Westfälische Wilhelms-Universität

Institut der Landschaftsökologie

Diploma Thesis

Water Vapour Fluxes

Above a Mountain Cloud Forest in Taiwan

Presented by

Veronika Wolff

Examiner: Prof. Dr. Otto Klemm

Westfälische Wilhelms-Universität, Münster

Co-Examiner: Prof. Dr. Yue-Joe Hsia

National Donghwa University, Hualien

Münster, May 2006

Table of Contents

Table of Contents I
List of Figures III
List of Tables VI
Symbols and Abbreviations VII
Abstract IX
Zusammenfassung X
1. Introduction 1
1.1 General 1
1.2 Study site 4
1.3 Experimental setup 5
1.4 Aims of the study 6
2. Methods and Materials 8
2.1 Methods for estimating water vapour flux 8
2.1.1 Bowen Ratio Method 8
2.1.2 Eddy Covariance 11
2.1.3 Penman approach 13
2.1.4 Penman-Monteith Method 14
2.2 Flux measurements above high vegetation and forest 16
2.3 Monte Carlo Method 19
2.4 Footprint analysis 20
3. Results 25
3.1 General 25
3.1.1 Weather conditions 25
3.1.2 Roughness parameter 30
3.1.3 Stability 33
3.2 Bowen Ratio 35
3.2.1 Calibration 35
3.2.2 Data quality for Bowen Ratio Measurement 38
3.2.3 Bowen Ratio 42
3.2.4 Water vapour fluxes 43
3.3 Eddy Covariance 46
3.3.1 Data quality for eddy covariance measurement 46
3.3.2 Eddy covariance water vapour fluxes 47

3.4 Penman fluxes 49
3.5 Penman Monteith fluxes 52
3.6 Comparison 55
3.6.1 Bowen Ratio and Eddy Covariance 55
3.6.2 Bowen Ratio, Penman, Penman-Monteith and Eddy Covariance 59
3.7 Monte Carlo Results 63
3.8 Footprint analysis 65
4. Discussion and Conclusion 71
Appendix 76
Acknowledgments 77
References 78
Statement 81

List of Figures

Figure 1: Study site (KLEMM, CHANG & HSIA, 2006) 4
Figure 2: Illustration of Taylor's hypothesis. (a) An eddy that is 100 m in diameter has a 5 °C temperature difference across it. (b) The same eddy 10 seconds later is blown downwind at a wind speed of 10 m s^{-1} (STULL 1988).....11
Figure 3: Contribution to the surface energy balance a) for a finite thickness box and b) for an infinitesimally thin layer. R_{net} is the net radiative contribution, Q_H is the turbulent heat flux, Q_E is the turbulent latent heat flux, H_{soil} is the molecular flux into the ground, and ΔH_S is storage (STULL, 1988) 17
Figure 4: The constant flux layer and its sub layers. The depth of the constant flux layer is about 15 % of the surface boundary layer (MONTEITH & UNSWORTH, 1990). 18
Figure 5: The source weight function, or footprint function, and its relation to the source area (SCHMID, 1994).....22
Figure 6: Schematic 50 % source areas for an eddy covariance and a profile measurement system (AMMANN, 1998) 23
Figure 7: Characteristics dimensions of the source areas as provided by Schmid's model (SCHMID 1994).....23
Figure 8: Temperature and fog during the first half of the study. 25
Figure 9: Temperature and fog during the second half of the study.....25
Figure 10: Wind speeds measured at 23.6 m (16.95 m above displacement height) 27
Figure 11: Wind direction a) of all data sets and b) after applying quality criteria (refer to Section 3.2.2) 28
Figure 12: Wind direction of data a) without fog and b) with fog 29
Figure 13: Net radiation during fog and in non foggy conditions.....30
Figure 14: Wind profile wind speeds plotted against height and the natural logarithm of height.....32
Figure 15: Wind Profile and roughness parameters 33
Figure 16: Stability conditions according to wind sectors. 34
Figure 17: Calibration data with more than 1m s^{-1} wind speed and wind direction between 100° and 200°.....36
Figure 18: Calibration Plot Doro and Egon.....37
Figure 19: Histogram of Bo before and after applying the first criterion (OHMURA, 1982) 39
Figure 20: Criterion for data quality considerations (Criterion 2).....40
Figure 21: Bo after applying quality criteria 1 to 3 41

Figure 22: Differences in temperature and water vapour pressure in times with and without fog. 42
Figure 23: Mean water vapour fluxes determined with the Bowen Ratio method. The black line gives an overall mean per hour, the black dots are single measured values, and the grey line shows the number of data sets available at that time. 44
Figure 24: Differences in measured values depending on the wind direction for a) sensible and latent heat flux (Q_H and Q_E) and b) the water vapour flux (Q_W). 45
Figure 25: Means of sensible (Q_H) and latent (Q_E) heat flux per hour of a day. 45
Figure 26: Part of the water vapour fluxes separated for wind directions. 48
Figure 27: Mean water vapour flux at a day. 48
Figure 28: Potential evaporation rates calculated with the penman approach separated for times with and without fog. 50
Figure 29: Potential evaporation separated for different wind directions 51
Figure 30: Potential evaporation rates of a day separated for the energy and the ventilation part of Penman's formula. 52
Figure 31: Mean evaporation rates for a day calculated with the Penman Monteith method....53
Figure 32: Differences in evaporation rates determined with the Penman Monteith method for a) times with and without fog and b) the two main wind directions, each time in comparison with the whole data set's mean. 54
Figure 33: Comparison between Bowen Ratio and Eddy Covariance fluxes during the last week of the study....55
Figure 34: Eddy Covariance results plotted against Bowen Ratio results. 56
Figure 35: Differences between eddy covariance and Bowen Ratio against energy budget's closure. 57
Figure 36: Difference in energy partitioning by the EC and the BR method. 58
Figure 37: Sums of latent and sensible heat flux for the Bowen Ratio and the eddy covariance set up. 58
Figure 38: Evaporation rates determined with the Bowen Ratio method, the Penman approach, the Penman-Monteith method, and the eddy covariance method. 59
Figure 39: Box-Plot for hourly water vapour flux averages calculated with the Bowen Ratio method (Q_W BR), the Penman Monteith method (ET_{PM}), the Penman approach (ET_{pot}), and the Eddy Covariance method (Q_W EC). 60

Figure 40: Hourly average values of water vapour flux determined by a) the Bowen Ratio method, b) the Penman Monteith method, and c) the Penman approach plotted against the fluxes by the eddy covariance method. 61
Figure 41: Daily values of water vapour fluxes determined with the Bowen Ratio method, the Penman Monteith method, the Penman method, and the eddy covariance method. 62
Figure 42: Standard deviation of hourly and daily values, expressed as percentage of the mean. 62
Figure 43: Comparison of the overall sums of measured water vapour fluxes. 63
Figure 44: Footprint areas for stable conditions. 66
Figure 45: Footprint areas for unstable conditions. 67

List of Tables

Table 1: Installed instruments 6
Table 2: Constants to determine the canopy resistance (MENZEL 1997) 16
Table 3: Results of the Kolmogorov-Smirnov-test. DE is the difference between the dry, and GF the difference between the wet temperatures, in the first (1) and second (2) calibration period. 36
Table 4: Overview of the data set size changes with quality criteria 41
Table 5: Statistical parameter of Bo 43
Table 6: Fluxes determined by the Bowen Ratio method separated for different wind directions 46
Table 7: Water vapour fluxes determined with the eddy covariance method, separated for fog and clear times and for wind directions 47
Table 8: Potential evaporation rates, energy, and ventilation parts for different situations determined with the Penman formula 49
Table 9: Evaporation rates determined with the Penman Monteith method (all data, data in times with and without fog (No fog, Fog), data with south easterly winds (SE) and data with northerly and north westerly winds (N/NW)). 54
Table 10: Rank order correlation results for hourly averages 60
Table 11: Calculated fluxes (Monte Carlo method). 64
Table 12: Footprint results 68
Table 13: Input and quality check parameter for footprint calculation. 69

Symbols and Abbreviations

Abbreviations

Bo	Bowen Ratio	ET_{POT}	Penman method
BR	Bowen Ratio method	ET_{PM}	Penman Monteith method
EC	Eddy covariance method	LAI	Leaf area index

Symbols

Δ	[hPa K^{-1}]	slope of the saturated water vapour pressure graph
Δe	[hPa]	Differences in humidity
ΔH_S	[W m^{-2}]	rate of energy storage within the canopy
ΔT	[°C]	Differences in temperature
c_p	[J kg^{-1} K^{-1}]	specific heat capacity of air at constant pressure
d	[m]	Displacement height
E	[hPa]	Saturation vapour pressure
e	[hPa]	Vapour pressure
$E(q)$		limit of resolution for specific humidity
$E(T)$		limit of resolution for temperature
g	[m s^{-1}]	Gravity acceleration
h	[m]	Height of the forest; vegetation
h_{BL}	[m]	boundary layer thickness
H_{soil}	[W m^{-2}]	Soil heat flux
L	[m]	Obukhov length
L_v	[J kg^{-1}]	latent heat of vaporization
p	[hPa]	Air pressure
Q_E	[W m^{-2}]	Latent heat flux
Q_H	[W m^{-2}]	Sensible heat flux
Q_W	[kg m^{-2} s^{-1}]	Water vapour flux
r_a	[s m^{-1}]	aerodynamic resistance
r_c	[s m^{-1}]	canopy resistance
R_{net}	[W m^{-2}]	Net Radiation
T	[°C]	Dry temperature
t	[s]	Time
T'	[°C]	Wet temperature
U	[m s^{-1}]	Wind speed

u^*	[m s^{-1}]	Friction velocity
WD	[°]	Wind direction
z	[m]	Aerodynamic height above the surface (above the displacement height)
z_0	[m]	roughness length
z_{0H}	[m]	Roughness length for heat and water vapour
z_{0W}	[m]	Roughness length for momentum transport
z_g	[m]	Geometric height above solid ground surface
z_H	[m]	Height of temperature and humidity measurement
z_m	[m]	Measurement height
z_W	[m]	Height of wind measurement
γ	[hPa K^{-1}]	Psychrometer constant
δv	[m s^{-1}]	Standard deviation of the lateral wind component
$\delta\Theta$	[mm]	Soil humidity deficit
κ		Kármán – constant
ρ	[kg m^{-3}]	Density of air

Footprint dimensions

a	[m]	Minimum distance from the tower
e	[m]	Maximum distance from the tower
d	[m]	Maximum lateral extension
xd	[m]	Distance between the maximum lateral extension and the tower
x_m	[m]	Maximum source location
ar	[m^2]	Area of the footprint

Abstract

From September through November 2005, fluxes of latent and sensible heat and water vapour fluxes from a cypress trees forest in north east Taiwan were studied. The aims of this study were to quantify the site's evapotranspiration rates, to find a statistically significant answer to the question if there is evaporation during fog or not, and to calculate footprint areas for the observed water vapour fluxes.

Four methods to quantify the evaporation were employed: the energy balance Bowen Ratio method, the eddy covariance measurement, the Penman approach, and the Penman Monteith method. Problems of measurement above high vegetation are discussed. Differences between the results of the methods were surprisingly large. Taking the eddy covariance results as the standard (100 %), the Bowen Ratio method overestimated fluxes by about 50 %. The Penman method agreed best with an underestimation of 26 %. Penman Monteith daily results showed no significant correlation to the other method's results and underestimated the fluxes by about 32 %. Differences between eddy covariance and Bowen Ratio results were found to be correlated to the energy budget closure; with improving closure, differences decreased. Energy partitioning of the eddy covariance and Bowen Ratio method were found to be different, with the eddy covariance favouring the latent heat flux and the Bowen Ratio favouring the sensible heat flux. Reasons for large differences between the eddy covariance and the Bowen Ratio are discussed.

A Monte Carlo type simulation was applied. Water vapour fluxes from the forest to the atmosphere, as determined with the Bowen Ratio method during fog proved to be statistically significant different from zero.

Footprints were calculated using the model by Schmid (1997). The footprint analysis showed excellent footprint conditions into south easterly directions. For stable conditions and wind directions other than south east little data was available.

Zusammenfassung

Zwischen September und November 2005 wurden im Nordosten Taiwans Messungen zum Wasserdampffluss über dem dort endemischen Zypressenwald durchgeführt. Ziele der Arbeit waren, die Verdunstung des Standortes zu quantifizieren, Verdunstungsraten bei Nebel statistisch zu testen und für die gemessenen Wasserdampfflüsse Footprint Analysen durchzuführen.

Es kamen vier Methoden der Wasserdampfbestimmung zur Anwendung: die Bowen-Verhältnis-Methode, die Eddy-Kovarianz-Methode, die Methode nach Penman und die nach Penman-Monteith. In der Arbeit wurden zudem die auftretenden Probleme und Besonderheiten bei Durchführungen von mikrometeorologischen Messungen über hoher Vegetation und Wald diskutiert. Die Unterschiede zwischen den durch die verschiedenen Methoden gewonnenen Ergebnissen waren erstaunlich groß. Im Vergleich zu den Ergebnissen der Eddy-Kovarianz-Messung (100 %), überschätze die Bowen-Verhältnis-Methode den Wasserdampffluss um 50 %. Die Ergebnisse der Penman-Methode wiesen die besten Übereinstimmungen auf und unterschätzen den Wasserdampffluss um 26 %. Die durch die Penman-Monteith berechneten Wasserdampfflüsse zeigten keinen statistischen Zusammenhang zu den anderen Ergebnissen und unterschätzen die Eddy-Kovarianz Ergebnisse um 32 %. Es stellte sich heraus, dass die Unterschiede zwischen Eddy-Kovarianz und Bowen-Verhältnis mit der Energiebilanzschließung korrelieren; mit sich verbessernder Schließung, verringerten sich die Differenzen. Des Weiteren war die Aufteilung der vorhandenen Energie in sensiblen und latenten Wärmestrom durch die Eddy-Kovarianz und die Bowen-Verhältnis Methode unterschiedlich. Die Eddy-Kovarianz-Methode begünstigt dabei den latenten Wärmestrom, während die Bowen Verhältnis Methode den sensiblen Wärmestrom bevorzugt. Die Gründe für die großen Unterschiede zwischen Eddy-Kovarianz und Bowen-Verhältnis werden diskutiert.

In dieser Studie wurde eine Simulation nach Monte Carlo durchgeführt. Bei Nebel mit der Bowen-Verhältnis-Methode gemessene Wasserdampfflüsse zwischen Wald und Atmosphäre zeigten sich dabei als statistisch signifikant von null verschieden.

Anhand des Modells nach Schmid (1997) wurden Footprints berechnet. Die Analyse zeigte exzellente Footprint Konditionen in südöstliche Richtungen. Für die weiteren Windrichtungen und für stabil geschichtete Atmosphäre waren wenige Daten zur Footpintanalyse vorhanden.

1. Introduction

1.1 General

Cloud forests are defined as forests that are frequently covered in cloud or mist (STADTMÜLLER, 1987). In the tropics, cloud forests are mainly located on high mountains between 1'200 and 2'500 meters above sea level (asl), where cloud belts are formed by moist ascending air masses. Mountain cloud forests represent an ecosystem that is extremely rich in plant diversity with more than 5000 species in a 10,000 square kilometre (km^2) area. They constitute a biodiversity hot spot and are considered as extremely fragile ecosystems playing an important hydrological an ecological role. (STADTMÜLLER, 1987)

The frequent occurrence of fog may result in the special structure and functioning of the tropical mountain cloud forest. Among others, the abundance of epiphytic bryophytes is a typical feature found in the tropical mountain cloud forest (CHANG ET AL., 2006). Fog also acts as an important stress factor in the ecosystem. Fog droplets may remain on a leafs surface for up to 4 hours before moistening capacity is reached and the droplets fall to the ground. In addition, fog contains ion concentrations that are 10 to 100 times larger than that of rain droplets, so pH can also vary. Fog impaction can constitute up to 48 % of the total water input of an ecosystem (BEIDERWIEDEN, 2004). In high mountain regions, fog is the most important source of soil and vegetation pollution. Further, the presence of fog reduces incoming short wave solar radiation (KLEMM, CHANG & HSIA, 2006). These properties of fog make it an important component of the hydrological and nutrient cycling (CHANG ET AL., 2006).

The study site, part of the Yuan Yang Lake (YYL) ecosystem, is located in the mountain regions of north eastern Taiwan and experiences frequent fog immersion (CHANG ET AL., 2006). The frequent occurrence of fog and the large amount of epiphytic bryophytes were believed in former studies to be important factors for the establishment and regeneration of the forest (WU ET AL., 2001).

The predominant species in the mountain cloud forest are cypress (*Chamaecyparis obtuosa var. formosana* and *Chamaecyparis formosensis*) with an under story of predominantly rhododendron (*Rhododendron formosanum*). The wood of these trees is valuable in Taiwan, not only for its high quality, but also as a symbolic element in the Taiwanese heritage and culture (KLEMM, CHANG & HSIA, 2006). It is not yet clear what the limiting factors of the *Chamaecyparis* species are and why

they occur mainly in the subtropical mountain cloud forest (KLEMM, CHANG & HSIA, 2006).

Cypress trees have been logged extensively in the past and are now protected by national nature preservation regulations. The plantation in which this study was performed exists for the purpose of restoring strong populations of these cypress trees. A program to investigate the site's ecological properties builds the background to the study described herein.

One of the aims of the study is to estimate the site's evaporation rate. Next to the radiation and the heat budget, the water budget is of fundamental meaning for the earth's climate. Phase Changes of water in exchange processes is a key factor for the heat budget of a climate system (LAUER & BENDIX, 2004). As a result of evaporation, a considerable amount of energy is taken out of the ecosystem. This energy is later released at another place when vapour condenses. This principle provides the link between energy and water budgets. Knowledge of an ecosystem's evaporation rate helps in understanding its ecological processes. (ARYA, 2001)

There are both direct and indirect methods to estimate the evaporation rate of a site. Indirect methods rely on estimates based on meteorological parameters such as net radiation and soil heat flux. Direct measurements derive evaporation rates either from a gradient measurement of crucial parameters or through a direct flux measurement such as the eddy covariance system, which relies on measurement of fluctuation of the crucial parameters.

Every method offers advantages and disadvantages in terms of applicability, accuracy, resolution for small time scales, prerequisites on spatial properties of the study site, user-friendliness, or cost. These advantages and disadvantages will be discussed in Section 2.1.

The hypothesis that there is statistically-significant evaporation during fog will be tested by a Monte-Carlo-type simulation.

Conducting measurements at a study site at a deficit height the flux measurement does not represent the exchange properties below the instrument. It does represent the properties of a surface in upwind direction (Luv) of the study site. This influencing area is called a footprint or a source area (FOKEN, 2003). Functions describing this area (i.e., the spatial distribution of surface sources) and its relationship to a measured signal at height in the surface layer have been termed "footprint" function or "source weight" function (SCHMID, 1994). Especially in

heterogeneous terrain the source areas are of major interest regarding measurements results (AMMANN, 1998). Footprint models are used more and more for experimental set up planning and for quality considerations (FOKEN, 2003). In this study, a footprint analysis after Schmid (1997) will be conducted, to determine source areas of measured fluxes and to assess the site's suitability for certain measurements.

The following chapter describes the study site, the experimental set up, and the aims of this study. In the second chapter, the methods to determine water vapour fluxes applied are introduced. Furthermore, the statistical Monte-Carlo method will be described as well as the footprint analysis. In addition, one part of sector two talks about general aspects on performing micrometeorological flux measurements above high vegetation and forests. The third chapter presents the results of the water vapour fluxes and compares them among each other. In the third chapter also the results of the Monte-Carlo and the Footprint analysis are given. The fourth chapter discusses and concludes the work done in this study.

1.2 Study site

The study was conducted close to the Yuang Yang Lake Nature Preserve, which is located in the north-eastern part of Hsinchu County, Taiwan. The site is at the uppermost head water of the Tahan River watershed with an elevation of 1 650 to 2 432 m (CHOU ET AL, 2000).

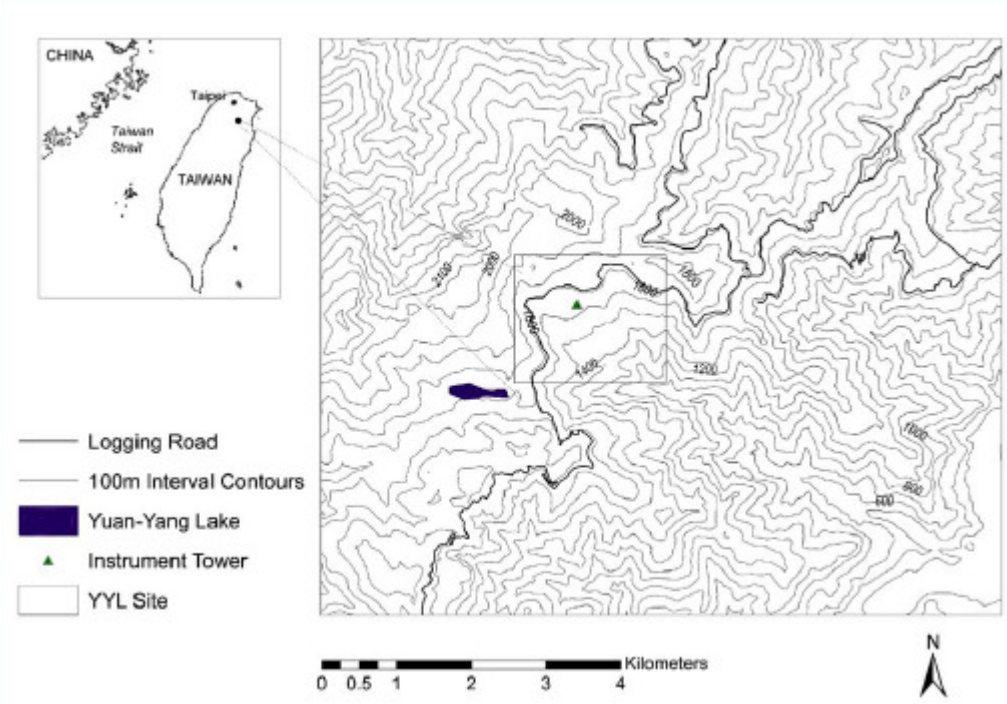

Figure 1: Study site (KLEMM, CHANG & HSIA, 2006)

The site is one of Taiwan's Long Term Ecological Research sites and represents the middle-altitude forest ecosystems in Taiwan. It was declared a nature preserve due to the presence of the sub alpine lake, the Yuan Yang Lake, and the surrounding old-growth Taiwan yellow cypress forest (*Chamaecyparis obtuosa var. formosana)* (CHANG ET AL, 2002).

The ecological research program was initiated in 1992 and is sponsored by the Taiwan National Science Council in cooperation with the Taiwan Forestry Research Institute, several universities, and the Institute of Botany of the Academia Sinica in Taipei. Its aims are to understand ecological processes in the ecosystem, investigating the hydrological and nutrient fluxes of the ecosystem and providing data for the global change research program (CHOU ET AL., 2000; KLEMM, CHANG & HSIA, 2006).

The climate of the study area is characterized as temperate heavy moist. According to the weather data recorded at this site, the mean annual temperature is 13 °C, and

annual rainfall averages over 4000 millimetres (mm). The high frequency of fog and cloud coverage accounts for significant reduction of solar radiation, and thus an important ecological factor for the cypress forest (HWANG ET AL., 1996, CHANG ET AL., 2002;KLEMM, CHANG & HSIA, 2006).

There are no apparent wet and dry seasons. However, the precipitation types can be differentiated between summer and winter: the source of rainfall in summer is mainly orographic precipitation and typhoons, while in winter the precipitation is dominated by the north eastern monsoon (CHANG ET AL., 2002). Due to high humidity the forest is rich in epiphytes, mainly mosses and liverworts (KLEMM, CHANG & HSIA, 2006).

The study was conducted in the partly managed forest surrounding the nature preserve. The canopy of the cypress forest is closed and extraordinarily uniform. Trees were planted between 1961 and 1978 (Klemm, Chang & Hsia, 2006) and their heights range from 11 to 14.3 m. The average height is 13.7 m.

The plantation is 300 hectares in size and is located within a valley on a relatively flat section which slopes downward at an angle of approximately 15 degrees in the south easterly direction (120 ° from true north). In 2002, an experimental tower reaching 23.4 m at its upper most platform was established within the plantation. The location (24°35'27.4"N, 121°29'56.3", and 1650 m asl.) was selected based on meteorological considerations (KLEMM, CHANG & HSIA, 2006). The tower is positioned at the north-westerly end of the plantation (KLEMM, CHANG & HSIA, 2006). The site was determined to be one of the optimum sites with the best possible footprint conditions for micrometeorological studies of the respective mountain cloud forest (KLEMM, CHANG & HSIA, 2006).

Former studies showed a wind regime with two dominating wind directions: north to northwest (mountain wind) and south to southeast (valley winds). Fog seemed to be highly correlated with wind directions from southeast to south. This observation lead to the hypothesis that the fog at the site is formed orographically due to cooling of air during its uphill transport (KLEMM, CHANG & HSIA, 2006).

1.3 Experimental setup

From the 21st of September through the 8th of November, 2005, an experimental setup to study the fluxes of energy and water vapour was installed at the

meteorological tower in the Chamaecyparis plantation. The equipment used is summarized in Table 1.

Table 1: Installed instruments

Method	Parameter		height
Bowen Ratio	Wet and dry temperature (ΔT and Δe)	Psychrometer (Frankenberger)	15.05 m 23.12 m
	Radiation	Kipp&Zonen CNR 1 net radiometer	22.50 m
	Soil Heat Flux	Hukseflux Thermal sensors	ground
Eddy covariance	ultrasonic anemometer	Young	23.40 m
	Optical combined CO_2/H_2O-analyzer	LI-COR 7500	23.40 m
Further parameters	Pressure	Model 61202 Barometric Pressure Senor	ground
	Wind direction & Wind speed	Young Model 05305 Wind Monitor-AQ	23.60 m
	Visibility	Aanderaa instruments, mira visibility sensor 3544	22.20 m 4.90 m
	Wind profile	Micro response anemometer 3-cup assembly	13.20 m 14.60 m 16.60 m 18.70 m 20.50 m 23.30 m

The soil heat flux was measured by five Hukseflux thermal sensors. The soil at the YYL site is highly heterogenic, thus five sensors were put into the soil at locations representative of the area; the mean result of the five was used for the analysis. Barometric pressure (Aanderaa instruments at two heights, 22.20 m and 4.90 m) and visibility data were made available to the investigators.

1.4 Aims of the study

This study is part of a cooperative effort of the universities of Muenster, Germany, and Donghwa, Taiwan. Its principal aim is to enhance the understanding of the water and nutrient cycling processes within a subtropical rainforest.

Furthering scientific work at the site in the areas of soil science, hydrology, forestry and botany, the work presented herein has been completed in addition to a PhD thesis about the area's climatology. This thesis adds valuable information to our understanding of ecological processes at the study site.

The specific goals of this study were, first, to determine water vapour fluxes using four different methods (Bowen Ratio method (BR), the eddy covariance method (EC), the Penman approach (ET_{POT}) and the Penman Monteith method (ET_{PM})) and to compare and discuss the results. The suitability of various methods to accurately measure water vapour fluxes at this study site will be evaluated. Special emphasis will be placed on measurements collected during the presence of fog.

Second, statistical methods will be used to determine whether the existence of water vapour fluxes during foggy conditions can be proved. The analysis will reveal whether evaporation occurs during periods of fog.

Third, analytical footprints (i.e. the source weight functions) will be determined for the EC method with varying wind directions and stability conditions in order to make general conclusions about the study site and to evaluate the suitability of various meteorological study methods for this site.

2. Methods and Materials

2.1 Methods for estimating water vapour flux

2.1.1 Bowen Ratio Method

The Bowen Ratio method was introduced by Bowen in 1926 as a simplification of the well known flux gradient similarity. It is now one of the most widely known methods for determining latent (Q_E) and sensible heat flux (Q_H). The method is based upon the Bowen Ratio similarity (1) and the equation for the surface energy balance (2). (ARYA, 2001)

$$Bo = \frac{c_p \cdot p}{L_v \cdot 0.622} \cdot \frac{\Delta T}{\Delta e} \quad (1)$$

$$R_{net} = Q_H + Q_E + H_{soil} \quad (2)$$

with

Δe	Difference between upper and lower water vapour pressure	hPa
ΔT	Difference between upper and lower dry temperature	°C
Bo	Bowen Ratio	
c_p	Specific heat of air at constant pressure	J kg^{-1} K^{-1}
H_{soil}	Soil heat flux	W m^{-2}
L_v	latent heat of vaporization	J kg^{-1}
p	Air pressure	hPa
Q_E	Latent heat flux	W m^{-2}
Q_H	Sensible heat flux	W m^{-2}
R_{net}	Net radiation	W m^{-2}

The sign convention used here is that radiation fluxes are positive towards the surface and that all other fluxes are positive away from the surface.

The Bowen Ratio is the ratio of the sensible and the latent heat flux:

$$Bo = \frac{Q_H}{Q_E} \quad (3)$$

Under certain circumstances, such as when measuring under near-neutral stability conditions and assuming the equality of the eddy exchange coefficients for heat and

water vapour, the flux gradient similarity can be simplified to the Bowen Ratio similarity. It states that the gradients of temperature and humidity between two heights act in the same way as the Bowen Ratio.

Thus, in order to determine *Bo* one needs to measure the differences in temperature and specific humidity at two levels in the surface layer (ARYA, 2001; FOKEN, 2003). To determine sensible and latent heat flux, the net radiation and the soil heat flux have to be measured also, and using equation (1) and (2) they can be calculated following

$$Q_H = \left(R_{net} - H_{soil}\right) \cdot \frac{Bo}{\left(1 + Bo\right)} \tag{4}$$

$$Q_E = \frac{\left(R_{net} - H_{soil}\right)}{\left(1 + Bo\right)} \tag{5}$$

From the latent heat flux the water vapour flux can be calculated with equation (5).

$$Q_W = \frac{Q_E}{L_v} \tag{6}$$

When employing the Bowen Ratio Method one has to keep in mind the assumptions made in the derivation. Turbulent atmospheric conditions are indispensable. Thus, although wind velocity does not appear in the formula, wind measurements should be included in the experimental set up.

Using this method, the closed surface energy budget (i.e., the validity of equation (2)) (refer to Section 2.2) also is of major importance. An imbalance in the surface energy budget can occur, for example, through measurement errors in one of the parameters or due to inaccurate estimation of the heat storage in the soil. Unbalanced energy budget closure may lead to overestimation of the latent and the sensible heat flux because storage terms are indirectly added to the net radiation (FOKEN, 2003). Furthermore, different footprint areas of parameters measured at separate heights (such as the soil heat flux and the temperature gradient) may lead to difficulties (refer to Section 2.4). To minimize data errors, the sensors should be arranged in such a way that ΔT and Δe (i.e., the difference in temperature and water vapour pressure) are maximized and one can obtain possibly large resolvable profile differences. To accomplish this, the vertical distance between the two levels was chosen as large as possible without introducing internal boundary layers between them.

The Bowen Ratio set up in Taiwan consisted of a net radiometer and five soil heat flux sensors, whose arithmetic mean was used for the calculation. The wet and dry temperature was measured at two heights, 15.05 m and 23.12 m, above the forest canopy. The lower level was thus approximately 1 m above the maximum height of the forest (14 m). Although a larger distance from the canopy would have been more appropriate to avoid roughness sublayer effects (refer to Section 2.2), a certain compromise had to be made in order to gain resolvable differences.

Each psychrometer consisted of two Pt 100 platinum resistance sensors; one of them was covered with wet gauze. The sensors were protected from radiation and constantly ventilated by electric fans to eliminate influences of wind, radiation, and evaporation.

The psychrometers were connected to a Delta-T DL2e data logger[1]. A four wire connection was used to eliminate cable resistance (difference circuit). Temperature was measured every 10 seconds and stored as a 10 minutes average.

From the dry and wet temperature psychrometers reading, the water vapour pressure (e) can be derived. The saturation vapour pressure can be calculated from the well-established Magnus' formula (constants from the VDI):

$$E = 6.11 \cdot e^{\frac{17.08 \cdot T'}{234.18 + T'}} \tag{7}$$

The actual water vapour pressure from:

$$e = E - \frac{c_p \cdot p}{0.622 \cdot L_v} \cdot (T - T') \quad \text{(MONTEITH \& UNSWORTH 1990)} \tag{8}$$

where:

e	Actual water vapour pressure	hPa
E	Saturation water vapour pressure	hPa
p	Air pressure	hPa
T	Dry psychrometers temperature	°C
T'	Wet psychrometers temperature	°C

The accuracy of the Bowen Ratio method for periods larger than one day at balanced energy budget is between 10 % and 30 % (FOKEN 2003). Among others, a study of Spittlehouse and Black (1980) confirms the suitability of the Bowen Ratio method for measuring forest evaporation. Further, former studies at this study site

[1] Delta-T Devices Ltd, 128 Low Road, Burwell, Cambridge, CB5 OEJ, UK

showed a well closed energy budget of the study site, and thus validate the application of this method here (KLEMM, CHANG & HSIA, 2006).

To achieve reliable data from this method several quality tests were run in this study (refer to Section 3.2.2).

2.1.2 Eddy Covariance

The eddy covariance method relies on measurements of the fluctuating components of wind in the constant flux region of the surface boundary layer and on the associated fluctuations in temperature, humidity or gas concentration.

Fundamental for this method is Taylor's hypothesis that suggested that turbulent eddies can be considered "frozen" as they are carried along with the mean wind speed and past a fixed point (e.g., the ultrasonic anemometer). This means that the measurement at a certain point as function of the time gives the same result as a spontaneous spatial measurement. In this way, Taylor's hypothesis allows interpreting time series and spectra as representative spatial series and spectra (STULL, 1988).

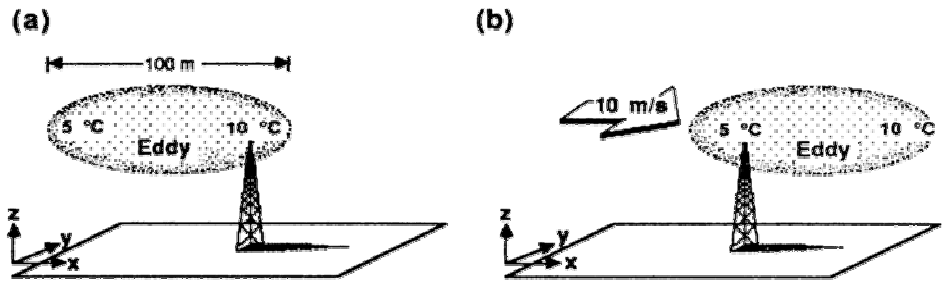

Figure 2: Illustration of Taylor's hypothesis. (a) An eddy that is 100 m in diameter has a 5 °C temperature difference across it. (b) The same eddy 10 seconds later is blown downwind at a wind speed of 10 m s^{-1} (STULL 1988)

Observing one point in the constant flux layer, the mean wind velocity is horizontal, but instantaneous values are in any direction and generally have a vertical component towards or away from the surface. Being in the constant flux layer, the mean of vertical flux of dry air is zero. The fluctuating vertical components carry other entities, such as sensible and latent heat. This net transport of heat by the vertical eddies shows fluctuations in temperature and water vapour concentration that are correlated to the fluctuations in vertical velocity. A flux of heat towards the surface arises when, on average, eddies moving towards the surface contain air at

higher than average temperature, and those moving away from the surface are at lower temperatures (MONTEITH & UNSWORTH, 1990).

From the measurement of the fluctuating components, the time averaged turbulent fluxes can be derived from the following equation, after applying the Reynolds averaging (in ARYA, 2001). For example the vertical flux of water vapour is thus

$$E = \rho\overline{wq} \qquad \text{(ARYA, 2001)} \qquad (9)$$

with $\overline{wq}$ as the covariance of the fluctuations of the vertical wind speed w and the fluctuation of the humidity q and ρ the density of the air (ARYA, 2001).

The assumptions used in the derivation of the method requirements must be honoured when using the method. One of the most important assumptions is that the horizontal homogeneity and the stationary conditions (i.e. average properties of turbulence and species concentration) must not change statistically over an averaging interval of 30 minutes. Furthermore, the correct estimation of the footprints (refer to Section 2.4.), which should be within uniform surface for all stability conditions, internal boundary layer exclusion and obstacle influence exclusion are of major importance for choosing the study site (FOKEN 2003).

The eddy covariance experimental set up used in this study consisted in a Young 8100 ultrasonic anemometer[2] and a LI-COR LI-7500[3] combined open path infrared CO_2/H_2O-analyser. Raw data were recorded continuously using the in-house software 'Acquisio'. After the removal of apparent outliners, data were computed by the in-house software 'DANA'. The following processing steps were conducted:

I. Coordinate rotation of u, v, w wind components using the planar fit method

II. Detrending of the data sets calculating moving average (1200 s intervals) of scalar data

III. Webb correction (WEBB ET AL., 1980)

IV. Determining time lag values by cross-correlation

V. Computing turbulent fluxes

[2] R.M. Young Company, 2801 Aero Park Drive, Traverse City, Michigan 49686 USA
[3] LI-COR Biosciences, 4421 Superior Street, P.O. Box 4425, Lincoln, Nebraska, USA

Data acquisition and computing were performed by E. Beiderwieden, and the results were provided for comparison.

2.1.3 Penman approach

Using a combination of the energy balance and the bulk transfer formulas, Penman (1948) derived a formula for evaporation from open water and saturated land surfaces. Penman's formula, either in the original or a slightly modified form, is widely used for estimating potential evaporation or evapotranspiration, especially in hydrological and agricultural applications (ARYA, 2001).

The Penman formula:

$$ET_{pot} = \frac{\Delta}{\Delta + \gamma} \cdot \frac{R_{net} - H_{soil}}{L_v} + \frac{\gamma}{\Delta + \gamma} \cdot f(U) \cdot \frac{E - e}{L_v} \quad \text{(ARYA, 2001)} \qquad (10)$$

with

ET_{POT}	Potential evaporation	kg m^{-2} s^{-1}
Δ	Slope of the saturated water vapour pressure graph	hPa K^{-1}
γ	Psychrometer constant	hPa K^{-1}
$f(U)$	Semi-empirically determined function of the wind velocity	

Crucial aspects of Penman's formula are, first, the energy for the evaporation provided by the net radiation, and second, the possibility of the removal of the evaporated water, calculated from the wind speed and the water vapour gradient.

In order to determine the evaporation rate from equation (10), measurements of the net radiation, and soil heat flux at ground level, together with the measurements of wind speed, temperature, and humidity at a low level above the surface are required.

The Penman formula gives the potential evaporation of a site. Its applicability is limited to wet, bare surfaces and vegetated surfaces with wet foliage over which evaporation is near its potential rate (ARYA, 2002). Arya points out that for water surfaces and those with tall vegetation, the use of the surface energy balance equation may not be appropriate (refer to Section 2.2).

This method was used during the study for two reasons: Firstly, water deficiency could be excluded as fog and rain kept the foliage at the study site wet (this assumption underlies the applicability of the formula above) and secondly, this method has previously been used at this site. The evaporation rates will be compared to results provided by other methods to determine accuracy and applicability to this study site. This would allow for the possibility to revise former study results.

2.1.4 Penman-Monteith Method

From Penman's formula Monteith (1965) developed a formula that includes properties of the vegetated and not-water-saturated surfaces. It considers the resistance to evaporation of the respective vegetation using the leaf area index and the stomata resistance of the vegetated surface. Evaporation resistance is principally based on the conductivity for water of the plants, which is regulated by its stomata and stomata resistance (MONTEITH & UNSWORTH, 1990). With the Penman-Monteith formula the actual evaporation rates can be calculated.

The Penman-Monteith formula is

$$ET_{PM} = \frac{\Delta\,(Q_S - H_{soil}) + \rho \cdot c_p \cdot \frac{(E-e)}{r_a}}{L_v \cdot (\gamma \cdot (1 + \frac{r_c}{r_a})} \quad \text{(MONTEITH \& UNSWORTH, 1990)} \qquad (11)$$

with

ET_{PM}	Actual evaporation after Penman-Monteith	kg m^{-2} s^{-1}
ρ	Density of the air	kg m^{-3}
r_a	Aerodynamic resistance	s m^{-1}
r_c	Canopy resistance	s m^{-1}

The aerodynamic resistance r_a can be calculated using this formula:

$$r_a = \frac{\ln\left(\frac{z_w - d}{z_{0w}}\right) \cdot \ln\left(\frac{z_H - d}{z_{0H}}\right)}{k^2 \cdot U_{zw}} \quad \text{(MONTEITH \& UNSWORTH, 1990)} \qquad (12)$$

With:

z_W	Height of wind measurement	m
z_H	Height of temperature and humidity measurement	m
z_{0W}	Roughness length for momentum transport	m
z_{0H}	Roughness lenth for heat and water vapour transport	m
d	Displacement height	m
U	Wind speed at height zw	m s^{-1}
κ	Kármán constant	0.40

The displacement height at the study site was calculated as 6.65 m (refer to Section 3.1.2). The roughness length for momentum transport is 1.37 m and the roughness length for the transport of heat and water vapour is 0.137 m.

Regarding the forest canopy as a surface at the displacement height rather than a layer of thickness h_0, and thus avoiding further complications (refer to Section 2.2), we measure z_W and z_H from the displacement height rather than from ground level. For temperature measurement, the dry temperature of the upper psychrometer was taken, the wind speed measurement was calculated from an extrapolation of the wind profile measurement conducted at the tower, thus $z_W = z_H = 16.47$ m.

The canopy resistance r_C depends on the vegetation. That is, it depends on the season of the year and the leaf area index (*LAI*) (MENZEL, 1997).

Menzel (1997) derived a model to estimate r_c based on the independent parameters leaf area index (*LAI*), air temperature (*T*) and soil humidity deficit ($\delta\Theta$):

$$r_c(T, LAI, \delta\Theta) = a_0 + a_1 r_c(T) + a_2 r_c(LAI) + a_3 r_c(\delta\Theta)$$

with the canopy resistance as the sum of the resistances for temperature ($r_c(T)$), for the leaf area index ($r_c(LAI)$) and for the soil humidity deficit ($r_c(\delta\Theta)$). These resistances can be calculated with the following equations (MENZEL, 1997):

$$r_c(T) = (\mathrm{T} + b_1)^4$$
$$r_c(LAI) = \exp(b_2 LAI)$$
$$r_c(\delta\Theta) = (\delta\Theta + b_3)^4$$

Depending on the LAI he gives the following constants for these equations:

Table 2: Constants to determine the canopy resistance (MENZEL 1997)

	a_0	a_1	a_2	a_3	b_1	b_2	b_3	r^2
LAI ≥ 2	*37.52*	*$5.4 \cdot 10^{-5}$*	*2420.5*	*$3.0 \cdot 10^{-5}$*	*4.43*	*-1.75*	*-20.51*	*0.67*
LAI ≤ 2	*-227.30*	*2.98*	*487.6*	*$2.5 \cdot 10^{-5}$*	*-*	*-0.33*	*-2.05*	*0.92*

The leaf area index of the vegetation within the study site was determined to be 6.3 $m^2 m^{-2}$ (CHANG, 2005, personal communication) and air temperature was constantly measured. The soil humidity deficit was not measured at the experimental site and therefore has to be estimated. The soil humidity deficit $\delta\Theta$ ($\delta\Theta$ = 0 mm corresponding to the field capacity of the soil) only strongly influences r_c at very little water availability ($\delta\Theta$ > 40 mm) or at excess supply of water ($\delta\Theta$ < 0 mm) (MENZEL, 1997). Due to the frequent occurrence of fog and rain and the good water drainage of the soil at the site, it could be estimated that there was no excess of water nor water shortage and set the soil humidity deficit to be 0 mm.

2.2 Flux measurements above high vegetation and forest

Several considerations have to be included when measuring turbulent fluxes and evaporation above high vegetation and forests. Methods to determine water vapour fluxes often contain the energy budget equation for the surface in some way or depend on its closure. The energy budget of vegetated surfaces such as canopies differs from that of bare surfaces as the growth of vegetation over an otherwise flat surface introduces several complications into the energy balance.

First, the ground surface may not be the appropriate reference for the surface energy as the radiative, sensible, and latent heat fluxes are spatially variable within the canopy. The equation of energy budgets for whole canopy layers

$$R_{net} = Q_H + Q_E + H_{soil} + \Delta H_s \qquad \text{(ARYA, 2001)} \qquad (13)$$

would be more appropriate to consider for forest and high vegetation. R_{net}, Q_H, and Q_E have to be measured well above the treetops where horizontal variation of fluxes may be neglected (ARYA, 2001).

Second, the rate of energy storage (ΔH_S) introduced in the canopy's energy budget consists of two parts, the rate of physical heat storage and the rate of biochemical heat storage (result of photosynthesis and carbon dioxide exchange). This rate of heat storage is not easily measured or calculated. Even if in some high vegetation canopies the storage rate may not be important on time scales used in micrometeorological measurements, the large heights of trees and the associated biomass of the forest canopy suggest that the heat storage of them may not be insignificant, even over short periods (ARYA, 2001).

For these first two points confer to Figure 3.

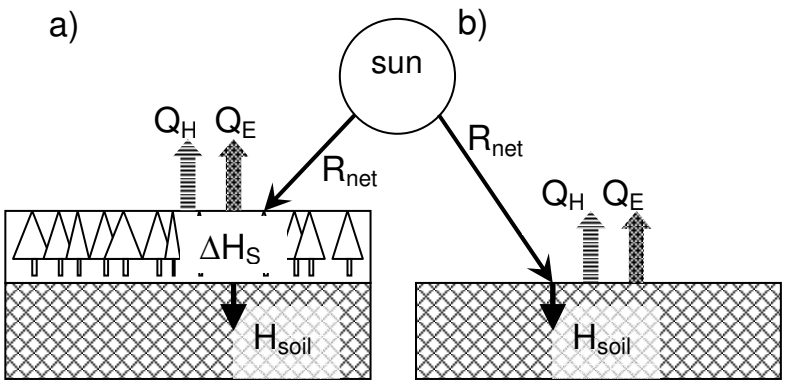

Figure 3: Contribution to the surface energy balance a) for a finite thickness box and b) for an infinitesimally thin layer. R_{net} is the net radiative contribution, Q_H is the turbulent heat flux, Q_E is the turbulent latent heat flux, H_{soil} is the molecular flux into the ground, and ΔH_S is storage (STULL, 1988)

Third, above vegetated canopy the latent heat flux is not only due to processes at the surface but also due to transpiration from the plants leaves. This evapotranspiration (evaporation + transpiration) produces nearly a constant flux of water vapour above the canopy layer (ARYA, 2001). Foken (2003) points out that within the complicated meteorological processes within the treetops and trunk space of a forest, the treetops act as a layer that separates the trunk space and the upper layer above the forest and that therefore energy fluxes between the atmosphere and upper treetops should be separated from the exchange fluxes between the lower treetops, the trunk space and the soil.

Another problem arises measuring fluxes above high vegetation. Very close to the roughness elements, the turbulent structure is influenced by the wake generated by the elements, thus establishing a roughness sub layer (MONTEITH & UNSWORTH, 1990) (refer to Figure 4). Significant deviations from the log law under neutral conditions and more general Monin-Obukhov-similarity profiles have been observed

to occur in this layer, which is a transition layer between the canopy layer below and the constant flux inertial sub layer above (ARYA, 2001). After Arya (2001) this roughness transition layer is characterized by relative small values of (z-d / z_0), ranging between 10 and 150. Thus, the roughness sub layer thickness may vary from less than a meter over short vegetation to several tens of meters over forest canopies (ARYA, 2001).

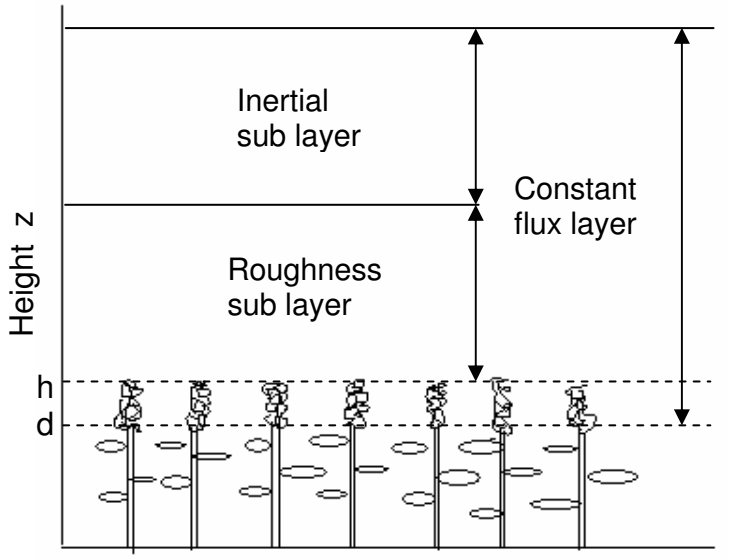

Figure 4: The constant flux layer and its sub layers. The depth of the constant flux layer is about 15 % of the surface boundary layer (MONTEITH & UNSWORTH, 1990).

Above the roughness sub layer is the inertial sub layer, in which fluxes are constant with height and the boundary layer structure depends only on scales as friction velocity and height. In this layer micrometeorological measurements can be used most easily to deduce fluxes from profiles (MONTEITH & UNSWORTH, 1990), i.e. Bowen Ratio measurement should at best be performed in this inertial sub layer. The gradient parameterizations can be applied in the above-canopy inertial sub layer, especially in the height range $0.1 \cdot h_{BL} > z > 2 \cdot h$ with h_{BL} being the boundary layer thickness (ARYA, 2001). Arya (2001) points out that the range of validity of the surface layer similarity relations becomes narrower for taller canopies and for shallow boundary layers and that it may disappear completely, when the planetary boundary layer thickness is less than 10-15 times the vegetation height, a distinct possibility, over mature canopies.

Monteith and Unsworth (1990) define the lower limit of this inertial sub layer by z_m-d >> z_0 and postulates for z_m, the measurement height, z_m–d = $10 \cdot z_0$, from which follows $z_m = 10 \cdot z_0 + d$.

As to Bowen Ratio and gradient measurement, McNeil and Shuttleworth (1975) note that gradients of temperature and water vapour are much smaller above forest canopies than over lower vegetation due to the aerodynamically very rough forest canopy that produces rapid exchange of latent and sensible heat to the atmosphere.

On the other hand it is found convenient and practicable to consider the canopy as an area source and sink of infinitesimal thickness located at an effective height d above the ground level, and to consider it an effective reference plane (ARYA, 2001). Foken (2003) further states that dense vegetation can be regarded as a porous sub layer and therefore there is only the displacement of the profiles with the displacement height. Measurements of turbulent fluxes of momentum, sensible heat, and water vapour have been conducted and turbulent fluxes were found to remain practically constant (independent of the height) in the height interval $h < z < 2.4 \cdot h$ studied, which includes the roughness sub layer (ARYA, 2001).

As it was neither possible nor practicable in this study to measure or estimate storage rates of the canopy layer or fluxes within it, we regard the canopy as an area source and sink of infinitesimal thickness located at an effective height d. With regards to the measurement heights for the Bowen Ratio set up, one has to weigh up the size of gradients and their measurability, against the danger to get into the roughness sub. In this study more emphasis was put on measurable gradient differences.

Measurement heights for the Bowen Ratio were 15.05 m (8.40 m above *d*) and 23.12 m (16.47 m above *d*) and the Eddy covariance set up was mounted at 23.4 m (16.75 m above *d*). For other instrument height, please refer to Section 1.3.

2.3 Monte Carlo Method

To examine the water vapour fluxes determined by the Bowen Ratio method during fog, a Monte-Carlo-type simulation routine was applied in order to determine for several data sets if there is statistically significant water vapour flux during fog or if fluxes found are statistically not significant.

The Monte-Carlo Method uses principals of probability calculation and statistics to solve complex problems. This is why it is also referred to as a “method of statistic tests”. It was named after Monte Carlo as first random number tables were filled by the roulette results of one of the casinos in Monte Carlo (LUTZ, 2006).

To apply this method here, for each data set and each sensor of the lower psychrometer, normal distributed random numbers were generated, taking the original measurement value as the mean value and the standard deviation between the dry and the wet sensors during fog (as determined during the calibration, see 3.2.1 Calibration) for the standard deviation. The lower dry and wet temperatures were randomly generated with their own normal distributed random numbers while the upper dry and wet temperatures were held at the original measurement value. Using these data sets, the Bowen Ratios and the water vapour fluxes were calculated. With growing number of repetitions and growing number of random numbers, the mean and the standard deviation of the fluxes calculated for one data set tend to a stable value. That way, for one data set (i.e. one situation at the study site during fog), a mean flux and its standard deviation are obtained.

The mean of the calculated fluxes is tested in a single-value-t-Test against zero to determine whether or not it is statistically different from zero, i.e. if there is water vapour fog and at what probability value.

2.4 Footprint analysis

When performing micrometeorological flux measurement, it is not easy to identify the surface area that is representative of the measured fluxes. All constant flux layer methods rely in their theory on the assumption of an ideal homogeneous surface. In practice, however, no vegetated surface is perfectly homogeneous and often shows spatial variability in its exchange activity. Moreover the surface is usually patchy with limited areas of different agricultural and natural vegetation canopies and is disturbed by single roughness elements such as isolated trees. Thus, it is of high importance for the micrometeorological methods to have quantitative information about the surface area that actually influences the flux measurement at a single point or several points in a vertical profile (AMMANN, 1998).

Footprint areas are governed by the properties of turbulent diffusion, with size and location dependant upon wind direction and other characteristic parameters influencing turbulent diffusion such as thermic layering and surface attributes (MANGOLD, 1999). In this study, the terms footprint and source area, and the terms footprint function and source weight function, are used synonymously.

Corresponding footprint models are based on the turbulent diffusion theory and consider the measured concentration or flux at a certain height z as a linear

superposition of disperses plumes of many distributed point sources at the surface. The concentration and vertical flux distribution in a turbulent dispersion plume may be determined either with a Lagrangian concept using the simulations of particle trajectories or with an analytical Eulerian approach using surface layer similarity theory (AMMANN, 1998).

Footprint models rely on certain presumptions. Legality of the surface layer is assumed, i.e. there is a logarithmic wind profile, a constant flux layer and a fully developed turbulent wind field. There are no further sources and sinks, and diffusion of regarded substance is passive and independent to each other. Furthermore, it is assumed that the turbulent flow field is homogeneous in wind direction, i.e. parameters as u^*, z/L, z_0, and wind fluctuation do not vary between emission and sensor. Diffusion parallel to the mean wind direction is disregarded. Thus, the source weight function is only due to the upwind position of the source (MANGOLD, 1999).

In this study the 'source weight function' after Schmid (1994), relying on the Eulerian approach, will be used. Important input parameters are aerodynamic measurement height (z_g-d), roughness length (z_0), stability (z/L), standard deviation of the lateral wind component (δv), friction velocity (u^*), and wind direction.

Measurement height, wind speed, and wind direction can be taken directly from the data set. The parameters z/L for stability and the friction velocity u^* are provided by the in-house software DANA to analyze data from the ultrasonic anemometer. The roughness length is calculated from these data using a rearranged formula of the logarithmic profile law:

$$z_0 = \frac{z-d}{e^{\frac{u\cdot\kappa}{u^*}}}. \qquad (14)$$

To determine the standard deviation of the lateral wind component a co-ordinate rotation is conducted. The three wind components have to be rotated into the mean wind direction; this corresponds to the classical first co-ordinate rotation (FOKEN, 2003). After doing so, the mean lateral wind speed is zero and its standard deviation is the one needed in further calculation.

The general form of the source weight function is as follows: It is small directly in front of the sensor, then rapidly rises to a maximum and falls off more slowly with increasing distance. It also decreases to both sides of the main upwind direction producing an ellipsis-like shape of the isopleths. The distance of the maximum point

and the longitudinal extension increases with z/L and z/z_0, i.e. with measurement height, stability, and inverse roughness length. The lateral extension is mainly dependant on the dimensionless crosswind standard deviation $\sigma v/u^*$ (refer to Figure 5).

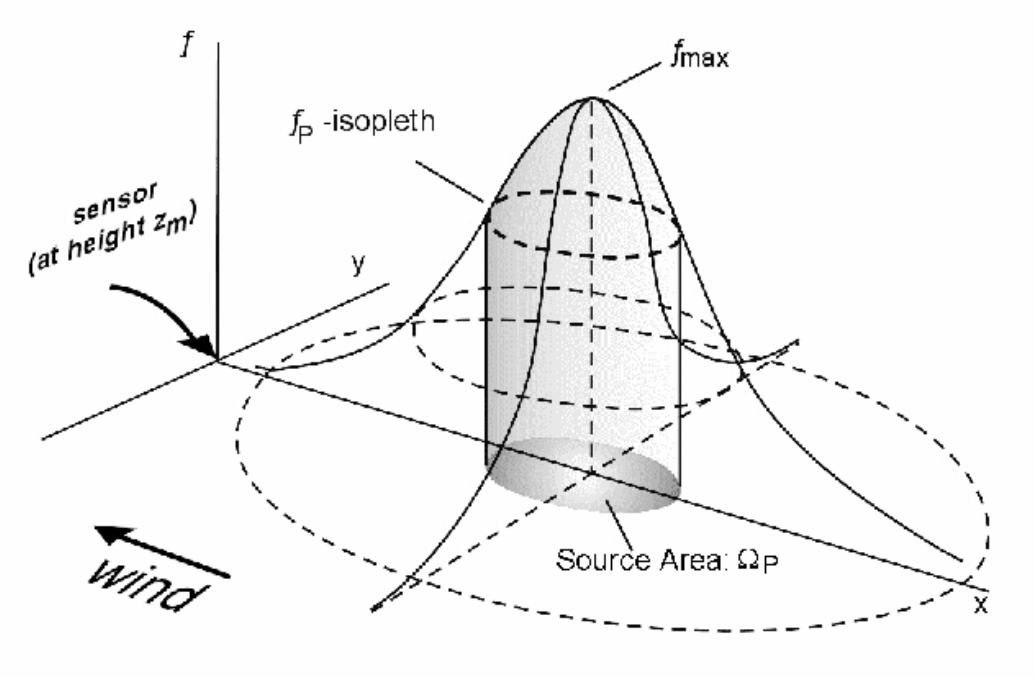

Figure 5: The source weight function, or footprint function, and its relation to the source area (SCHMID, 1994)

The source areas for eddy correlations flux measurements at a single point are found to be generally smaller than those for gradient concentration measurements under comparable conditions (AMMANN, 1998). The main problem for the profile methods is that each measurement level has its own distinct source area (refer to Figure 6). It is usually much smaller and closer to the tower for low profile levels than for the higher ones. Thus under inhomogeneous conditions, the profile levels are often influenced by different surface types no meaningful flux result can be obtained (AMMANN, 1998).

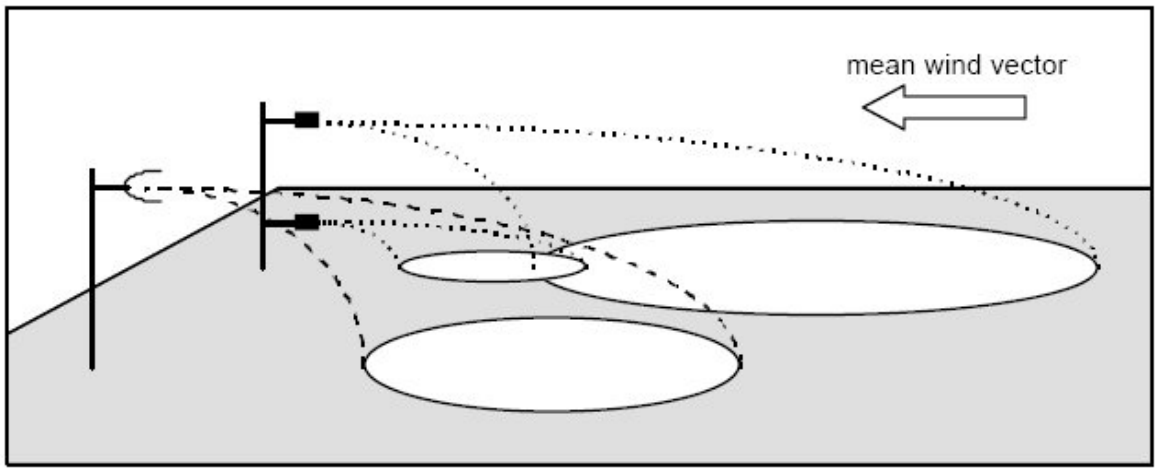

Figure 6: Schematic 50 % source areas for an eddy covariance and a profile measurement system (AMMANN, 1998)

As in this study only one 3D ultrasonic anemometer was installed at the tower, so it is not possible to compare footprints of the different methods used here. Footprints calculated are those for the eddy covariance set up. The results of the model are presented as characteristics dimensions of the P = 50 % and the P = 90 % source areas (i.e. the area responsible for 50 % and for 90 % of the surface influence): the maximum source location (i.e. the upwind distance of the surface element with the maximum-weight influence) (x_m), the near (a) and the far (e) end of the source area, and its lateral extension (d) (SCHMID, 1994) (cf. Figure 7).

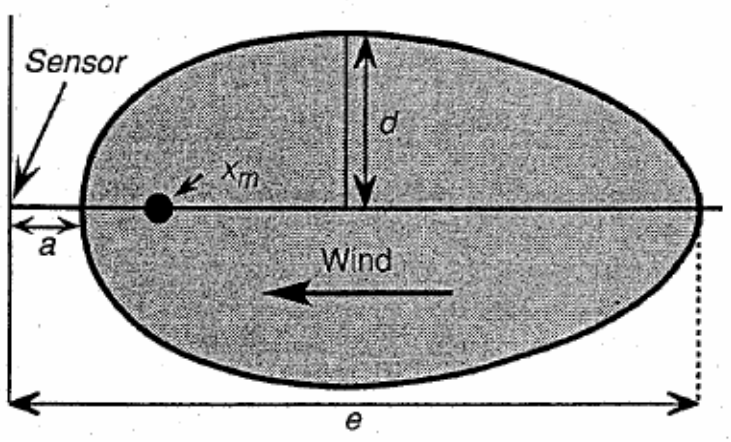

Figure 7: Characteristics dimensions of the source areas as provided by Schmid's model (SCHMID 1994).

Schmid defines certain ranges for input parameters for his method. One requirement is $z_0 << z_m$. Thus, values for z_m/z_0 have to range between 20 and 500 for stable conditions and between 40 and 1000 for unstable conditions. $\sigma v/u^*$ may range from 1 to 6. Numerical restrictions allow for z/L only values between $2 \cdot 10^{-4}$ and 0.1 for stable conditions and between $4 \cdot 10^{-4}$ and 1 for unstable conditions. Every single

input parameter has a special influence on the dimensions of the footprint. These influences are discussed, for example, in Schmid (1994) and in Mangold (1999).

The results of the calculations will be used to interpret fluxes measured with different wind directions and atmospheric conditions. These results are of importance to this study, not because of different canopy vegetation but because of changing topography and fetch properties in different wind directions. Thus, the footprint analysis may help in interpreting fluxes and their data quality regarding their fetch situations.

3. Results

3.1 General

3.1.1 Weather conditions

During the measured period from 29th of September to 8th of November 2005 temperatures ranged between 6.8 and 23.5 °C (dry temperature at 15.05 m), its mean being 14.1 °C (Figure 8 and Figure 9).

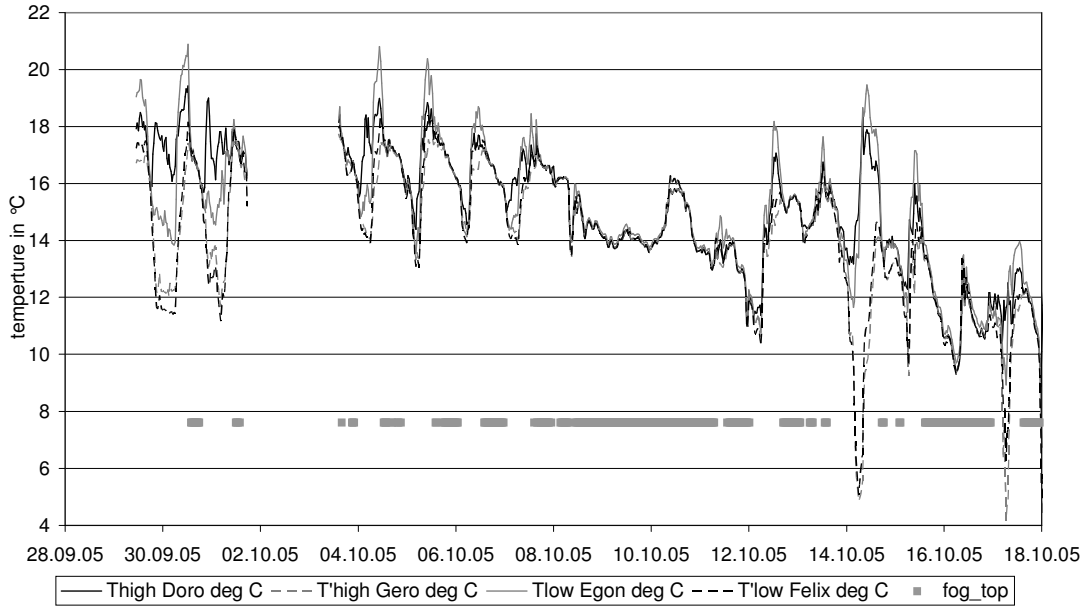

Figure 8: Temperature and fog during the first half of the study.

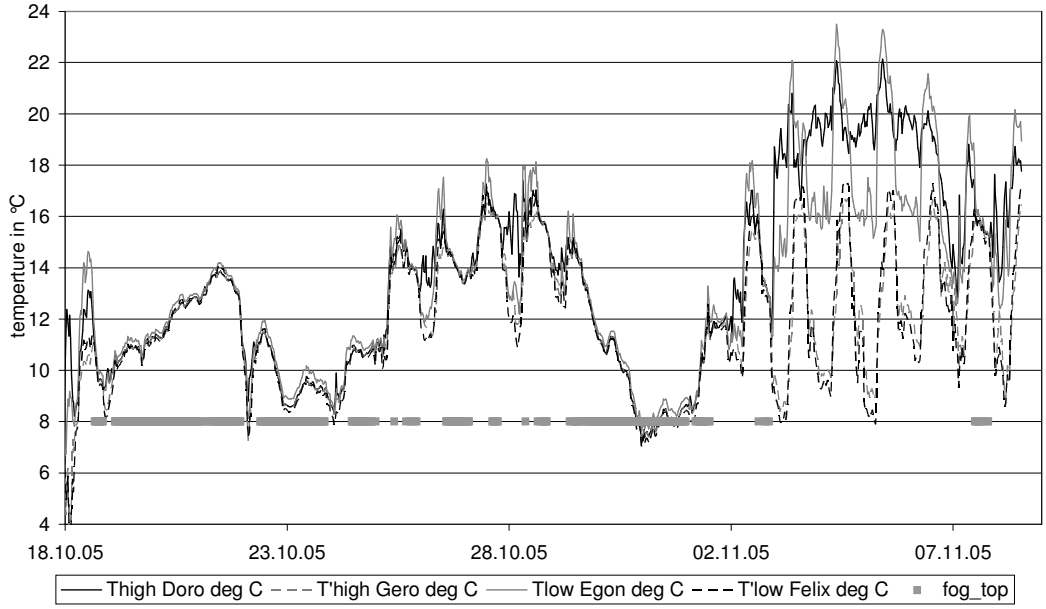

Figure 9: Temperature and fog during the second half of the study.

Figure 8 and Figure 9 display dry and wet temperatures measured during the study. The grey dots in the figures represent fog at the upper level (22.5 m). 42 % of the time conditions were foggy. Fog is defined at visibility below 1000 m (WRZESINSKY & KLEMM, 2000).

During the study period, a typhoon fell on Taiwan (refer to Figure 10) and forced a stop of the measurements for 2 days. For the first week of the study and the week following the typhoon, the weather displayed a rhythmic pattern, with sun and higher temperatures during morning hours and descending temperatures with raising fog in the afternoon, similar to the weather conditions as described in former studies (KLEMM, CHANG & HSIA, 2006). Days with fog and rain followed. From the 19th of October to the 26th it was very rainy and foggy and temperatures reached a minimum.

The last ten days were very sunny with little fog and great temperature differences between night and day and between the dry and the wet sensors (high water vapour pressure differences).

Wind speed was measured on top of the tower (see Section 1.3 Experimental setup). Wind speeds were generally low; the mean of all 10-minute averages was 1.5 m s^{-1}, with a maximum wind speed of 4 m s^{-1}. During the typhoon, the wind speed reached a maximum of 23 m s^{-1}. This data was not used in the study as all other instruments were taken down from the tower for security reasons.

More than one quarter of the wind speed were less than 1 m s^{-1} and could therefore not be used in the Bowen Ratio method, as one could not be certain about turbulent conditions in the atmosphere. More than 50 % of the data had wind speeds between 1 and 2 m s^{-1}. Less than one-fourth of all wind speeds were higher than 2 m s^{-1} (refer to Figure 10).

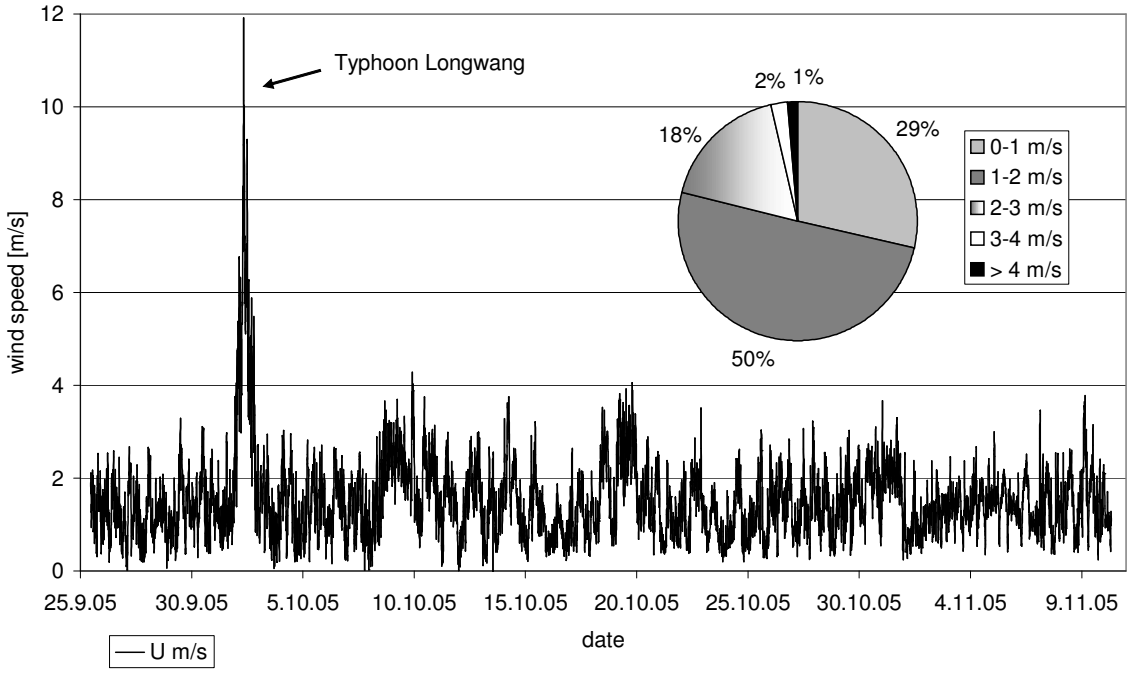

Figure 10: Wind speeds measured at 23.6 m (16.95 m above displacement height)

The results of the wind profile measurement are discussed in Section 3.1.2 Roughness parameter.

The data set showed a pronounced bimodal distribution of the wind directions for the measurement period with the main peak from southeast and a secondary maximum from north/northwest. This behaviour can be explained by the topographic effects at the study site, i.e. the mountain range in westerly and easterly directions have a channelling effect. As described in former studies (KLEMM, CHANG & HSIA, 2006), fog was highly correlated with wind direction. Fog occurred only with southerly or south easterly winds and thus came with valley winds, therefore it has been described as advective and orographic fog, respectively (KLEMM, CHANG & HSIA, 2006).

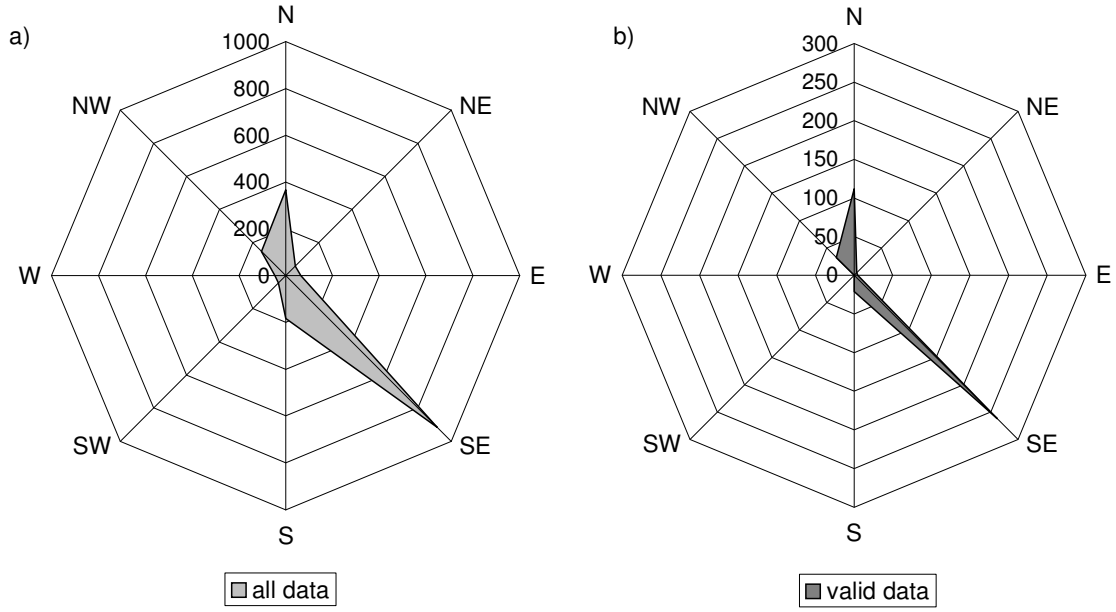

Figure 11: Wind direction a) of all data sets and b) after applying quality criteria (refer to Section 3.2.2)

Figure 11 shows wind direction a) of the whole data set as measured during the study and b) of the data valid after applying quality criteria for Bowen ratio described in chapter 3.2.2. Please note the different scales in the wind roses. The number of valid data points decreased to about 24 % after applying the quality criteria.

The wind directions of the valid data further underline the bimodal distribution and only show south easterly and north/north westerly directions.

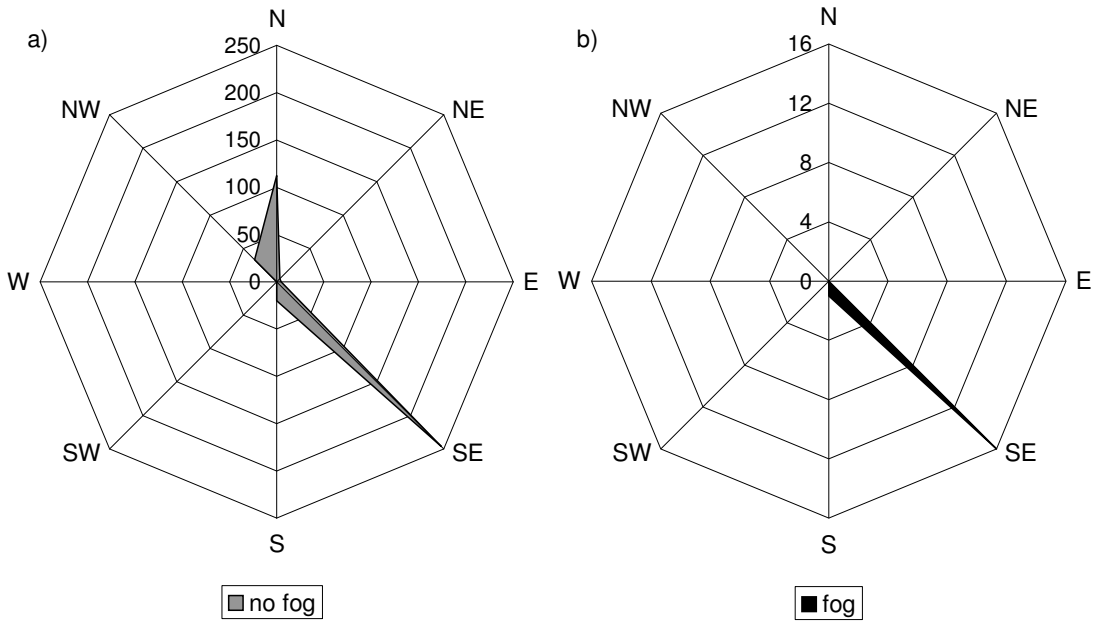

Figure 12: Wind direction of data a) without fog and b) with fog

Figure 12 shows the wind direction distribution of the valid data set a) without fog and b) during foggy conditions. The latter comprises only 4 % of the valid data. The correlation between fog and south easterly winds is clearly shown. Furthermore, it can be observed that in the valid data set, north and north westerly winds dominate at night time and south easterly winds at daytime. Night winds roughly range between 300 ° and 60 °, daytime winds between 100 ° and 200 °. Wind speeds were lower during night time.

During fog net radiation was diminished in general to one third of the value from non foggy conditions (refer to Figure 13).

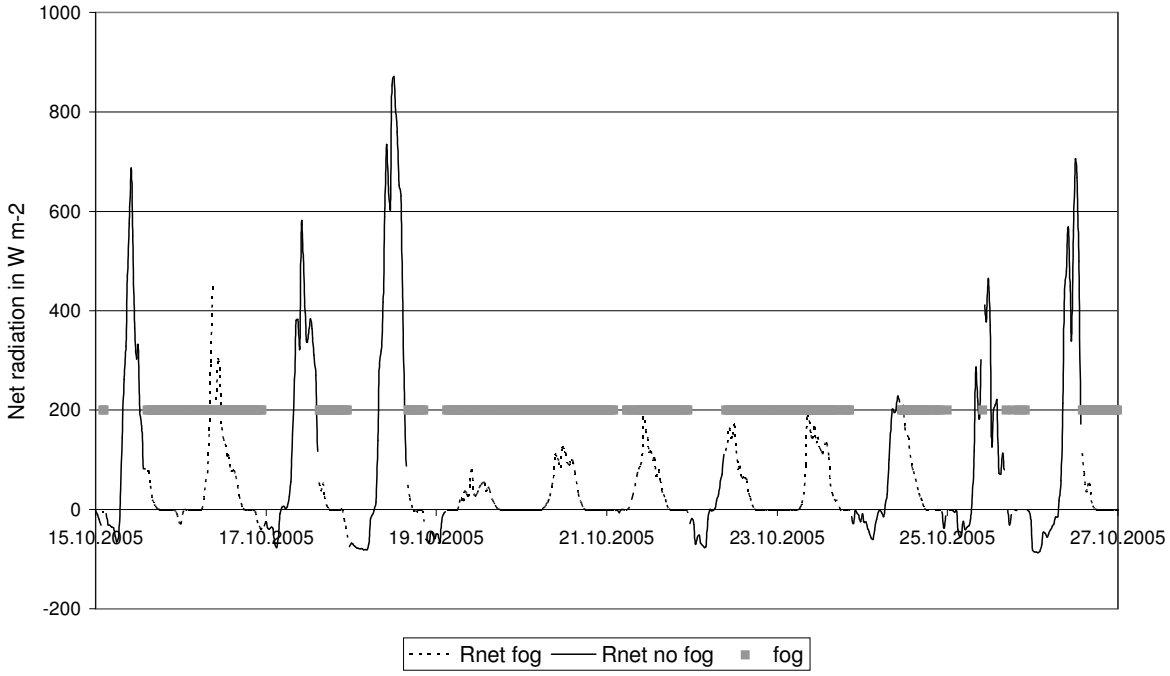

Figure 13: Net radiation during fog and in non foggy conditions

3.1.2 Roughness parameter

While investigating turbulent fluxes, it is essential to know the surfaces roughness of the surface above which the study is conducted.

The roughness is characterized by two parameters, the roughness length and the displacement height, which can be empirically determined from wind-profile observations.

The roughness length is a dimensional constant of integration introduced by the logarithmic velocity profile law (ARYA, 2001):

$$U = \frac{u*}{\kappa} \cdot \ln\left(\frac{z}{z_0}\right) \qquad (15)$$

It varies over five orders of magnitude according to the type of terrain or the average height of the roughness elements.

In practice, z_0 is determined either from the least-square fitting of Equation (15) through the wind-profile data, or by graphically plotting *ln z* versus *U* and extrapolating the best fitted straight line down to the level where $U = 0$; its intercept on the ordinate axis must be $ln\ z_0$ (ARYA, 2001).

On vegetated surfaces the air flow above the top of roughness elements is influenced by the ground surface as well as by the individual roughness elements. Densely vegetated surfaces may thus have a different reference datum than the top of the ground. It should lie somewhere between the actual ground level and the tops of roughness elements.

In practice, the reference datum is determined empirically from wind profile measurements in the surface layer under near neutral stability conditions.

The modified logarithmic wind-profile law used for this purpose is

$$U = \frac{u*}{\kappa} \cdot \ln\left(\frac{z-d}{z_0}\right) \quad \text{(ARYA, 2001)} \tag{16}$$

in which d is called the zero plane displacement or displacement height and z is the height measured above the ground level.

Plotting $ln\ z$ versus U the extrapolated best fitted straight line intercepts the ordinate axis at $ln\ (z_0+d)$. Thus it is not possible to determine the roughness length and the displacement height at the same time with this method.

Generally a value for z_0 is taken from literature and d is calculated. A rough estimation is z_0 = 0.1*canopy height (FOKEN, 2003).

As values for z_0 for forests vary between 1 and 2, the rough estimation mentioned above was used and calculated z_0 = 1.37.

To determine d the wind profile measurement installed at the tower was used. Six cup anemometers were placed at 13.20 m, 14.60 m, 16.60 m, 18.70 m, 20.50 m and 23.30 m. Since the anemometer at 20.5 m showed problems during the study, it was excluded from further calculation.

As the above mentioned logarithmic velocity profile law is only valid in near-neutral stability conditions, only selected data from mid day with high wind speeds were used, as it is more common to find near-neutral stability during daytime and with comparatively high wind speeds.

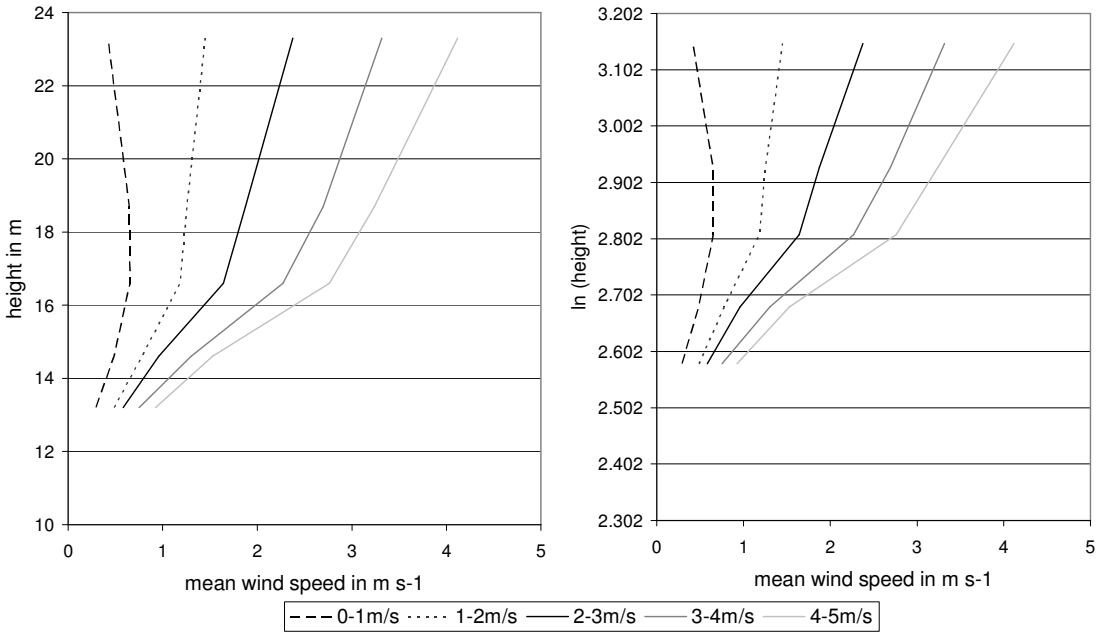

Figure 14: Wind profile wind speeds plotted against height and the natural logarithm of height.

The wind regime of these selected data is characterized through average profiles in Figure 14. On the left hand side the mean wind speed is plotted against the height and on the right hand side it is plotted against the natural logarithm of the height. From 10 minute wind speed profiles at the tower as measured during the study, five average profiles were computed. For the first average profile, all individual profiles with wind speeds between 0 and 1 m s^{-1} at the 23.30 m level were combined. For the average profile number 2, all individual profiles with wind speeds between 1 and 2 m s^{-1} were combined, and so forth.

From these profiles as shown in Figure 14, conclusions can be drawn: Firstly, the wind speed profiles number 2 through 5 (top level wind speeds > 1 m s^{-1}) of the three levels above the tree tops (23.30 m, 18.70 m, and 16.60 m above ground) exhibit log-normal profiles (squared regression coefficients with altitude > 0.99). As for the graphs bend below 16.60 m it is clear that the lower anemometers are within great influence of the canopy layer of the forest. Thus, also the lower psychrometer used in the Bowen Ratio method, which is at 15.05 m, is inside this influence, is inside the roughness sublayer. This collides with the prerequisites of this method and has to be discussed evaluating the results.

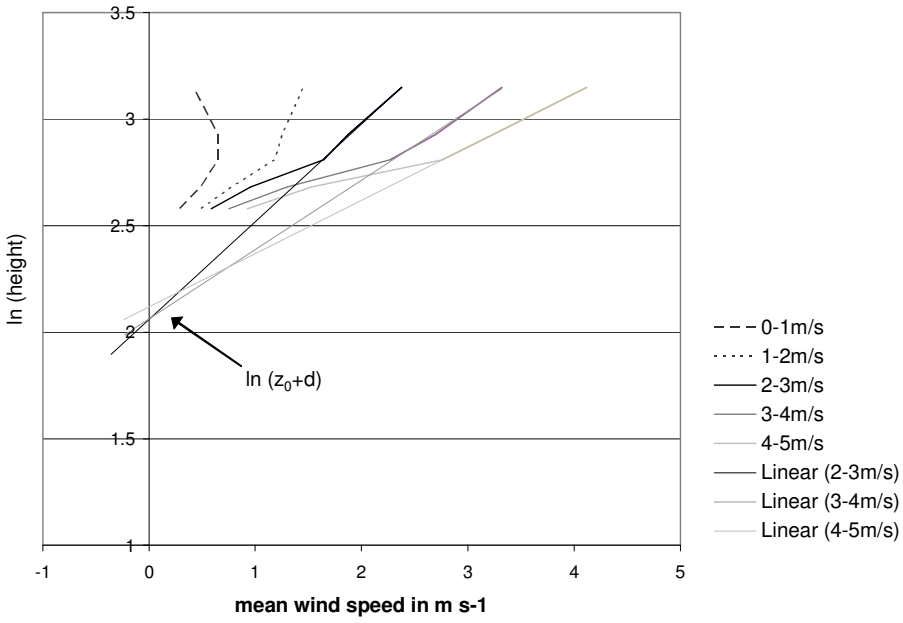

Figure 15: Wind Profile and roughness parameters

The upper three levels with wind speeds greater than 2 m s^{-1} were used to determine d. The zero points of the three profiles are at 7.86 m, 7.87 m and 8.33 m above ground. The average zero displacement height (plus roughness length) of the forest is thus 8.02 m, which is 56 % of the maximum tree height.

The displacement height can thus be calculated to be 6.65 m.

3.1.3 Stability

To describe the influence of thermic layering on turbulent exchange, Monin and Obukhov (1954) introduced the dimensionless scaling parameter *z/L*. The underlying hypothesis is that every parameter determining the properties of the surface layer can be described within this layer through the four terms, height *z*, friction velocity *u**, kinematic heat flux $\overline{w'T'}$ and prompting term *g/T*. As a measure of length for vertical exchange *L*, the Obukhov length, was introduced (FOKEN, 2003).

$$L = -\frac{u^{*3}}{\kappa \frac{g}{T} \frac{Q_H}{\rho \cdot c_p}} \qquad \text{(FOKEN, 2003)} \qquad (17)$$

At values of *z/L* close to zero, the surface layer is neutral, i.e. there is convection forced by turbulence. For negative values of *z/L* the surface layer is unstable. For

values smaller than -1 exchange relies only on thermic conditions. Positive values of *z/L* stand for stable conditions, when vertical exchange is made difficult. For values greater than 1, eddies are no longer dependants on *z* but on *L*, i.e. turbulence dies out.

Thus, the ratio *z/L* is an important parameter measuring the relative importance of buoyancy versus shear effects in the stratified surface layer (ARYA, 2001).

In this study the stability parameter *z/L* was provided by the in-house software "DANA" which interprets the data collected with the ultrasonic anemometer and provides among other data half-hourly values of *z/L*.

This data was classified according to the descriptions above into "unstable", "neutral" and "stable". Figure 16 shows the stability conditions according to two wind sectors; the first one from 67.5 ° to 202.5 °, the second from 247.4 ° to 22.5 °.

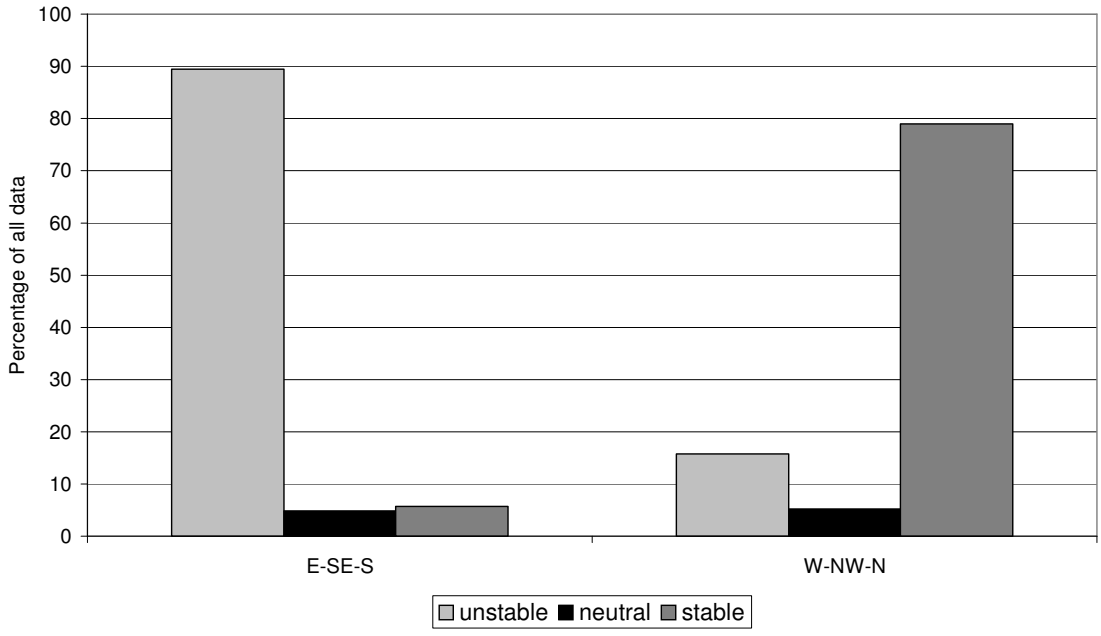

Figure 16: Stability conditions according to wind sectors.

During easterly to southerly winds unstable conditions prevailed while during westerly to northerly winds stable conditions dominated. Neutral conditions occurred when wind direction changed. As north westerly winds occurred mainly during the night, the correlation between stable conditions and north westerly winds can be explained.

Stability and the parameter *z/L* will be important in this study when calculating the source areas for the fluxes (refer to Section 3.8).

3.2 Bowen Ratio

3.2.1 Calibration

A calibration took place prior to the study to choose the best sensors and to check the actual values the sensors show at given temperatures. All sensors, after being named and labelled to separate them clearly, were arranged in a water bath, which was constantly stirred and slowly heated from 0 °C to 34 °C while the temperature was recorded. Differences between the sensors range between 0.28 °C and 0.41 °C depending on the temperature. The sensors were plotted against a calibration standard and a regression was calculated for each sensor. The calibration standard was the mean out of the two new sensors bought in July 2005 that showed the smallest differences in actual temperature value and responding time to changes in temperature.

Four instruments were chosen to use in the study. These were the sensors with the smallest differences in actual value and responding time to changes in temperatures. On the raw data the regression formula drawn from the calibration was used. The four sensors were the ones named ‘Doro’, ‘Gero’, ‘Egon’ and ‘Felix’.

For the application of flux-profile-relationships, the relative precision of the measurements at the different levels (i.e. the precision of the profile difference) is most important, rather than the absolute measurement accuracy (AMMANN, 1998). Thus, another calibration, this time with the whole psychrometers, took place at the study site. To do this the psychrometers were placed on the same level side by side, their sensors facing the same direction. To minimize the differences between the sensors two more regressions, one for the wet temperature and one for the dry temperature, were calculated this time taking one of the sensors as calibration standard.

This inter-calibration was repeated at the end of the measurement period.

Weather conditions, temperatures and temperature changes of the two calibration periods showed great difference. While in the first period, temperatures ranged from 14.3 to 18.7 °C, during the second period between 10 and 19 °C. Mean values differed almost by one degree. During the first period cloudy and foggy conditions predominated, while later sunny and foggy conditions occurred. Wind speeds during the calibration periods were generally low and showed means of 1.4 and 1.47 m s^{-1}.

Data with less than 1 m s^{-1} was excluded from the calculation; furthermore only data with wind directions between 100° and 200° (southeast east to south southwest) was used. This was due to the orientation of the sensors of the psychrometers at the tower and due to quality considerations, which are explained in chapter 3.2.2.

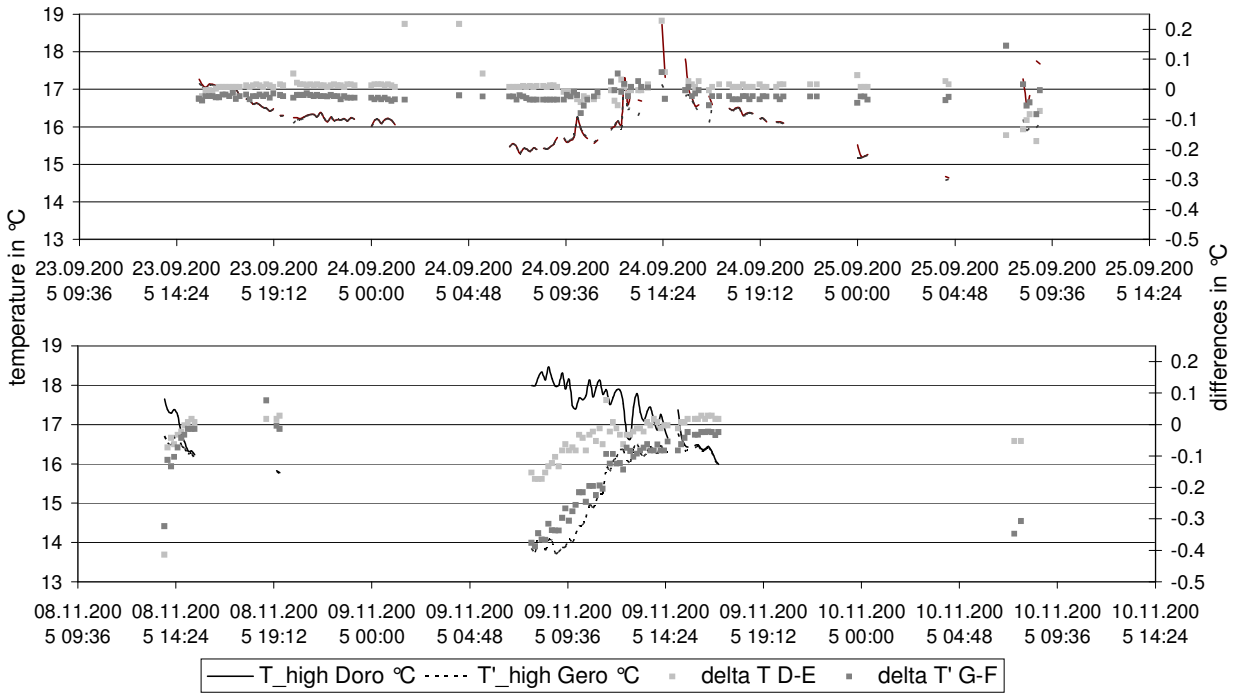

Figure 17: Calibration data with more than 1m s^{-1} wind speed and wind direction between 100° and 200°

Figure 17 shows the first (above) and the second calibration period (below) with their temperatures (left scale) and differences in the wet temperature (right scale), this one being the worse of the two couples concerning the differences between the two periods and the fluctuation around the mean.

Statistical test showed that neither ΔT nor $\Delta T'$ are normal distributed nor have their means a statistical relevant relation (refer to Table 3).

Table 3: Results of the Kolmogorov-Smirnov-test. DE is the difference between the dry, and GF the difference between the wet temperatures, in the first (1) and second (2) calibration period.

		DE1	GF1	DE2	GF2
N		379	379	260	260
Parameter of the normal distribution	Mean	0,019	-0,022	-0,015	-0,137
	Standard deviation	0,053	0,029	0,091	0,117
differences	Total	0,31	0,29	0,23	0,11
	Positive	0,31	0,29	0,21	0,06

Negative	-0,21	-0,22	-0,23	-0,11
Kolmogorov-Smirnov-Z	5,986	5,582	3,710	1,830
Asymptotic Significance (2-sides)	,000	,000	,000	,002

As it was not possible to determine the reason for these unexpected statistical results and differences, it may be assumed they are due to the extremely different weather conditions and temperature intervals which occurred during calibration periods.

To obtain the best results possible for the measurement periods we used all data (the one from the first and the one from the second period) to calculate the calibration factors for the sensors. One sensor of a couple was used as a calibration standard to obtain a regression formula which was later on used as the calibration factor.

In Figure 18 one can see all data of the two dry sensors plotted against each other and the regression calculated.

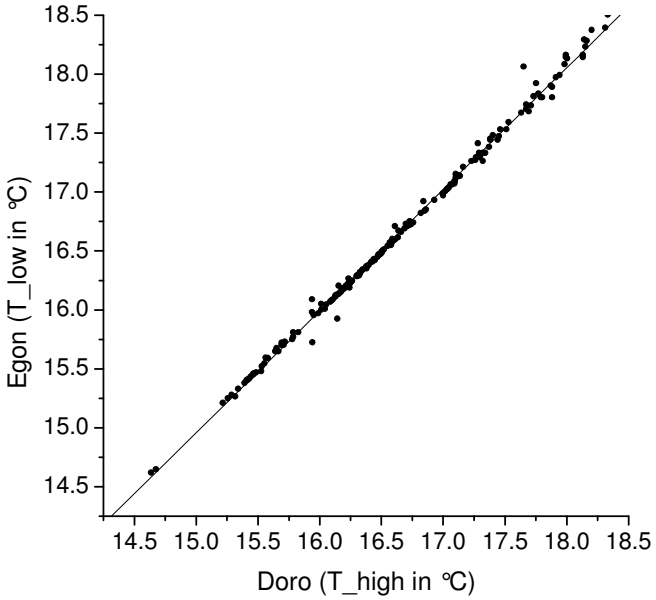

Figure 18: Calibration Plot Doro and Egon

Calibration formulas were:

$$Doro = 1.00199 \cdot rawDoro - 0.014186$$
$$Egon = 0.9703 \cdot rawEgon + 0.32072$$
$$Gero = 1.00065 \cdot rawGero + 0.01258$$
$$Felix = 1.09005 \cdot rawFelix - 1.53139$$

For calculations in the measurement period these regression formulas were combined with the ones from the former calibration and used on the raw data collected by the data logger.

After applying these formulas the standard deviation of the differences between the dry and wet temperatures were 0.22 °C and 0.56 °C. During fog, differences were smaller and standard deviation became 0.075 °C and 0.066 °C.

3.2.2 Data quality for Bowen Ratio Measurement

Data for Bowen Ratio flux calculation were rejected following several quality criteria.

Criterion 1: Ohmura (1982) showed the possibility of obtaining wrong signs for the turbulent fluxes under certain circumstances, when the flux calculation gives a flux direction the same as that of the gradient ("counter gradient flux"). Such a situation is not consistent with the definition of the flux/gradient relationship on which the Bowen Ratio flux calculation method is based and the data fulfilling these situations should be excluded from further calculation.

Following this we excluded data where the inequality $\frac{L_v \cdot \Delta q + c_p \cdot \Delta T}{Rnet - Hsoil} < 0$ was not valid.

After excluding this data, the distribution of values of Bo changes, Bo between 0 and -1.5 are reduced to only a fraction of the former number. The number of all valid data decreases by 35 % (see Figure 19). Data excluded was primarily from late evening and night time, some from early morning and from foggy conditions

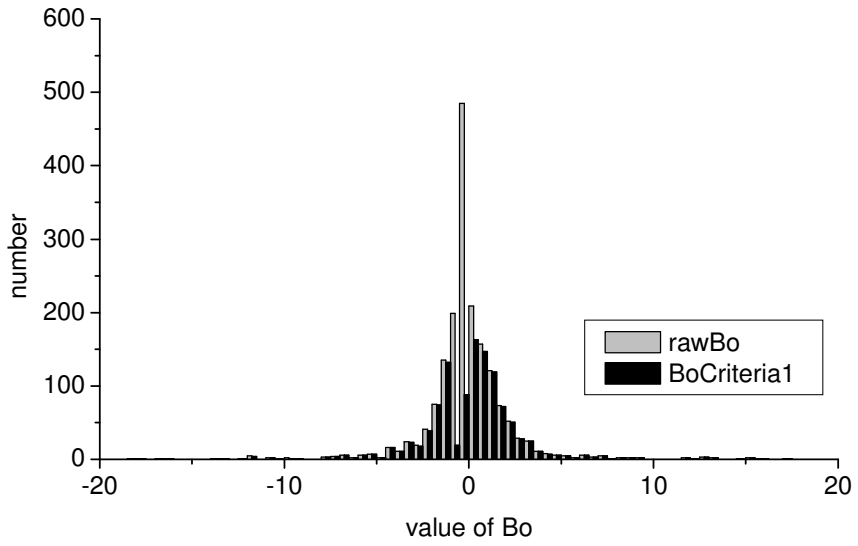

Figure 19: Histogram of Bo before and after applying the first criterion (OHMURA, 1982)

Criterion 2: From the calibration carried out before and after the study it was possible to obtain exact values for the resolution limits of the instrument of the set up used in this study. These were used to introduce criterion for rejecting data. For every value of T_high (Doro) and T'_high (Gero), i.e. the dry and the humid temperature of the upper Psychrometer, the expected value and 95 % confidence interval of that value were computed as if they were showing the same values. In the criterion every value for T_low and T'_low was checked considering its relationship to the 95 % confidence interval. Data inside this interval was rejected, data outside the interval was accepted for being significantly different from T_high and T'_high (see Figure 20). This data was used in further calculations.

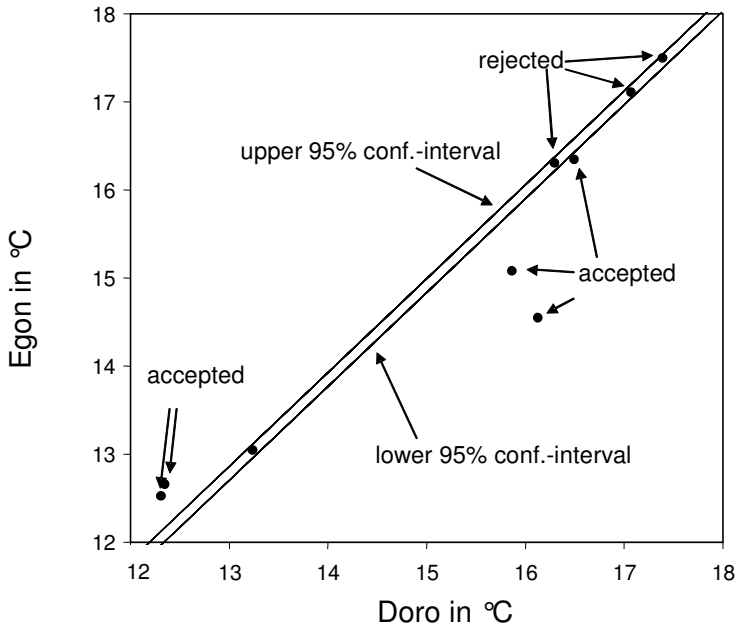

Figure 20: Criterion for data quality considerations (Criterion 2)

Applying this, 1.97 % of all data was excluded for ΔT and 3.18 % for $\Delta T'$. Together they reduce the data set to 95 % of the original size. Most data excluded was obtained during foggy periods.

Criterion 3: To ensure the disposition of a sufficiently developed turbulent measurement regime only data with wind speeds of more than 1 m s-1 was used (FOKEN, 2003). This excluded about 31 % of the data. Low wind speeds occurred mainly during early morning and night time. For further information about the wind regime see Section 3.1.1.

These three criteria reduced the data set to 44 % of its original size. Values of Bo ranged between -218.3 and 405.9, its Median was 0.6. The distribution (without the extreme values) can be seen in Figure 21.

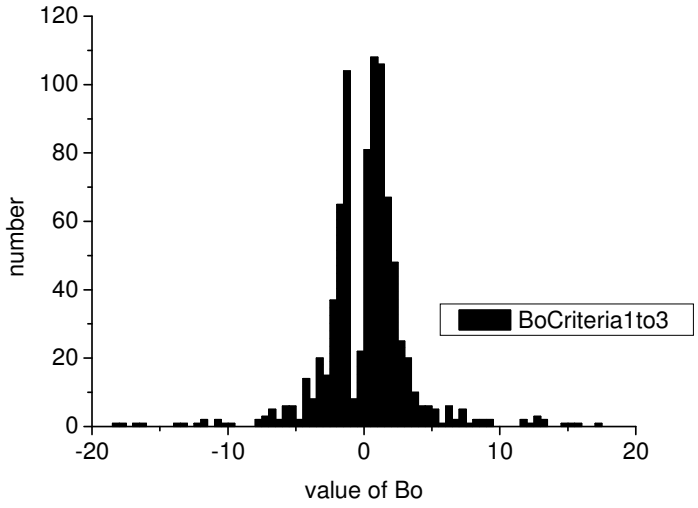

Figure 21: Bo after applying quality criteria 1 to 3

Criterion 4: To apply Bo in the calculation of sensible and latent heat flux and the water vapour flux, further considerations have to be taken into account. Since in the formulas (see equations (3) and (4)) for both latent and sensible heat flux (*1+Bo*) constitutes the denominator, with Bo becoming -1 the resulting fluxes may loose their numerical meaning. Ohmura (1982) introduced criterion for rejecting data were this can occur. Data that satisfied the inequality

$$-\frac{L_v}{c_p}\cdot\Delta q-2\left[\frac{L_v}{c_p}\cdot E(q)+E(T)\right]<\Delta T<-\frac{L_v}{c_p}\cdot\Delta q+2\left[\frac{L_v}{c_p}\cdot E(q)+E(T)\right] \qquad (18)$$

was therefore excluded from the calculation.

The number of data sets decreases to 24 % of the original size. Values close to -1 and some possible outliers with comparatively great values were excluded. Values now range between -212.8 and 405.9; the median is 1.08.

Table 4 shows a summary of the data set size before and after applying the quality criterion described above. Criteria 1 to 3 were first applied on the original data set and later on combined with each other. Criterion 4 was directly applied on the combination of criteria 1 to 3.

Table 4: Overview of the data set size changes with quality criteria

	data set size		name and appearance	
	No.	%		
Original	1826	100	rawBo	Figure 19
After criterion 1	1175	64	BoCriterion1	Figure 19

After criterion 2	1734	95	
After criterion 3	1257	68	
Combination of criteria 1 to 3	798	44	BoCriterion1to3 Figure 21
Combination of criteria 1 to 4	438	24	

3.2.3 Bowen Ratio

The Bowen Ratio was calculated from the data of the two psychrometers as described in Section 2.1.1.

Weather conditions during the campaign were changeable and fog was frequent (refer to Section 3.1.1). During fog, differences in wet and dry temperatures dropped to a minimum. Values of ΔT and Δe during fog ranged between -1.01 and 0.55 °C and -0.83 and 0.59 hPa with a mean of -0.23 °C and 0.11 hPa, respectively. During times of insolation and without fog, temperature differences grew and reached a maximum around midday. During these times ΔT and Δe ranged between -1.95 and 4.98 °C and -4.01 and 1.90 hPa with means of 1.07 °C and -0.26 hPa (see Figure 22).

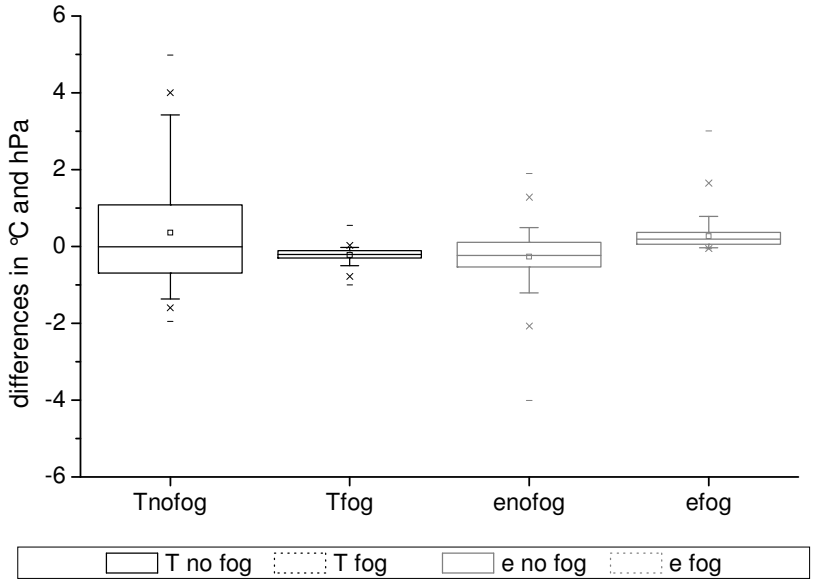

Figure 22: Differences in temperature and water vapour pressure in times with and without fog.

Both, ΔT and Δe values, i.e. the difference between the upper and the lower psychrometer, have negative signs in over half (66 %) of the valid data set. Negative signs stand for higher temperatures and higher water vapour pressures at the lower psychrometer and thus positive fluxes of sensible and latent heat. In one fifth of the data sets valid for calculation, ΔT and Δe have different signs and thus lead to a

negative Bowen Ratio. A negative Bowen Ratio further means that latent and sensible heat fluxes divert into different directions. These negative Bowen Ratios are mainly due to positive ΔT- and negative Δe-values, i.e. there is upward latent heat flux and downward sensible heat flux. With both ΔT and Δe values positive, the Bowen Ratio is positive and fluxes of sensible and latent heat are negative, i.e. downwards.

Statistical parameters of the Bowen Ratio differ after applying the quality criterion (refer to Table 5).

Table 5: Statistical parameter of Bo

	median	25 Quartile	75 Quartile	Min	Max	No. of data sets
Bo 1 to 3	0.74	-1.7	1.6	-201	437	789
Bo 1 to 4	1.06	0.5	1.6	-54	240	438

After applying criteria 1 to 3 it ranges between -201 and 437, with a median of 0.74 and the 25 % and 75 % Quartile being -1.7 and 1.6. After including the fourth criterion that excludes Bowen Ratios close to -1 for calculation reasons, the data set shrinks to almost half its size, the new median being 1.06. Under the assumption that the Bowen Ratio ranges around the median within the 25 % and the 75 % quartile ($0.5 \leq Bo \leq 1.6$) fluxes generally have the same direction and are more or less of the same size. A Bowen Ratio of 0.5 standing for a latent heat flux that is double the size of the sensible heat flux and so forth (refer to Equation (3)).

Other studies above forests report of Bowen Ratio between 1 and 4 on fine days (MONTEITH & UNSWORTH, 1990), 0.8 to 2 for tall coniferous forests (BERNHOFER, 1992), 0.5 over forests (STULL, 1988), and Oke (1987) reports of Bowen Ratio between 0.4 to 0.8 for temperate forests.

3.2.4 Water vapour fluxes

After excluding the data that does not fulfil the quality criteria described in the previous chapter, the remaining data is mainly from non foggy conditions and from morning to noon hours and late night hours (refer to Figure 23). Only 4 % of the data is from times with fog.

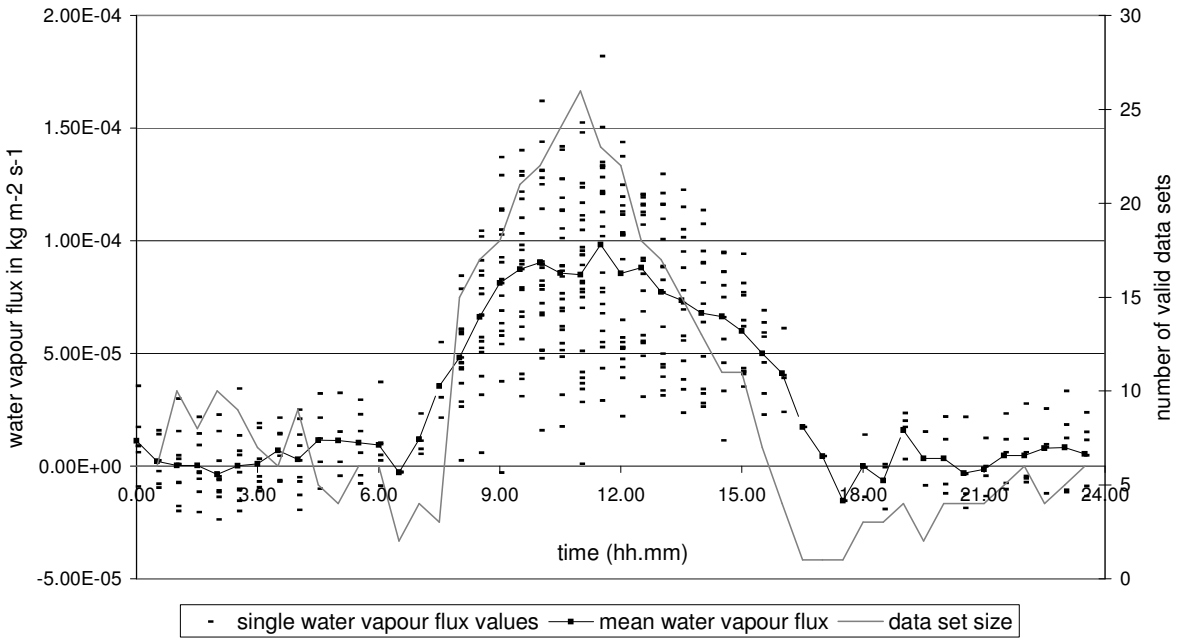

Figure 23: Mean water vapour fluxes determined with the Bowen Ratio method. The black line gives an overall mean per hour, the black dots are single measured values, and the grey line shows the number of data sets available at that time.

Water vapour fluxes determined with the Bowen Ratio method ranged between $-2.37 \cdot 10^{-6}$ and $1.82 \cdot 10^{-4}$ kg m^{-2} s^{-1}; their mean was $5.34 \cdot 10^{-5}$; their median $5.22 \cdot 10^{-5}$ kg m^{-2} s^{-1}. Values for sensible and latent heat flux and water vapour fluxes differed for different wind directions (cf. Figure 24 a)). Water vapour fluxes were much smaller for north and north-westerly winds, e.g. the mean of water vapour flux at south easterly winds was twenty times higher than the mean of water vapour flux at north to north westerly winds (cf. Figure 24 b)).

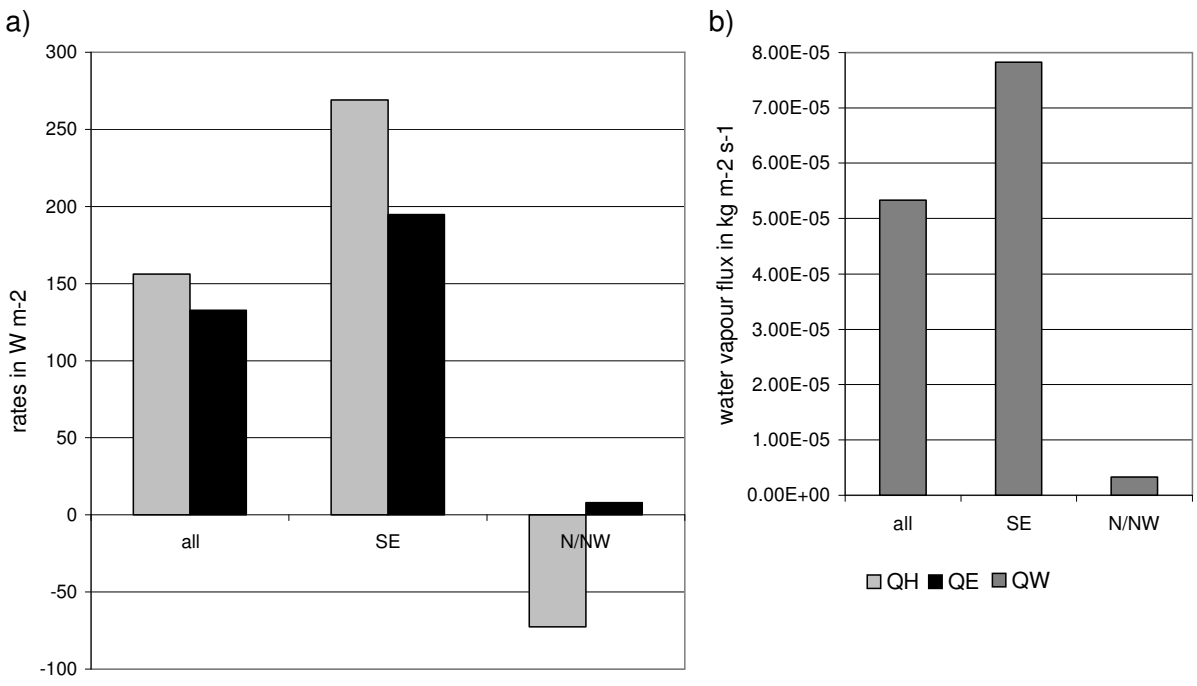

Figure 24: Differences in measured values depending on the wind direction for a) sensible and latent heat flux (Q_H and Q_E) and b) the water vapour flux (Q_W).

Northerly and north westerly winds occurred mainly at night, while south easterly winds prevailed at day time. The Bowen Ratio partitioned the available energy into sensible and latent heat flux (Q_H and Q_E) differently throughout the day (see Figure 25).

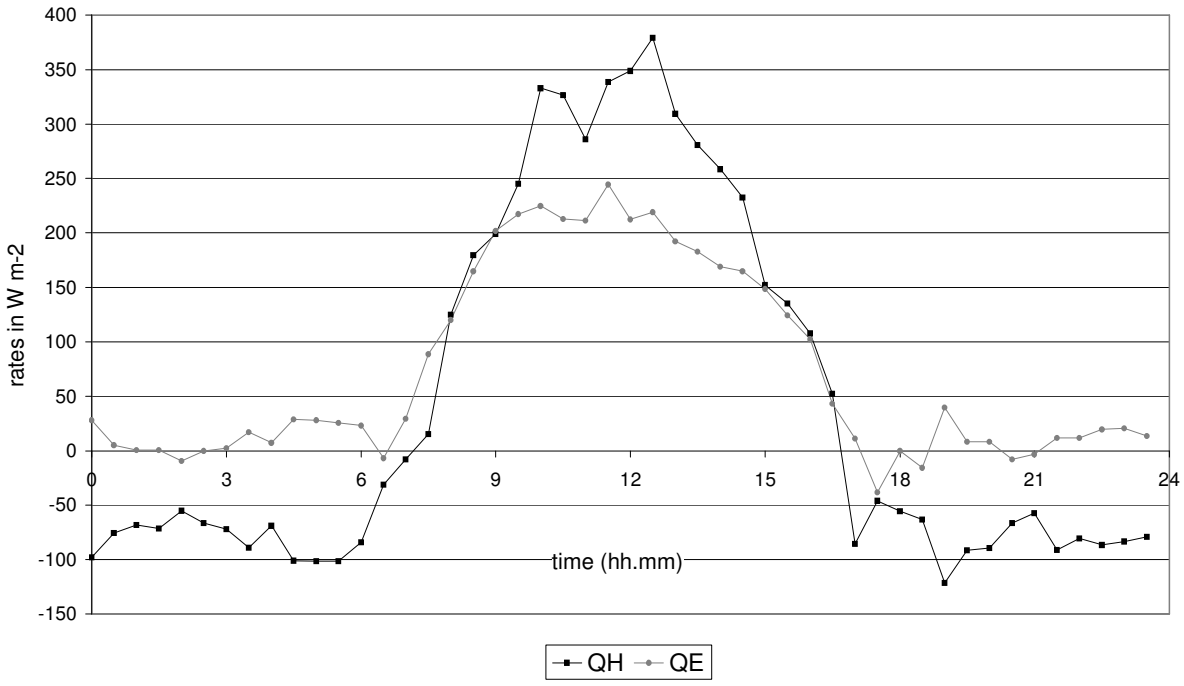

Figure 25: Means of sensible (Q_H) and latent (Q_E) heat flux per hour of a day.

Since night time fluxes are smaller because of lesser energy due to missing insolation, the small size of the fluxes at northerly and north westerly winds can easily be explained.

In Table 6 maxima, minima, mean values and medians are listed for northerly to north westerly winds, south easterly winds and both wind directions.

Table 6: Fluxes determined by the Bowen Ratio method separated for different wind directions

		SE	N/NW	Both Wind directions
Q_H in Wm^{-2}	Max	771.29	$4.30 \cdot 10^{-3}$	771.29
	Min	20.95	-171.21	-171.21
	Median	258.34	-77.21	165.59
	Mean	269.15	-72.74	156.05
Q_E in Wm^{-2}	Max	454.12	136.77	454.12
	Min	-7.42	-59.58	-59.58
	Median	194.23	5.70	130.02
	Mean	194.67	8.12	132.76
Q_W in $kgm^{-2}s^{-1}$	Max	$1.82 \cdot 10^{-4}$	$5.49 \cdot 10^{-5}$	$1.82 \cdot 10^{-4}$
	Min	$-2.95 \cdot 10^{-6}$	$-2.37 \cdot 10^{-5}$	$-2.37 \cdot 10^{-5}$
	Median	$7.80 \cdot 10^{-5}$	$2.27 \cdot 10^{-6}$	$5.22 \cdot 10^{-5}$
	mean	$7.83 \cdot 10^{-5}$	$3.29 \cdot 10^{-6}$	$5.34 \cdot 10^{-5}$

The fluxes during foggy conditions ranged between the measured fluxes for south easterly wind directions. Fluxes during fog are discussed in detail in chapter 3.7 Monte Carlo Results.

The results given by this method are compared to the eddy covariance method and to the methods of Penman and Penman Monteith in chapter 3.6.

3.3 Eddy Covariance

3.3.1 Data quality for eddy covariance measurement

To assure data quality the above mentioned prerequisites (refer to Section 2.1.2 Eddy Covariance), stationary of the observed time series (30 min), horizontal homogeneity, and a well developed turbulence regime due to stability of atmospheric stability structure, were tested. To test stationary for each 30-minute

interval, the variance $w'x'_{30}$ min was computed and compared with the variance of the six 5-minutes intervals $w'x'_5$ min of the same time period. With a deviation of less than 30 %, the averaging interval is assumed to be stationary. In former studies it has been pointed out that spatial homogeneity of the surface is given due to an area of 300 hectares cypress plantation with a uniform vegetation canopy (HSIA ET AL., 2004). The data file was provided by E. Beiderwieden from the University of Muenster.

3.3.2 Eddy covariance water vapour fluxes

During the study period heavy rain and fog lead to difficulties with the sonic anemometer. After control of data quality this data was excluded from further analysis.

Overall during the time studied here (29th September 2005 11:00 until 8th October 2005 13:00), 817 half hour data was available. Fluxes ranged between $-6.0 \cdot 10^{-5}$ and $3.3 \cdot 10^{-4}$ kg m^{-2} s^{-1} with a mean of $2.2 \cdot 10^{-5}$ and a median of $6.5 \cdot 10^{-6}$ kg $m^{-2}s^{-1}$.

Values of the water vapour flux differed in times with and without fog and with winds from different wind directions (refer to Table 7).

Table 7: Water vapour fluxes determined with the eddy covariance method, separated for fog and clear times and for wind directions

	All data	during fog	without fog	south easterly winds	northerly and north westerly winds
Number	817	104	713	382	382
Max*	$3.3 \cdot 10^{-4}$	$8.3 \cdot 10^{-5}$	$3.3 \cdot 10^{-4}$	$3.3 \cdot 10^{-4}$	$1.6 \cdot 10^{-4}$
Min*	$-6.1 \cdot 10^{-5}$	$-6.1 \cdot 10^{-5}$	$-3.6 \cdot 10^{-5}$	$-6.1 \cdot 10^{-5}$	$-3.6 \cdot 10^{-5}$
Mean*	$2.2 \cdot 10^{-5}$	$1.3 \cdot 10^{-5}$	$2.3 \cdot 10^{-5}$	$4.3 \cdot 10^{-5}$	$1.8 \cdot 10^{-6}$
Median*	$6.5 \cdot 10^{-6}$	$7.9 \cdot 10^{-6}$	$5.8 \cdot 10^{-6}$	$3.4 \cdot 10^{-5}$	$4.2 \cdot 10^{-7}$
* in kg m^{-2} s^{-1}					

During fog (12 % of the data set) the mean water vapour flux shrank to about 59 % of the mean flux in times without fog. Like the Bowen Ratio fluxes, the eddy covariance water vapour fluxes differed with wind direction (refer to Figure 26).

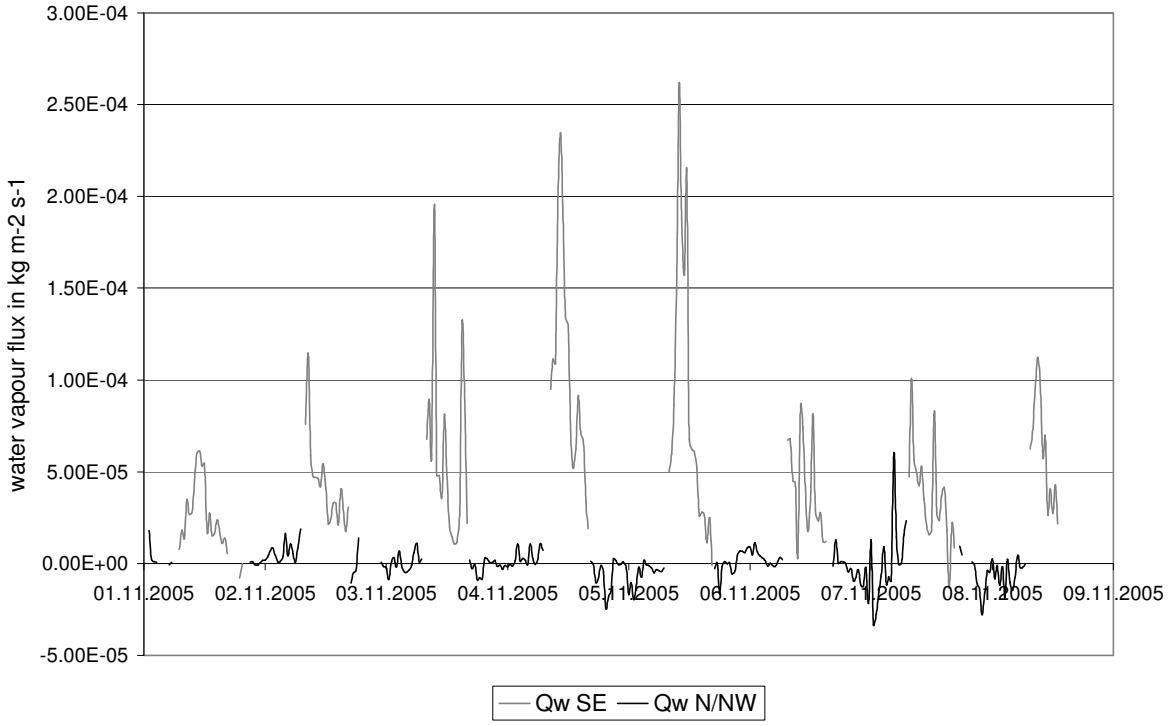

Figure 26: Part of the water vapour fluxes separated for wind directions.

Fluxes were almost twice as large with south easterly wind directions than with north and north westerly wind directions. Like with the Bowen Ratio fluxes this can be explained by reference to the time of day when north and north westerly winds occur.

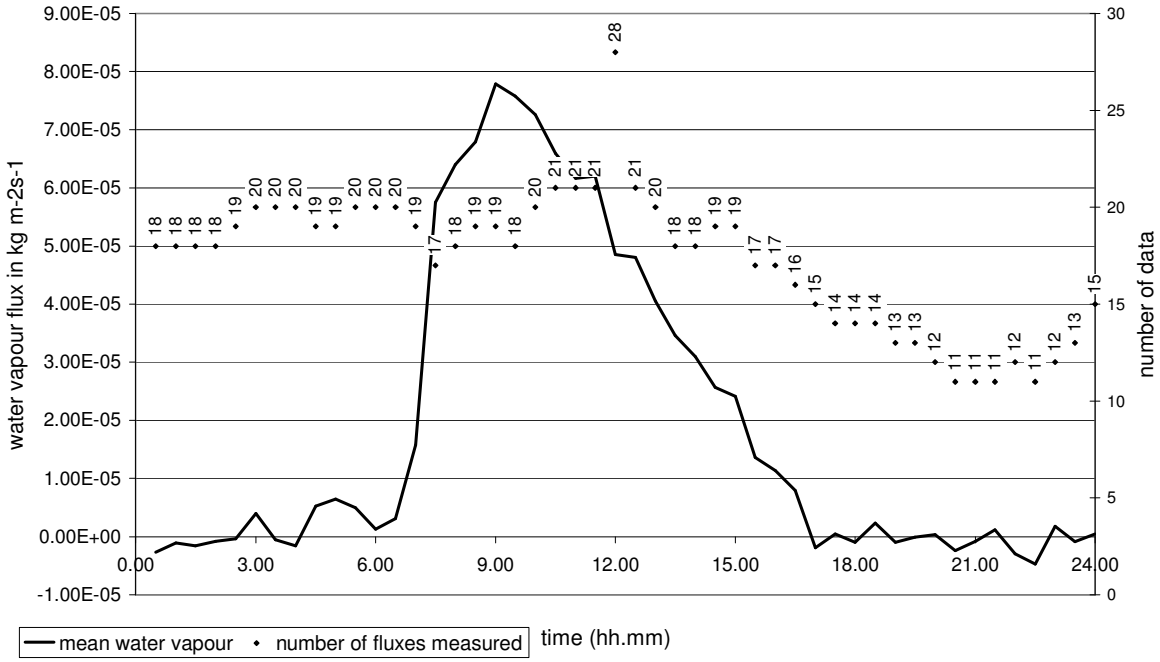

Figure 27: Mean water vapour flux at a day.

Figure 27 shows the mean water vapour flux for the time of day. During the study time, fluxes were largest around 9 and 12 o'clock, rapidly growing between 6:30 h and 8:00 h and slowly decreasing in the afternoon. The diminishing size of the water vapour flux values in the afternoon could be correlated with the fog that typically arrived at the study site during those hours which led to lessening net radiation.

Furthermore, in Figure 27, as indicated on the right hand side, the numbers of data sets available at that hour of the day are shown. This demonstrates the effect of the quality criteria applied on the data. Most data available is from noon; very little night time data is valid. During night time prerequisites like steady state conditions of the observed time series and well developed turbulence regime were more likely to be violated than during day time (ARYA, 2001), which explains the comparatively small size of the valid data sets during night time.

3.4 Penman fluxes

Penman data is available for the whole study period, except during the typhoon and one morning, when the system was switched off for 5 hours.

As described in chapter 2.1.3 Penman approach, Penman's formula calculates the potential evaporation for a specific time under given circumstances. This potential evaporation can further be divided into the energy part and the ventilation part, i.e. the part of the potential evaporation which is provided by net radiation and soil heat flux and the part where energy necessary to vaporize water is provided by the wind speed and the water vapour pressure saturation deficit.

Potential evaporation rates ranged between $-4.8 \cdot 10^{-6}$ and $7.9 \cdot 10^{-5}$ with a mean of $8.5 \cdot 10^{-6}$ and a median of $1.3 \cdot 10^{-6}$ kg m^{-2} s^{-1}. Table 8 gives an overview of calculated rates for the energy and the ventilation part and on the potential evaporation during the whole study time, in times with and without fog and for the two main wind directions.

Table 8: Potential evaporation rates, energy, and ventilation parts for different situations determined with the Penman formula

		N	Maximum*	Minimum*	Mean*	Median*
TOTAL	Energy part	1826	$6.7 \cdot 10^{-5}$	$-7.2 \cdot 10^{-6}$	$6.1 \cdot 10^{-6}$	$3.4 \cdot 10^{-7}$
	Ventilation part		$2.2 \cdot 10^{-5}$	$-9.2 \cdot 10^{-8}$	$2.4 \cdot 10^{-6}$	$2.0 \cdot 10^{-7}$
	Pot. evaporation		$7.5 \cdot 10^{-5}$	$-4.8 \cdot 10^{-6}$	$8.5 \cdot 10^{-6}$	$1.3 \cdot 10^{-6}$

NO FOG	Energy part	1054	$6.7 \cdot 10^{-5}$	$-7.2 \cdot 10^{-6}$	$8.9 \cdot 10^{-6}$	$-4.4 \cdot 10^{-8}$
	Ventilation part		$2.2 \cdot 10^{-5}$	$-6.1 \cdot 10^{-8}$	$4.1 \cdot 10^{-6}$	$2.2 \cdot 10^{-6}$
	Pot. Evaporation		$7.5 \cdot 10^{-5}$	$-4.8 \cdot 10^{-6}$	$1.3 \cdot 10^{-5}$	$3.9 \cdot 10^{-6}$
FOG	Energy part	772	$2.8 \cdot 10^{-5}$	$-2.5 \cdot 10^{-6}$	$2.4 \cdot 10^{-6}$	$4.3 \cdot 10^{-7}$
	Ventilation part		$1.1 \cdot 10^{-6}$	$-9.2 \cdot 10^{-8}$	$4.1 \cdot 10^{-8}$	$2.9 \cdot 10^{-8}$
	Pot. Evaporation		$2.8 \cdot 10^{-5}$	$-1.9 \cdot 10^{-6}$	$2.4 \cdot 10^{-6}$	$4.7 \cdot 10^{-7}$
SE	Energy part	1115	$6.7 \cdot 10^{-5}$	$-5.6 \cdot 10^{-6}$	$1.1 \cdot 10^{-5}$	$3.1 \cdot 10^{-6}$
	Ventilation part		$2.1 \cdot 10^{-5}$	$-9.2 \cdot 10^{-8}$	$1.3 \cdot 10^{-6}$	$4.0 \cdot 10^{-8}$
	Pot. Evaporation		$7.5 \cdot 10^{-5}$	$-1.6 \cdot 10^{-6}$	$1.3 \cdot 10^{-5}$	$3.2 \cdot 10^{-6}$
N/NW	Energy part	537	$2.0 \cdot 10^{-5}$	$-7.2 \cdot 10^{-6}$	$-3.4 \cdot 10^{-6}$	$-4.1 \cdot 10^{-6}$
	Ventilation part		$2.2 \cdot 10^{-5}$	$1.2 \cdot 10^{-8}$	$5.2 \cdot 10^{-6}$	$3.3 \cdot 10^{-6}$
	Pot. Evaporation		$3.9 \cdot 10^{-5}$	$-4.8 \cdot 10^{-6}$	$1.8 \cdot 10^{-6}$	$1.7 \cdot 10^{-7}$
* values in kg m^{-2} s^{-1}						

During fog, the mean potential evaporation rate diminished to roughly one fifth of the evaporation rate without fog. Further, the partition of energy and ventilation part is different during times with and without fog (refer to Figure 28).

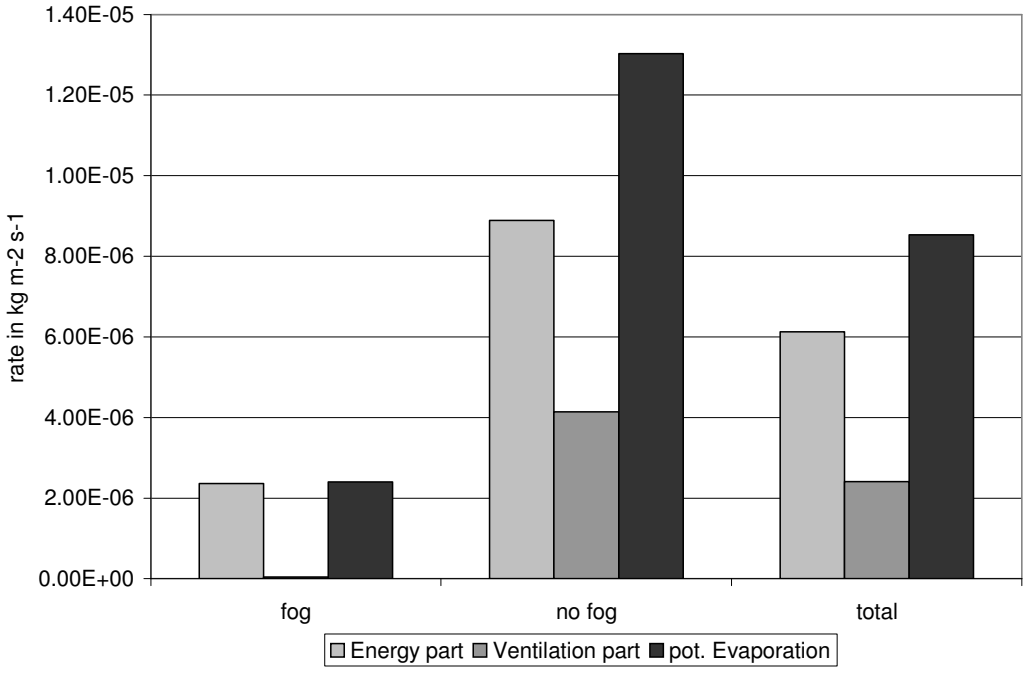

Figure 28: Potential evaporation rates calculated with the penman approach separated for times with and without fog.

During fog, the ventilation part decreases to a minimum; all the potential evaporation is due to the energy part. The water vapour pressure saturation deficit is part of the ventilation term of the Penman approach. This saturation deficit shrinks during fog due to high relative humidity.

Furthermore, evaporation rates vary with different wind directions (see Figure 29).

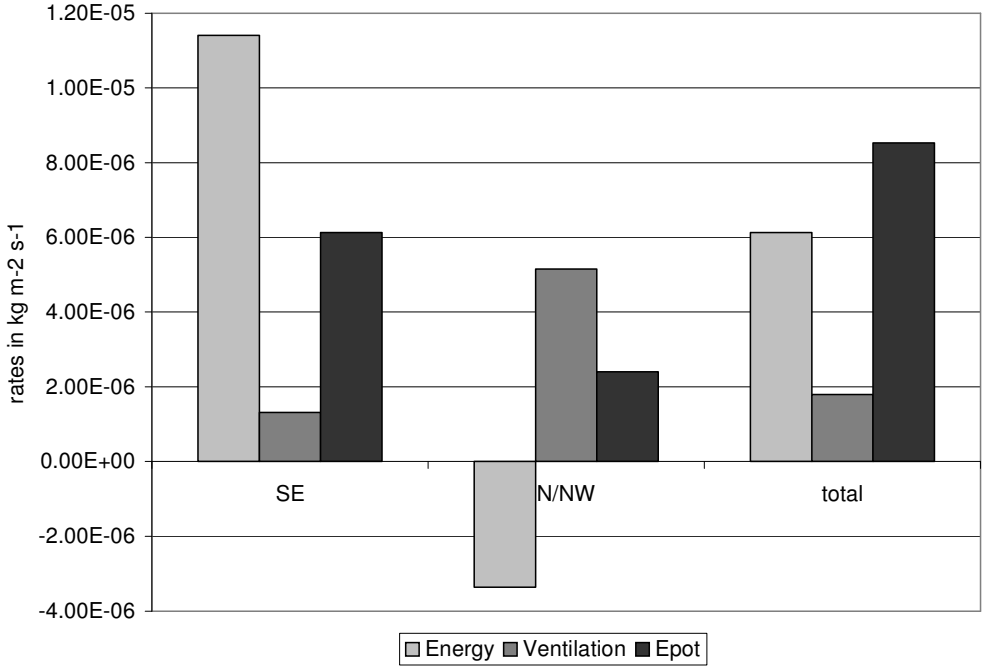

Figure 29: Potential evaporation separated for different wind directions

Figure 29 displays the different distributions of the two main wind directions of this study. The properties of air masses of these wind directions are reflected in the distribution of the potential evaporation rate into energy and ventilation part. During south easterly winds the energy part of the Penman formula clearly dominates. This is suggested to be due to the time of the day during which these winds occurred, i.e. mainly daytime hours. Thus, energy to evaporate water was available and the energy part was large. The ventilation part is small due to small water vapour pressure saturation deficit in the humid air masses rather than great wind speed differences.

North and north westerly winds occurred mainly during night time. The missing solar radiation explains the negative sign of the energy part of the penman formula. Descending from the mountains, the air masses coming from north and north westerly directions show a great water vapour pressure saturation deficit, thus they can take up water vapour and produce evaporation.

Figure 30 gives an impression on the potential evaporation rates per hour of a day. For this graph all data was used and an arithmetic mean was calculated.

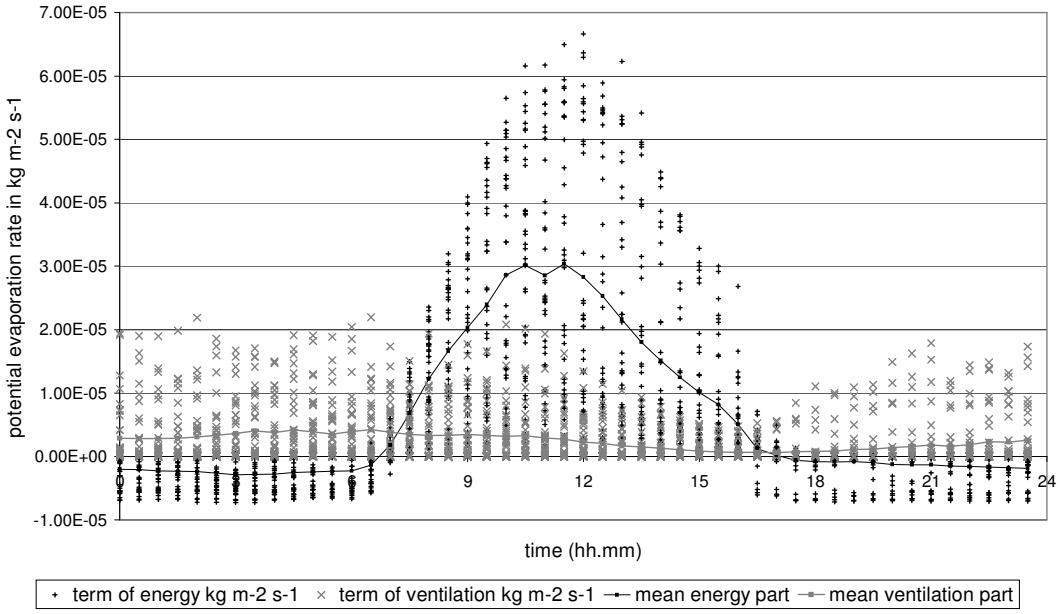

Figure 30: Potential evaporation rates of a day separated for the energy and the ventilation part of Penman's formula.

The great influence of the ventilation part on daytime evaporation rates is clearly demonstrated with the large peak at daytime. Furthermore, the small but very balanced size of the energy part is shown. The potential evaporation rates calculated with the Penman formula (refer to equation (10)) will be compared to the actual evaporation rates determined by the other methods in chapter 3.6.2.

3.5 Penman Monteith fluxes

As pointed out in 2.1.4, the Penman Monteith method is based on the Penman formula and develops it further in order to allow an estimation of the actual evaporation including the considerations of vegetated surface and its resistance against evaporation, mainly due to the plants' resistance against water loss.

Fluxes calculated by this method are generally smaller than those calculated by Penman's formula. Figure 31 gives an overview on evaporation rates on a average day. For this graph all data were used and an arithmetic mean was calculated.

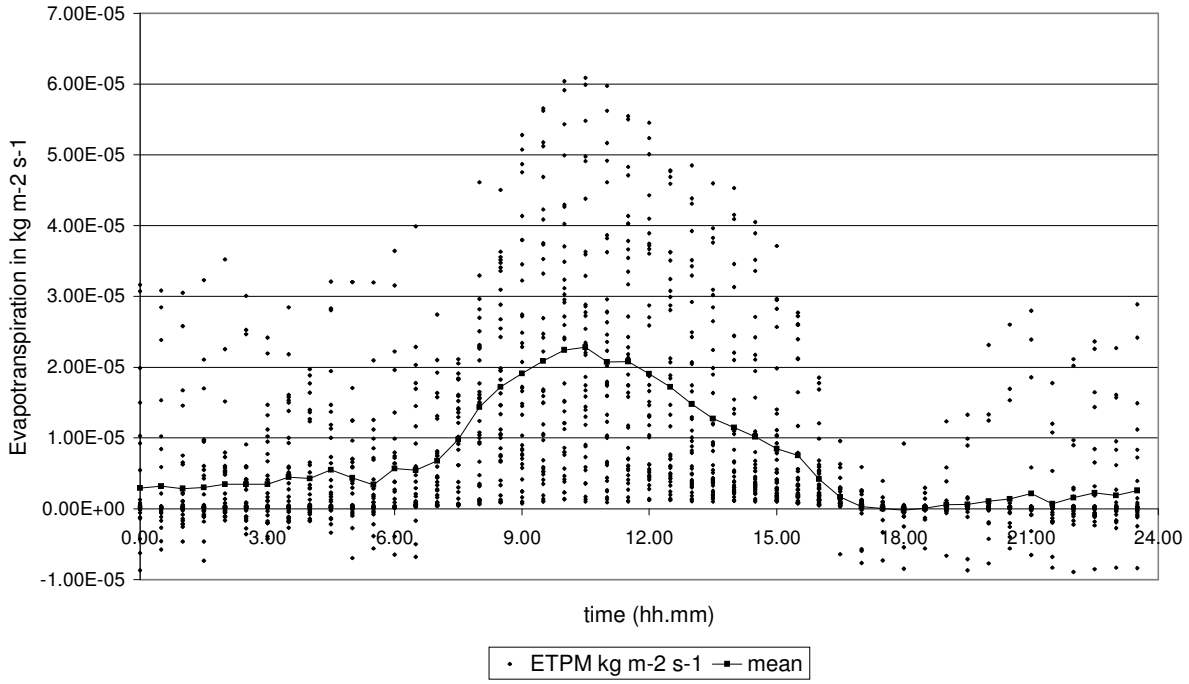

Figure 31: Mean evaporation rates for a day calculated with the Penman Monteith method

Evaporation comes to a minimum at sunset; its maximum is shortly before noon. Overall evaporation ranges between $-8.9 \cdot 10^{-6}$ and $6.1 \cdot 10^{-5}$ kg m^{-2} s^{-1}; its mean is $7.5 \cdot 10^{-6}$ kg m^{-2} s^{-1} and the median is $1.7 \cdot 10^{-6}$ kg m^{-2} s^{-1}.

Further, the evaporation calculated by the Penman Monteith method differs during times with and without fog and between the two main wind directions (refer to Figure 32).

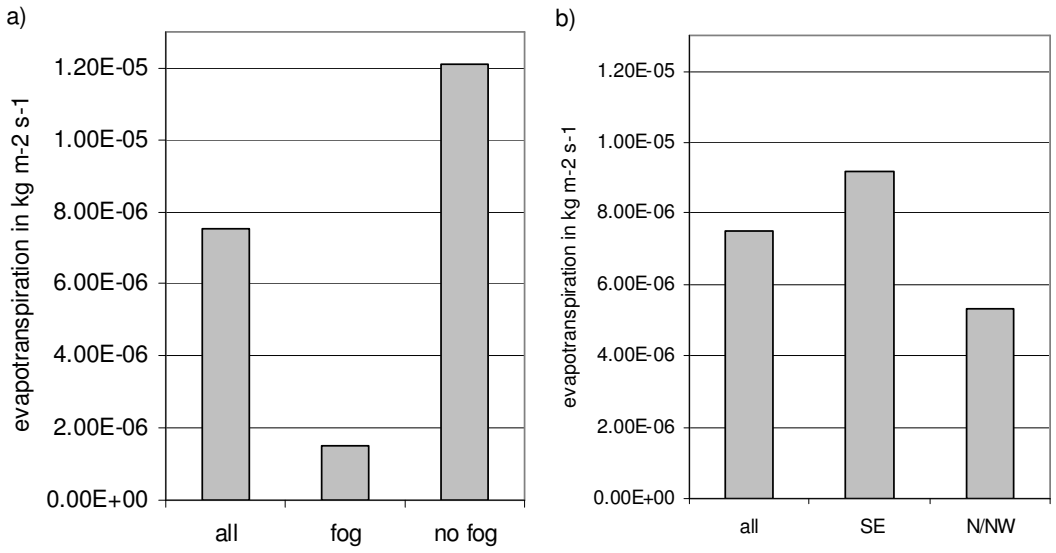

Figure 32: Differences in evaporation rates determined with the Penman Monteith method for a) times with and without fog and b) the two main wind directions, each time in comparison with the whole data set's mean.

Fog occurred during 40 % of the study time; during fog, mean evaporation was reduced to one fifth of the original mean. With northerly and north westerly wind, evaporation was smaller than with south easterly winds, although the difference was not as large as the differences observed in the fluxes calculated with the other methods. Evaporation rates calculated with this method are listed in Table 9.

Table 9: Evaporation rates determined with the Penman Monteith method (all data, data in times with and without fog (No fog, Fog), data with south easterly winds (SE) and data with northerly and north westerly winds (N/NW)).

	N	Maximum*	Minimum*	Mean*	Median*
All data	1714	$6.1 \cdot 10^{-5}$	$-8.9 \cdot 10^{-6}$	$7.5 \cdot 10^{-6}$	$1.7 \cdot 10^{-6}$
No fog	975	$6.1 \cdot 10^{-5}$	$-8.9 \cdot 10^{-6}$	$1.2 \cdot 10^{-5}$	$7.6 \cdot 10^{-6}$
Fog	739	$2.1 \cdot 10^{-5}$	$-1.8 \cdot 10^{-6}$	$1.5 \cdot 10^{-6}$	$3.5 \cdot 10^{-7}$
SE	1084	$6.1 \cdot 10^{-5}$	$-1.0 \cdot 10^{-6}$	$9.2 \cdot 10^{-6}$	$2.2 \cdot 10^{-6}$
N/NW	489	$4.6 \cdot 10^{-5}$	$-8.9 \cdot 10^{-6}$	$5.3 \cdot 10^{-6}$	$1.9 \cdot 10^{-6}$
*values in kg m^{-2} s^{-1}					

3.6 Comparison

3.6.1 Bowen Ratio and Eddy Covariance

Bowen Ratio and Eddy Covariance data could be compared at half hour level, due to the high time scale resolution of both systems.

A number of observations are possible once the results of the Bowen Ratio and the eddy covariance methods are plotted against time. For example, peaks of Bowen measurements are broader with a lower maximum and they show less fluctuation (refer to Figure 33).

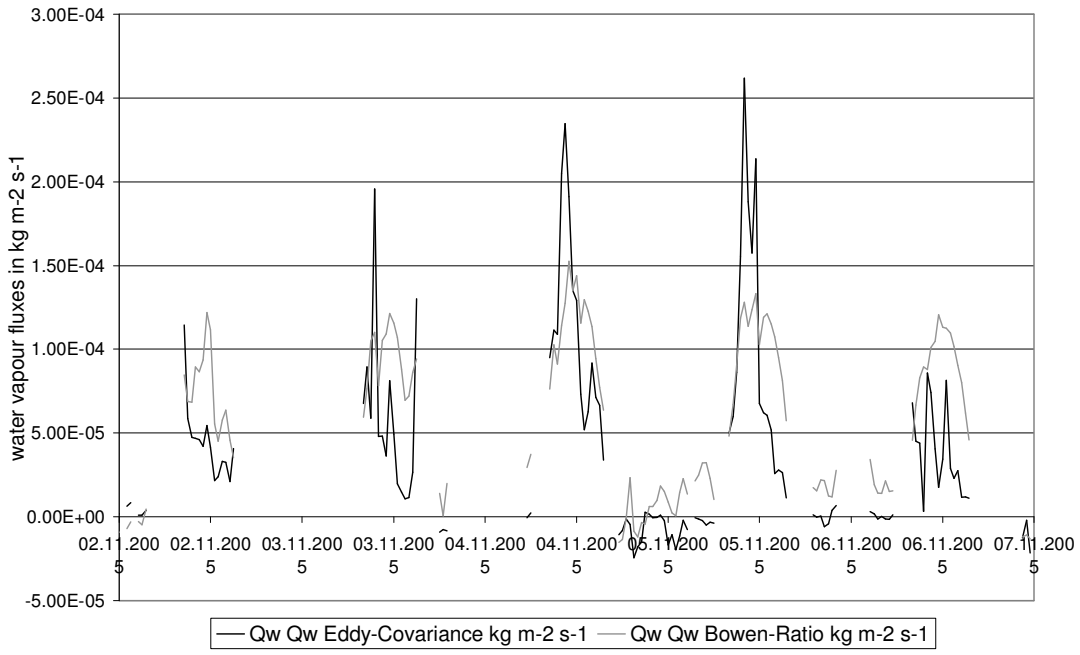

Figure 33: Comparison between Bowen Ratio and Eddy Covariance fluxes during the last week of the study.

A noticed time shift between the Bowen Ratio and the eddy covariance data is not persistent in one direction. This time shift could be due to the method's differing response times to parameter changes. Rank order correlation shows significant correlation between Bowen Ratio and eddy covariance data on the $p < 0.01$ level. Plotting eddy covariance and Bowen Ratio against each other separated for different wind directions, their similar behaviour depending on the wind direction becomes visible (Figure 34).

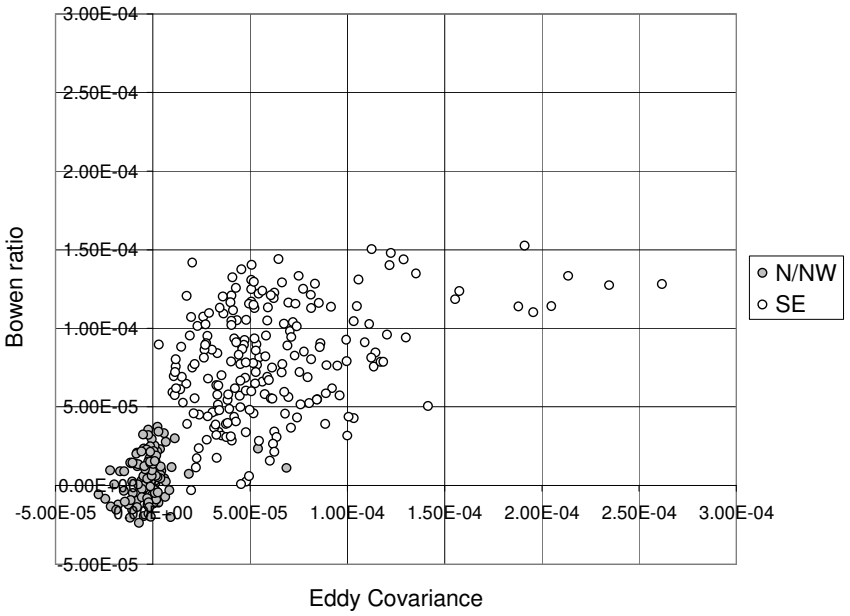

Figure 34: Eddy Covariance results plotted against Bowen Ratio results.

Both Bowen Ratio and eddy covariance fluxes are larger with south easterly winds. The mean difference between eddy covariance and Bowen Ratio fluxes and its standard deviation during northerly and north westerly winds are almost three times smaller than the mean difference and standard deviation during south easterly winds. Six data sets are from foggy conditions. Mean differences during fog are slightly smaller than differences from times without fog but standard deviation during fog is about 5 times larger.

As the Bowen Ratio method and therefore the quality and accuracy of its results rely on the validity of the energy budget closure, differences between eddy covariance and Bowen Ratio measurement are compared to energy budget's closure. To do so, absolute values of the energy budget (calculated from the eddy covariance data, net radiation and soil heat flux) and the absolute values for the difference between Bowen Ratio and eddy covariance measurements are plotted against each other.

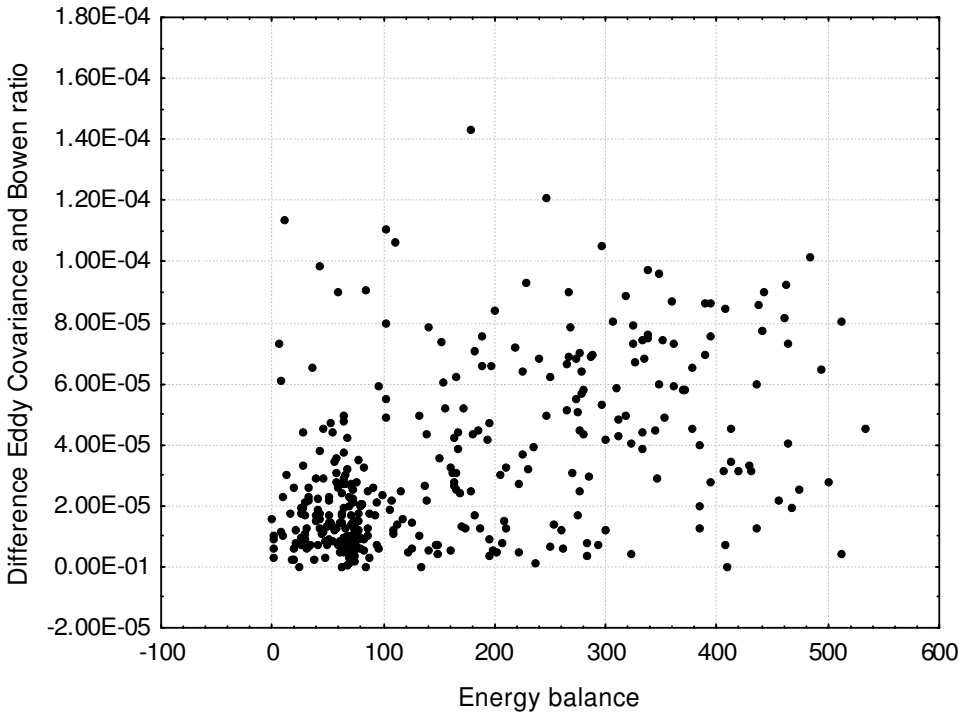

Figure 35: Differences between eddy covariance and Bowen Ratio against energy budget's closure.

Rank order correlation tests show significant correlation on the $p < 0.01$ level. Thus, as closure rates improve differences between eddy covariance and Bowen Ratio measurements decrease.

Other studies report of different energy partitioning of eddy covariance and Bowen Ratio in latent and sensible heat flux (BARR ET AL., 1994). Regarding sensible and latent heat flux as percentage of the sum of both, the different energy partitioning becomes visible (Figure 36); with the eddy covariance favouring latent heat flux and the Bowen Ratio system favouring sensible heat flux.

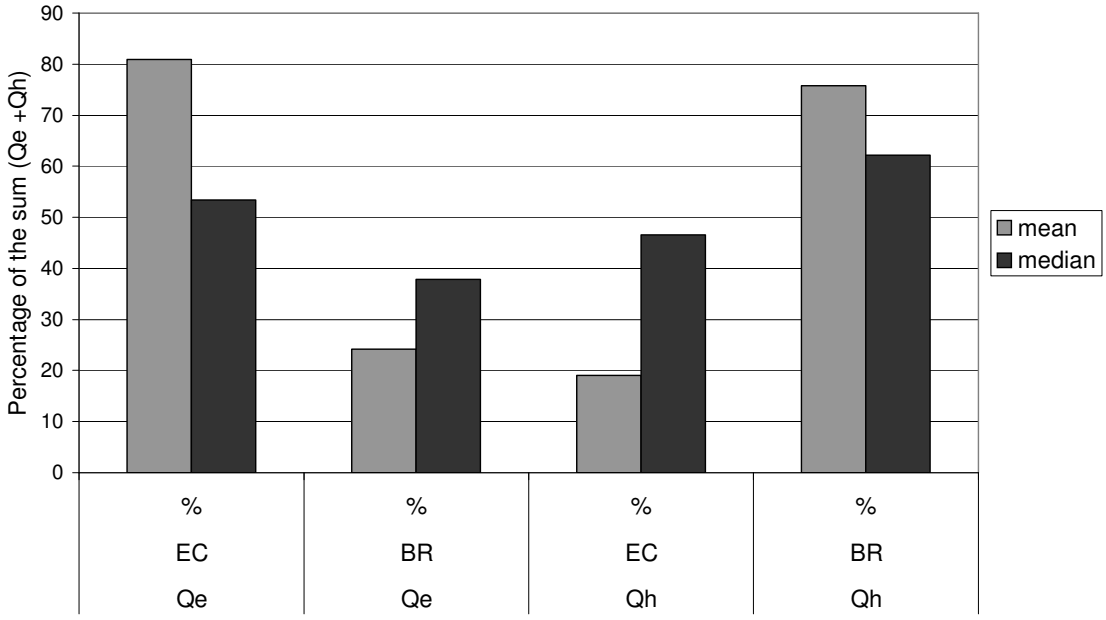

Figure 36: Difference in energy partitioning by the EC and the BR method.

The eddy covariance method splits available energy in 53 % latent heat flux and 47 % sensible heat flux, while the Bowen Ratio method splits into 38 % Q_E and 62 % Q_H (median values). This is not reflected in the size of water vapour flux, which then should be larger with the eddy covariance method, because of the larger sum of Q_E+Q_H determined with the Bowen Ratio system, the median of this sum for Bowen Ratio is twice as large as the sum for eddy covariance (Figure 37).

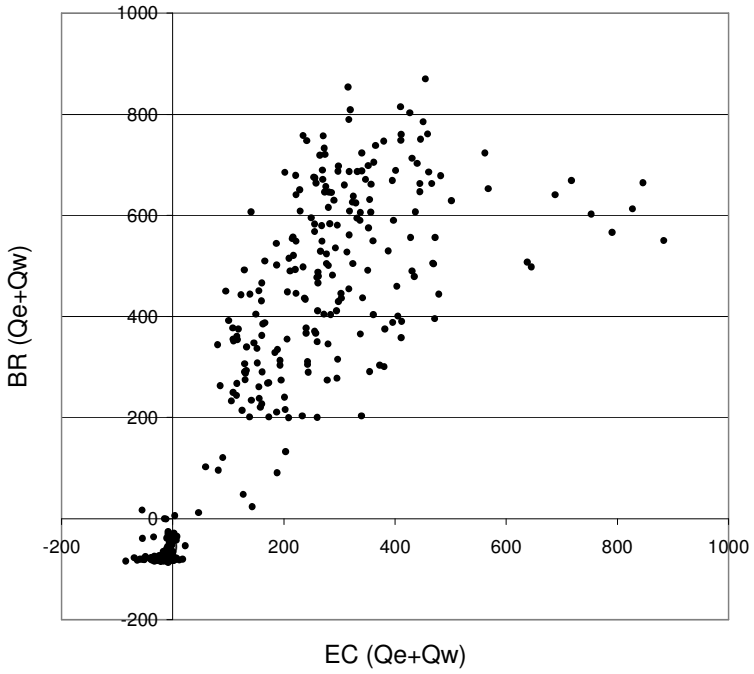

Figure 37: Sums of latent and sensible heat flux for the Bowen Ratio and the eddy covariance set up.

Thus, water vapour flux rates determined with Bowen Ratio method are larger than eddy covariance flux rates, although this method favours the sensible heat flux.

3.6.2 Bowen Ratio, Penman, Penman-Monteith and Eddy Covariance

The results provided by all the methods used are compared with each other. Doing so, one has to keep in mind the different resolution limits of every method. The Penman approach is suitable to gain precise estimates for daily to monthly evaporation while the Penman Monteith method to provides good daily values. The Bowen Ratio and eddy covariance as direct measurements provide accurate 10 to 30 minutes averages under appropriate circumstances (e.g. the closed energy budget) (FOKEN, 2003).

For every conducted method hourly averages were computed and results were put in one data set. For 216 hours, data from all methods are available. Plotting these against the time some observations can be made (Figure 38).

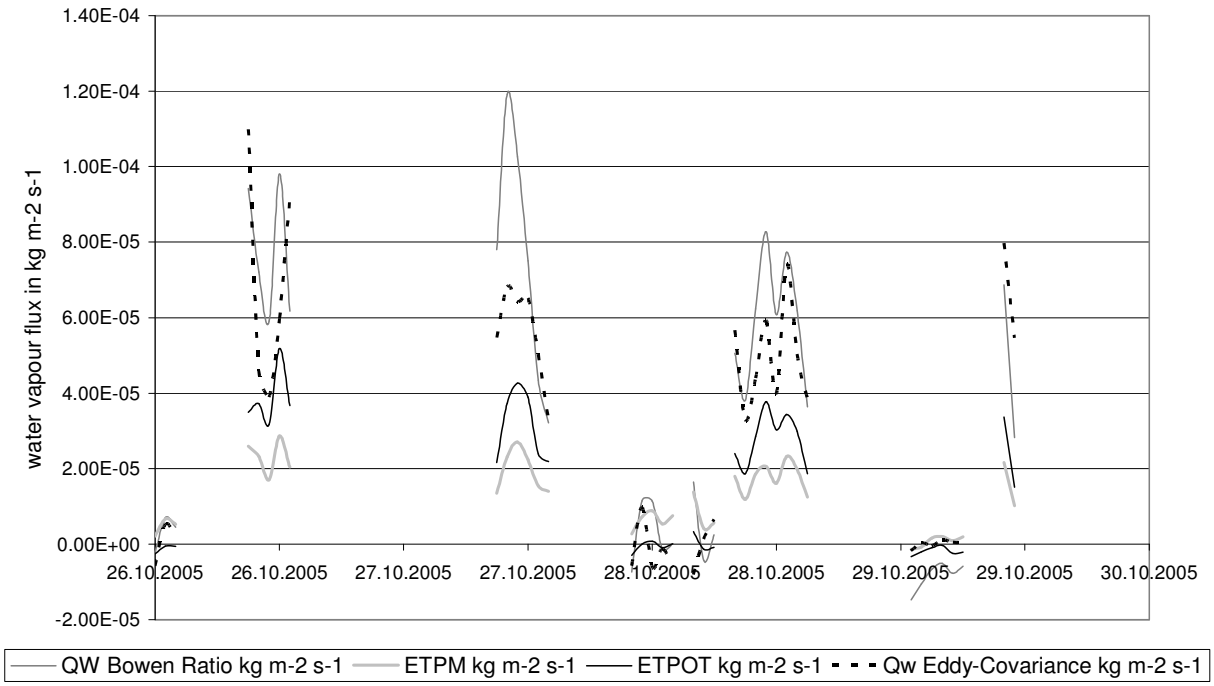

Figure 38: Evaporation rates determined with the Bowen Ratio method, the Penman approach, the Penman-Monteith method, and the eddy covariance method.

Figure 38 shows part of the fluxes measured in the study. The fluxes calculated by the different methods show similar behaviour, i.e. peaks can be found at all methods and lines simultaneously rise and fall. Results obtained by the Penman, the

Penman-Monteith, and the Bowen Ratio method, match better to each other than to the results of the eddy covariance measurement. Great differences concerning the calculated flux size can already be seen in Figure 38. The Bowen Ratio methods tends to provide largest fluxes, eddy covariance ranges in between Bowen Ratio and Penman, and Penman Monteith' fluxes are smallest.

In a second step, daily average sums were calculated. To do so 24 hour data with 18 or more valid data sets were summarized and missing data was interpolated to fill data gaps. Rank order correlation tests were conducted for hourly and daily values and Box & Whisker Plots were computed to visualize results.

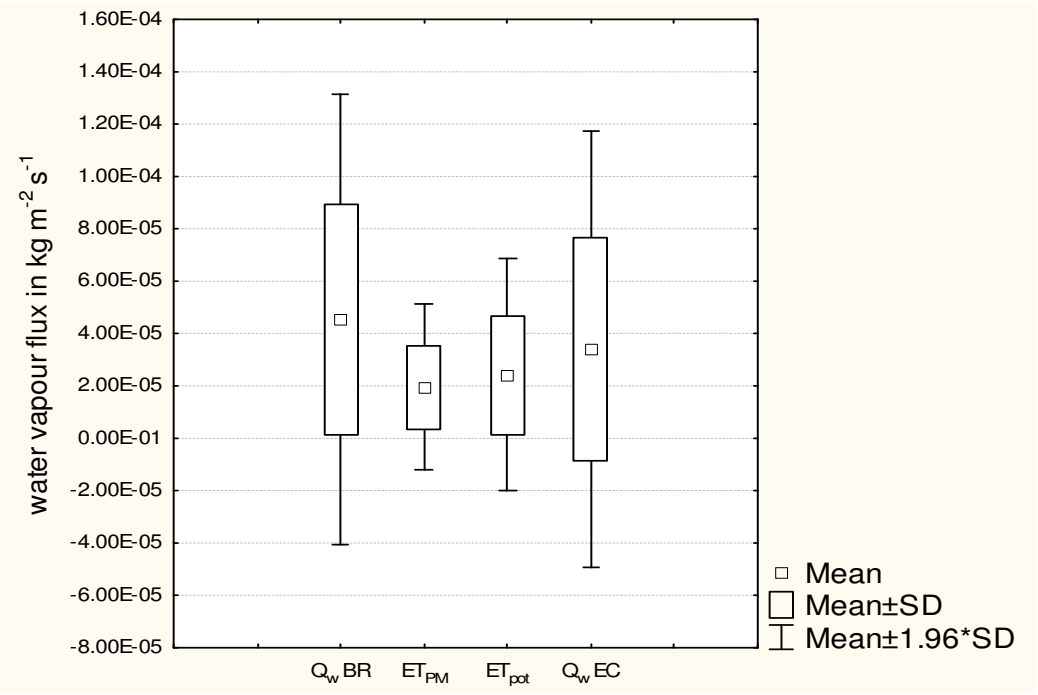

Figure 39: Box-Plot for hourly water vapour flux averages calculated with the Bowen Ratio method (Q_W BR), the Penman Monteith method (ET_{PM}), the Penman approach (ET_{pot}), and the Eddy Covariance method (Q_W EC).

Different sizes and ranges of the method's results are demonstrated (see Figure 39). The rank order correlation termed all methods to be significantly correlated at the p = 0.01 level with high R^2 numbers between 0.72 and 0.93 (refer to Table 10).

Table 10: Rank order correlation results for hourly averages

	Q_W BR	ET_{PM}	ET_{pot}	Q_W EC
Q_W BR	1.00	0.84*	0.93*	0.78*
ET_{PM}	0.84*	1.00	0.93*	0.72*
ET_{pot}	0.93*	0.93*	1.00	0.79*

Q_W EC	0.78*	0.71*	0.79*	1.00
* Marked correlations are significant at p <.01				

Since the eddy covariance method is said to be most suitable for inhomogeneous terrain because the spatial context of this method is most clearly defined (SCHMID, 1997); all the other methods were compared to it.

a)

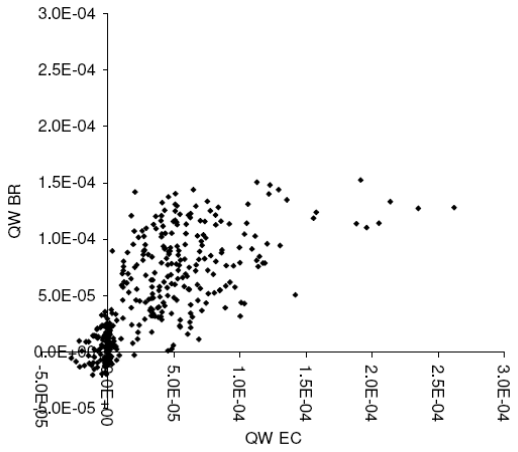

b)

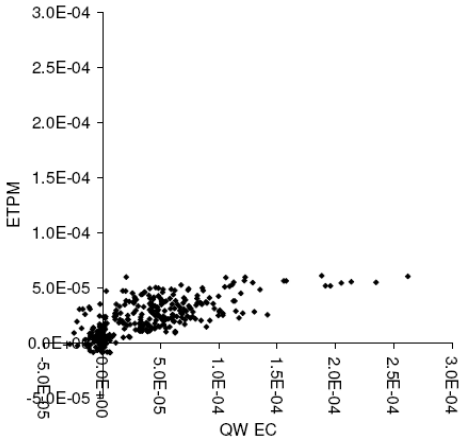

c)

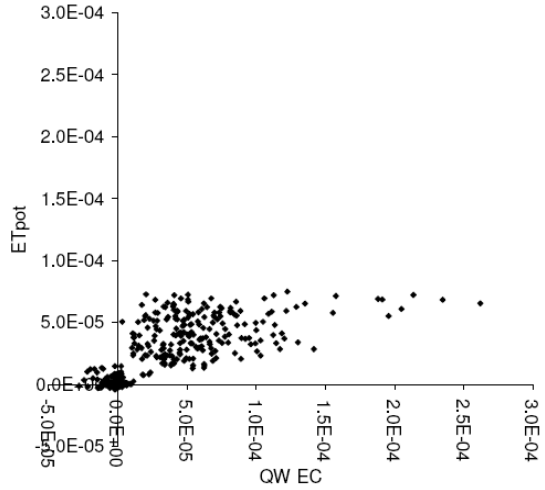

Figure 40: Hourly average values of water vapour flux determined by a) the Bowen Ratio method, b) the Penman Monteith method, and c) the Penman approach plotted against the fluxes by the eddy covariance method.

Differences in size and distribution can clearly be seen. Bowen Ratio results are high and differences to the eddy covariance results are large and variable. Penman and Penman Monteith values are generally much smaller than eddy covariance values. Here, differences are also variable in size and direction.

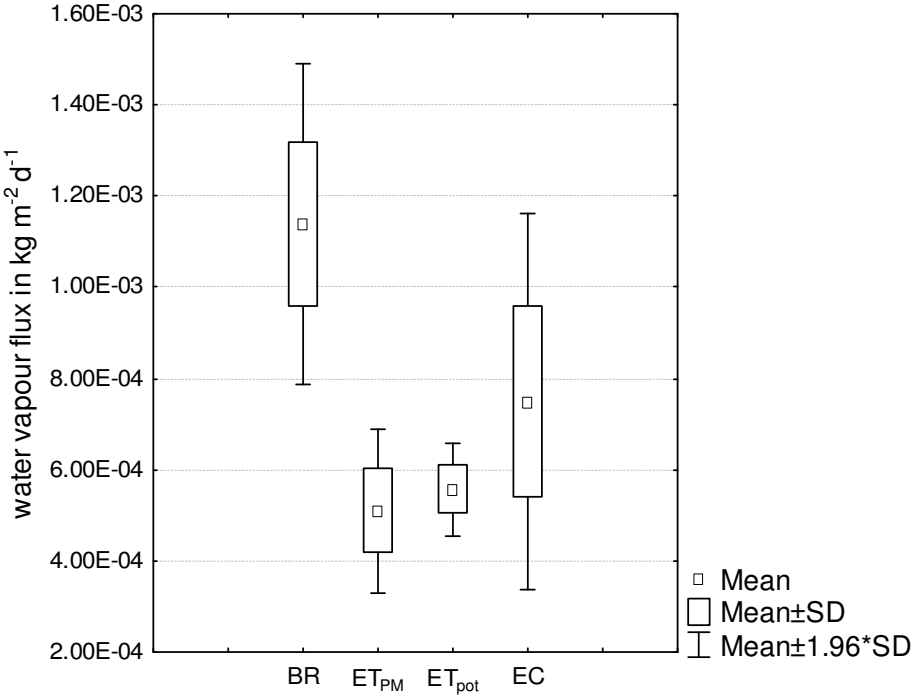

Figure 41: Daily values of water vapour fluxes determined with the Bowen Ratio method, the Penman Monteith method, the Penman method, and the eddy covariance method.

Conducting the rank order correlation test, daily values of the Bowen Ratio, the Penman and the eddy covariance method correlate significantly (with $p < 0.01$); they do not correlate with the Penman Monteith method. Daily values show less variation than hourly values do. This is shown in Figure 42, expressing the standard deviation as percentage of the mean.

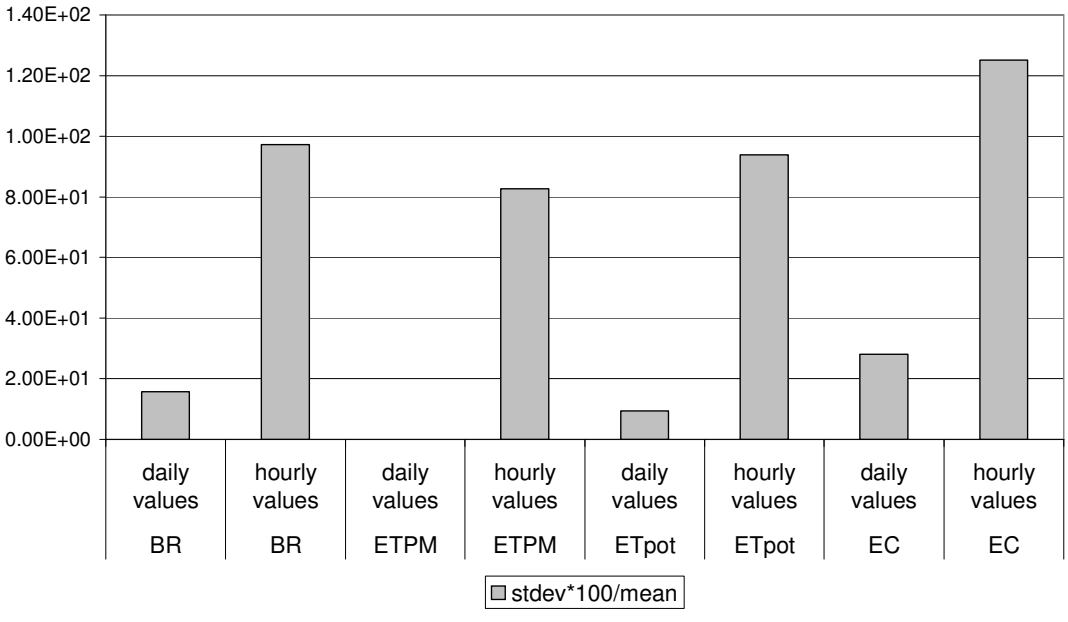

Figure 42: Standard deviation of hourly and daily values, expressed as percentage of the mean.

In order to compare the four methods used in this study, an overall sum of the measured fluxes was calculated for the valid data set. These sums are presented as percentages of the eddy covariance result in Figure 43.

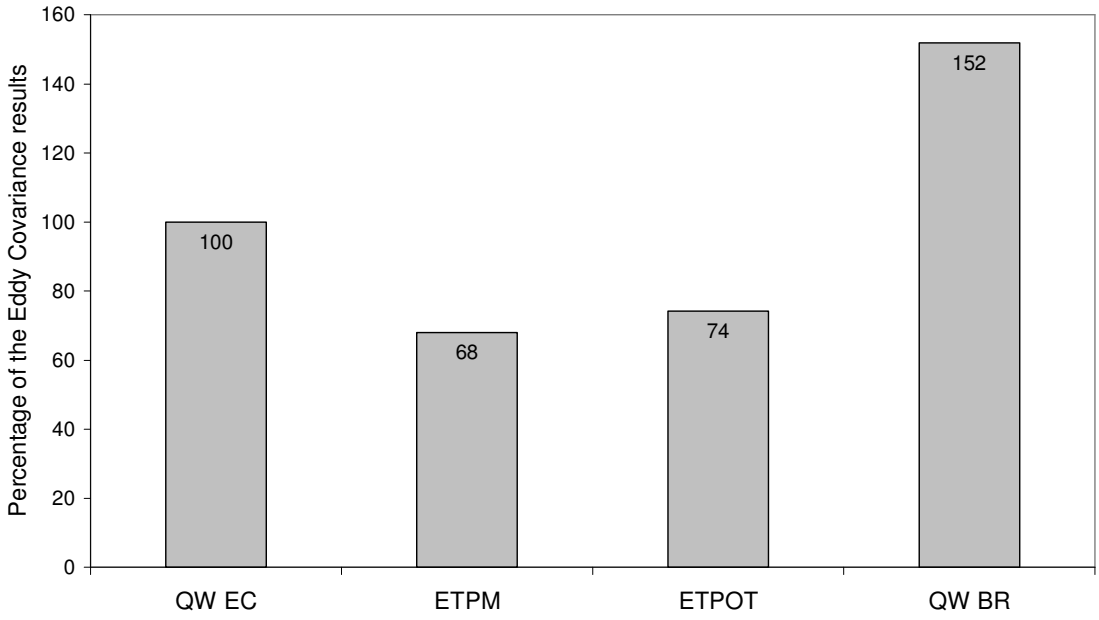

Figure 43: Comparison of the overall sums of measured water vapour fluxes.

Splitting this result into the two prevailing wind directions, it can be observed that during north and north westerly winds percentage differences in the sum are up to six times larger than differences during south easterly winds. This does not change the final result, presented in Figure 43, as fluxes during northerly and north westerly winds are diminutive compared to those during south easterly winds.

In Figure 43 it becomes obvious that the Bowen Ratio method as applied here overestimates the evaporation to about 50 %. The Penman results are closest to the eddy covariance results, but underestimate the water vapour flux to about 25 %. The Penman-Monteith results are smaller than the Penman results. It has also been found in other studies that the Penman Monteith evaporation is smaller than the potential evaporation calculated by Penman's method (MENZEL, 1997).

3.7 Monte Carlo Results

The above explained procedure (refer to Section 2.3) was applied on 17 data sets that passed the quality criteria described in chapter 3.2.2. Furthermore it was applied on three randomly chosen data sets that failed these quality criteria.

First, calculations were performed without any quality criteria. For this purpose, 20'000 random numbers were calculated and fluxes computed; for these cases, the standard deviations were mostly larger than the fluxes themselves, due to extreme values where Bo was close to -1. As these values are not numerically meaningful (denominator close to zero in equation (3) and (4)), it was decided to apply criterion 4 after Ohmura (1982), explained in chapter 3.2.2, for the analysis. When applying quality criterion 4 one has to keep in mind that the associated change in distribution of Bo (skewness towards positive values) may introduce some bias: as values for Bo tend towards positive values, means of calculated fluxes also increase and are more likely to be significantly different from zero.

For further calculations 10'000 random numbers were calculated for each data set. 10'000 numbers were sufficient to get a stable value for the means and the standard deviations of the fluxes. By excluding Bo values close to -1, between 0.5 and 44.4 % of the data calculated from the first 17 data sets were banned from further calculation. From the three data sets randomly chosen from those that did not pass the quality check during the study, 87 to 100 % were excluded; thus only one of these data sets took part in additional calculation. The distribution of Bo changed after excluding these data and, as expected, exhibited skewness towards positive values (refers to Section 3.2.2).

Fluxes were determined and for each calculated flux a single sample t-test was conducted to test the hypothesis that the mean value is significantly different from zero.

For all data sets tested tests showed significant difference between their means and zero at the $p < 0.01$ level. Thus, it can be stated, that fluxes measured during fog in this study are statistically significant and therefore that there is evaporation, i.e. upward water vapour fluxes during fog.

Calculated fluxes, their mean and standard deviation, size of data set, standard error and test results can be taken from Table 11.

Table 11: Calculated fluxes (Monte Carlo method).

variable	Mean	Std.Dv.	N	Std.Err.	Ref. Const.	t-value	df	p
5th Oct 14:30	$3.52 \cdot 10^{-5}$	$4.60 \cdot 10^{-6}$	7105	$5.46 \cdot 10^{-8}$	0.00	645.1256	7104	0.00
6th Oct 14:00	$2.98 \cdot 10^{-5}$	$3.36 \cdot 10^{-6}$	5759	$4.43 \cdot 10^{-8}$	0.00	673.9509	5758	0.00

7th Oct 16:00	$2.61 \cdot 10^{-5}$	$3.17 \cdot 10^{-6}$	5559	$4.26 \cdot 10^{-8}$	0.00	612.0966	5558	0.00
8th Oct 11:00	$7.72 \cdot 10^{-5}$	$1.44 \cdot 10^{-5}$	9962	$1.44 \cdot 10^{-7}$	0.00	536.4329	9961	0.00
8th Oct 12:00	$5.35 \cdot 10^{-5}$	$8.35 \cdot 10^{-6}$	8752	$8.92 \cdot 10^{-8}$	0.00	599.6290	8751	0.00
10th Oct 09:30	$8.70 \cdot 10^{-5}$	$9.68 \cdot 10^{-6}$	9703	$9.83 \cdot 10^{-8}$	0.00	885.8282	9702	0.00
10th Oct 10:00	$6.80 \cdot 10^{-5}$	$7.57 \cdot 10^{-6}$	8383	$8.27 \cdot 10^{-8}$	0.00	821.7235	8382	0.00
10th Oct 10:30	$7.40 \cdot 10^{-5}$	$8.15 \cdot 10^{-6}$	9539	$8.35 \cdot 10^{-8}$	0.00	886.0570	9538	0.00
10th Oct 11:00	$7.08 \cdot 10^{-5}$	$7.76 \cdot 10^{-6}$	8779	$8.28 \cdot 10^{-8}$	0.00	854.9306	8778	0.00
10th Oct 11:30	$6.09 \cdot 10^{-5}$	$6.42 \cdot 10^{-6}$	8303	$7.05 \cdot 10^{-8}$	0.00	864.5306	8302	0.00
10th Oct 12:00	$5.36 \cdot 10^{-5}$	$5.77 \cdot 10^{-6}$	7447	$6.68 \cdot 10^{-8}$	0.00	802.7474	7446	0.00
16th Oct 11:00	$4.49 \cdot 10^{-5}$	$9.98 \cdot 10^{-6}$	7895	$1.12 \cdot 10^{-7}$	0.00	399.6969	7894	0.00
25th Oct 10:00	$5.00 \cdot 10^{-5}$	$1.36 \cdot 10^{-5}$	9896	$1.37 \cdot 10^{-7}$	0.00	366.0382	9895	0.00
28th Oct 09:00	$3.63 \cdot 10^{-5}$	$1.27 \cdot 10^{-5}$	9948	$1.27 \cdot 10^{-7}$	0.00	285.4512	9947	0.00
28th Oct 15:30	$3.49 \cdot 10^{-5}$	$8.65 \cdot 10^{-6}$	7825	$9.78 \cdot 10^{-8}$	0.00	357.0679	7824	0.00
1st Nov 12:00	$2.65 \cdot 10^{-5}$	$1.56 \cdot 10^{-5}$	8116	$1.73 \cdot 10^{-7}$	0.00	153.1476	8115	0.00
2nd Nov 15:00	$3.60 \cdot 10^{-5}$	$9.59 \cdot 10^{-6}$	9016	$1.01 \cdot 10^{-7}$	0.00	356.0231	9015	0.00
1st Oct 14:00	$3.72 \cdot 10^{-5}$	$3.36 \cdot 10^{-6}$	1349	$9.14 \cdot 10^{-8}$	0.00	407.4320	1348	0.00

Determined fluxes from the first 17 data sets thus range around $5.09 \cdot 10^{-5} \pm 8.78 \cdot 10^{-6}$ kg $m^{-2} s^{-1}$. The determined flux for the data set that did not pass the measurement quality criterion calculated flux range around $3.72 \cdot 10^{-5} \pm 3.36 \cdot 10^{-6}$ kg $m^{-2} s^{-1}$.

3.8 Footprint analysis

The available data was divided according to their stability parameter z/L into those with stable ($z/L > 0$) and unstable conditions ($z/L < 0$). These data sets were checked respective to Schmid's specification for input parameter for his model (refer to Chapter 2.4 Footprint analysis). 15 data sets for unstable conditions were found that matched the prerequisites. For these, the standard deviation of the lateral wind component was calculated and quality checked, and footprints were calculated introducing the wind direction, the roughness length and dimensionless ratios z/L and $\sigma v/u^*$. There was no matching data set found with stable conditions, so Schmid's specifications for z/z_0 were changed to gain at least some footprints. Ignoring these specifications it can easily come to problems with the model such as unspecified stops. For four data sets footprints could be calculated.

The footprint model gives the source areas for every data set at different percentage levels (10, 30, 50, 70 and 90 %) of the whole source area. With growing percentage the minimum distance (*a*) to the tower diminishes and the maximum distance (*e*) as well as the maximum lateral extension (*d*) and the footprint area enlarge. In further considerations, only the 50 % and the 90 % values will be regarded.

Figure 44 and Figure 45 give examples for the calculated footprint areas for stable (Figure 44) and unstable (Figure 45) conditions. In these figures grey lines are contour lines, the black line is the logging road that goes through the area. The grey area is the 50 % footprint area and the hollow ellipse shows the 90 % area.

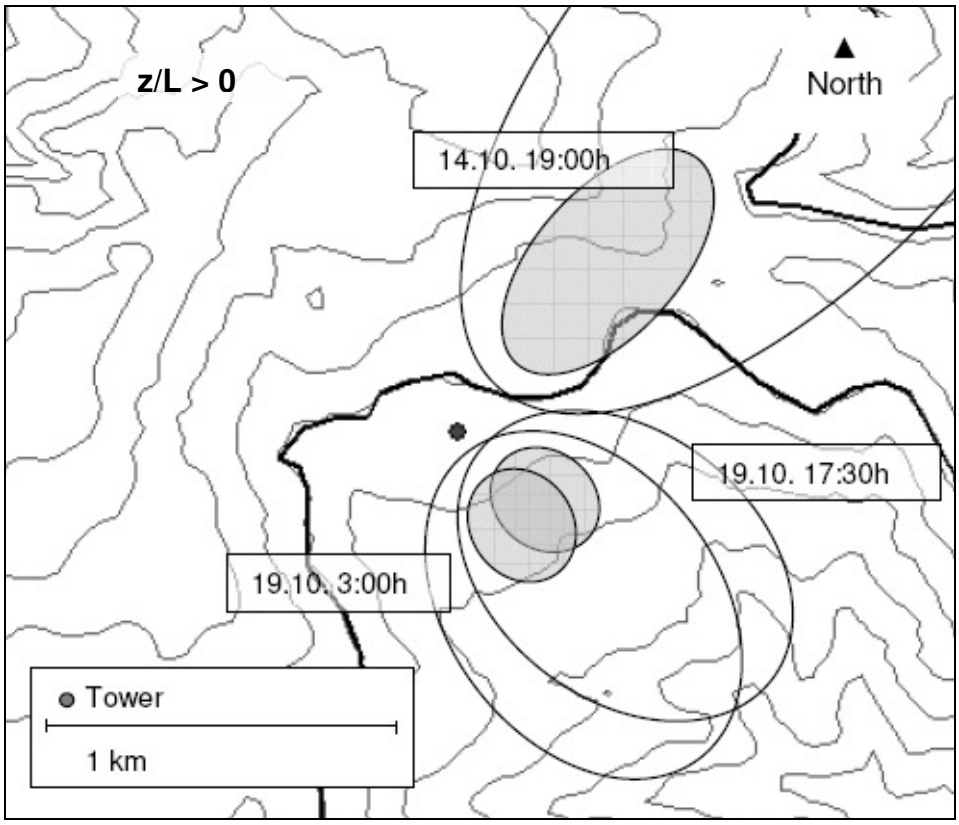

Figure 44: Footprint areas for stable conditions.

As reported from other studies (Schmid, 1994) footprint size differs significantly between stable and unstable conditions. The mean 50 % footprint area from stable conditions is more than 10 times larger than the mean footprint area in unstable conditions. Most of the determined footprint areas are from south easterly wind directions, only three of nineteen are from other wind directions, one of them from northerly wind directions. The majority of footprints are from times with fog.

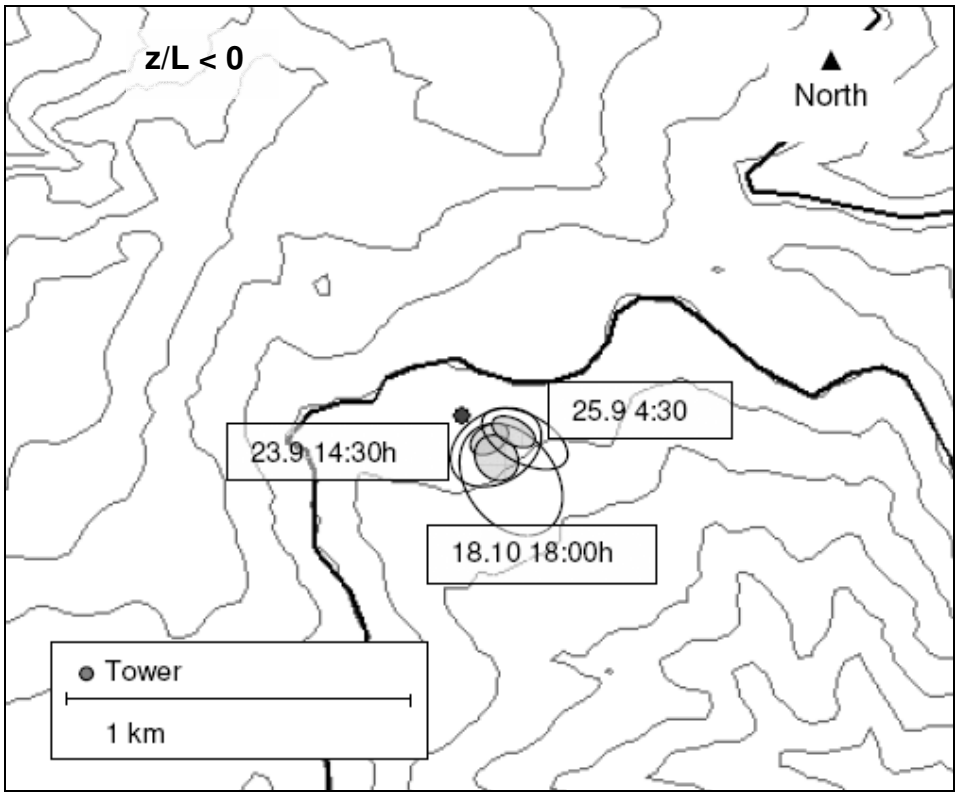

Figure 45: Footprint areas for unstable conditions.

Daytime footprint areas in south easterly wind direction range from 3'030 to 28'300 m² (0.30 to 2.83 ha) for 50 % area and 15'000 m² to 132'000 m² (1.50 to 13.20 ha) for 90 % area, their medians being 12'000 and 47'200 m² (1.20 and 4.72 ha).

Closest footprint distance extends from 25 to 115 m for 50 % areas and from 20.9 to 85.4 m for 90 % areas, their medians being 72.8 m and 56.1 m. The furthest distances for 50 and 90 % areas range between 79.1 and 341 m and between 144 and 622 m, their medians being 213 m and 347 m.

One footprint in northerly wind direction with near neutral stability was determined. Its size is comparatively large with a 50 % area of 58'700 m² (5.87 ha) and a 90 % area of 243'000 m² (24.30 ha). Minimum distance to the tower is 127 m (50 %) and 93.9 m (90 %), respectively. Furthest distances are 393 m for the 50 % area and 691 m for the 90 % area.

The two largest calculated footprint areas with 90 % areas of 54.90 and 241 ha are from stable conditions and are situated in north easterly directions. Their 90 % source areas start 87 m away from the tower and extend to the furthest distance of 2'810 m, i.e. almost 3 km. Though, these footprints are not as reliable as the ones calculated for unstable conditions because Schmid's prerequisites had to be changed to calculate them.

For most of the footprints calculated there are no water vapour flux data of the Bowen ratio measurement. In all cases except two, data was excluded applying the quality criteria described in chapter 3.2.2. For footprints calculated for the 30th September 2005 13:30h and 1st October 2005 05:00h comparable flux data exists. The first data set shows a perfect match of the two results with the Bowen Ratio result being almost the same as the eddy covariance result ($2.37 \cdot 10^{-5}$ and $2.36 \cdot 10^{-5}$). The second data set with comparable data comes from one of the data sets with large footprint areas in north easterly directions. Here, fluxes are negative and Bowen Ratio flux is twice the size of the eddy covariance flux. Due to topographic reasons and to the set up structure, with possible negative influences of the upper psychrometer by the tower, this data is less trustworthy than data from south easterly wind directions.

All calculated footprints are listed with their determining parameters in Table 12.

Table 12: Footprint results

	WD	a_{50}	e_{50}	d_{50}	xd_{50}	ar_{50}	a_{90}	e_{90}	d_{90}	xd_{90}	ar_{90}
23.09.2005 13:30	135.93 (SE)	72.8	213	69.2	132	$1.53 \cdot 10^{+4}$	56.1	414	147	235	$8.58 \cdot 10^{+4}$
23.09.2005 14:30	148.00 (SE)	40.1	119	61.3	76.2	$7.82 \cdot 10^{+3}$	32.3	239	142	136	$4.72 \cdot 10^{+4}$
25.09.2005 04:30	118.90 (SE)	78.5	217	36.8	153	$7.94 \cdot 10^{+3}$	59.5	333	71.2	210	$2.98 \cdot 10^{+4}$
25.09.2005 05:00	111.63 (E)	92.2	275	86	182	$2.40 \cdot 10^{+4}$	68.8	533	175	299	$1.26 \cdot 10^{+5}$
25.09.2005 20:00	359.81 (N)	127	393	141	263	$5.87 \cdot 10^{+4}$	93.9	691	304	395	$2.43 \cdot 10^{+5}$
26.09.2005 12:30	176.12 (S)	29.4	90.5	42.2	60.9	$4.03 \cdot 10^{+3}$	22.5	149	84	88.7	$1.67 \cdot 10^{+4}$
30.09.2005 13:30	146.54 (SE)	25	79.1	35.7	52.5	$3.03 \cdot 10^{+3}$	20.9	149	81.2	86.2	$2.34 \cdot 10^{+4}$
01.10.2005 05:00	61.50 (NE)	261	1100	216	695	$2.82 \cdot 10^{+5}$	488	488	0	488	$5.49 \cdot 10^{+5}$
14.10.2005 17:30	132.91 (SE)	52.9	152	35.7	105	5510	39.5	238	69.5	147	21200
14.10.2005 19:00	42.48 (NE)	237	1020	208	636	$2.55 \cdot 10^{+5}$	152	2810	599	1530	$2.41 \cdot 10^{+6}$
18.10.2005 16:30	134.03 (SE)	82.7	227	53.5	160	$1.20 \cdot 10^{+4}$	62.9	347	104	219	$4.50 \cdot 10^{+4}$

18.10.2005 17:00	132.33 (SE)	115	341	81.7	242	$2.83 \cdot 10^{+4}$	85.4	622	166	357	$1.32 \cdot 10^{+5}$
18.10.2005 17:30	140.04 (SE)	80.4	238	73.4	144	$1.78 \cdot 10^{+4}$	60.8	468	152	262	$9.89 \cdot 10^{+4}$
18.10.2005 18:00	142.91 (SE)	73.8	215	59.6	136	$1.34 \cdot 10^{+4}$	57	418	130	239	$7.42 \cdot 10^{+4}$
19.10.2005 03:00	143.61 (SE)	127	468	146	294	$7.85 \cdot 10^{+4}$	88	1190	390	652	$6.92 \cdot 10^{+5}$
19.10.2005 17:30	128.58 (SE)	124	455	145	286	$7.53 \cdot 10^{+4}$	86.2	1150	383	631	$6.49 \cdot 10^{+5}$
07.11.2005 15:00	156.17 (SE)	29.3	89.1	40	60.2	$3.74 \cdot 10^{+3}$	21.5	144	78.4	86.3	$1.50 \cdot 10^{+4}$
09.11.2005 16:30	139.46 (SE)	56.9	155	33.4	109	$5.12 \cdot 10^{+3}$	43.1	240	65.3	151	$1.97 \cdot 10^{+4}$
09.11.2005 17:00	135.82 (SE)	81	235	95.3	152	$2.35 \cdot 10^{+4}$	63	443	209	258	$1.25 \cdot 10^{+5}$
Grey data sets are from times with fog, black ones from times without fog											

Input parameters and parameters for quality check are listed in Table 13.

Table 13: Input and quality check parameter for footprint calculation.

	WD	z0	z/z0	z/L	σv/u*
14.10.2005 19:00	42.48	0.6	26.8	0.1	2.84
01.10.2005 05:00	61.50	0.5	35.7	0.2	3.08
19.10.2005 17:30	128.58	0.9	19	0	2.84
19.10.2005 03:00	143.61	0.9	19.3	0	2.84
25.09.2005 05:00	111.63	0.3	49.3	-0.1	3.15
25.09.2005 04:30	118.90	0	556.5	-0.5	3.20
18.10.2005 17:00	132.33	0.2	89.4	-0.1	3.1
14.10.2005 17:30	132.91	0.1	187.4	-0.7	3.38
18.10.2005 16:30	134.03	0	697.9	-0.5	4.66
09.11.2005 17:00	135.82	0.2	91	-0.2	5.13
23.09.2005 13:30	135.93	0.3	52.8	-0.2	3.32
09.11.2005 16:30	139.46	0	391.4	-1.0	3.54
18.10.2005 17:30	140.04	0.4	46.4	-0.1	3.00
18.10.2005 18:00	142.91	0.3	62.8	-0.2	3.04
30.09.2005 13:30	146.54	0.4	46.5	-0.9	3.91
23.09.2005 14:30	148.00	0.4	42.5	-0.4	4.63
07.11.2005 15:00	156.17	0.2	70	-1.0	4.50

26.09.2005 12:30	176.12	0.3	62.9	-0.9	4.57
25.09.2005 20:00	359.81	0.2	85.2	0	5.04

4. Discussion and Conclusion

Four methods to determine the water vapour flux have been conducted in this study, with special emphasis on the Bowen Ratio method, for which there were certain application difficulties. First of all, there seemed to be a change in sensor response when comparing data from the first and the second calibration period. This change in sensor response could be due to the different weather situations of the calibration periods, but no definitive reason could be determined. The second problem was the measurement height of the lower psychrometer. As stated in Section 2.1.1 Bowen Ratio Method, the danger of getting into the roughness sublayer (refer to Section 2.2 Flux measurements above high vegetation and forest) had to be evaluated against the need to obtain resolvable gradients of water vapour pressure and temperature. The rule-of-thumb introduced by Monteith and Unsworth (1990), requiring a measurement height z_m, that follows $z_m = 10 \cdot z_0 + d$, was ignored here. As noticed in Section 3.1.2 Roughness parameter, the lower psychrometer indeed was inside the roughness sub layer, which could have introduced inaccuracies to the results. Further, Barr (1994) points out that close to the forest canopy, where the Bowen Ratio is applied for practical reasons, several assumptions of gradient-diffusion theory are violated. However, Arya (2001) reports of measurements of turbulent fluxes that were found to remain practically constant in the height interval $h < z_m < 2.4$, which includes the roughness sub layer. All measurement heights studied here lay within this interval, which is why results of this study are considered valid.

In the derivation of the Bowen Ratio the similarity of the eddy diffusivities of heat and water vapour is assumed. Barr (1994) states, that this similarity could be violated when temperature or humidity variations dominate the buoyancy production of vertical motion. It is explained that K_H/K_V (the ratio of the eddy diffusivity of heat and the eddy diffusivity of water vapour) can depart from unity, increasing to as high as 3 when temperature dominates (high *Bo*) and decreasing to as low as 0.5 where humidity dominates. When $K_H/K_V > 1.0$, the Bowen Ratio method overestimates Q_E for $Bo > 0.0$ and underestimates Q_E for $Bo < 0.0$. When $K_H/K_V < 1.0$, the Bowen Ratio method underestimates Q_E for $Bo > 0.0$ and overestimates Q_E for $Bo < 0.0$. Spittlehouse and Black (1980) state that the assumption $K_H = K_V$ is acceptable for neutral to moderately unstable conditions. For stable conditions they say in their paper that K_H is larger than K_V. However, as no further information about the ratio K_H/K_V is available, it was assumed to be unity, as it is implied in the derivation of the Bowen Ratio method.

The eddy covariance method was accompanied by large problems that occurred mainly during foggy conditions, resulting in a data set that is even smaller than the valid data set for the Bowen Ratio method analysis. In addition, an instrument problem was determined after the study which could have lead to an error of up to 15 % (Wrzesinsky, 2006, personal communication). Nevertheless, data from this set up are available, and, since the eddy covariance method has been described as the one most suited for complex terrain (SCHMID, 1994), all other method results were compared to this one, putting its results as 100 % in the comparison.

The results of the Penman and the Penman Monteith methods were calculated as described above (refer to Sections 3.4 and 3.5).

No estimation has been made to describe the storage term of the forest layer. Spittlehouse and Black (1980) state that the sum of the heat storage term and the soil heat flux of a forest is less than 5 % of the net radiation except for periods around sunrise and sunset. However, an imbalance in the surface energy budget could be influenced by this missing factor. Comparing the energy balance and the differences between eddy covariance method and Bowen Ratio method results, a correlation has been found. With improving energy budget closure, the differences between the methods decrease. Because the Bowen Ratio method forces closure, errors are introduced when non-closure occurs. As described in Section 2.1.1, Foken (2003) states that with imbalanced energy budget, the Bowen Ratio method could overestimate latent and sensible heat flux. Barr (1994) assumes that as the eddy covariance method does not force closure of the of the surface energy budget, it may underestimate available energy. The energy budget was calculated using the eddy covariance data, the net radiation measurement, and the soil heat flux measurement. Aubinet et al. (2001) declares that non-closure of the energy budget is a common feature of the eddy-covariance measurements above forests. In this paper, it is said that this could be due to several causes and that it does not necessarily indicate errors in the eddy covariance only. Errors of the measurement technique are normally suggested to be the prevailing reason for energy balance non-closure. The accuracy of the net radiation measurement, for example, influences the calculation significantly as the net radiation plays a large part in the energy balance. The reasons for imbalance could not be fully explained in this study. Thus, it could not be explained if the improving match of eddy covariance results with the Bowen Ratio results with improving energy budgets closure is due to the lessening error of the eddy covariance setup or due to the diminishing influence of systematic restrictions of the Bowen Ratio setup.

Differences in results of the eddy covariance and the Bowen Ratio methods could also be due to different source areas of the systems. As mentioned in Section 2.4 and according to Schmid (1994), source areas for fluxes tend to be smaller than the concentration source areas. Schmid (1994) points out that this incongruity of the source areas may lead to considerable discrepancies between parameterized and actual fluxes in heterogeneous regions. He also states that the two components of the Bowen Ratio measurement are likely to respond to surface characteristics of different surface patches, and thus the gradients of humidity and temperature between the two levels are affected by advection, in addition to vertical transport (SCHMID, 1997). According to Schmid, this inconsistency may turn out to be irrelevant, as long as horizontal homogeneity in the partitioning of energy can be assumed and that the net radiation measurement reflects conditions that are local and representative of the surface of interest.

The study site shows horizontal homogeneity in plant composition of the forest, but it does not show homogeneity in topography and tree size outside the plantation. No further information was available on how changes in topography and canopy roughness structure influence the energy partitioning of the Bowen Ratio method. Comparing the two footprints associated with measured fluxes mentioned in Section 3.8, the influence of topography on the energy partitioning of the Bowen Ratio method could be an explanation for the large difference between Bowen Ratio and eddy covariance results with the north westerly footprint. This footprint from the 1st October is similar to the one from the 14th October, shown in Figure 44. It has a very large area and extends over surface with strong topography. Results of Bowen Ratio and eddy covariance from the regarded south easterly footprint (within the plantation) match almost perfectly. To further investigate this topic, equipment with several ultrasonic anemometers would be necessary in order to be able to calculate the footprint areas for every measurement level. From the example mentioned above, homogeneous energy partitioning is assumed for south easterly wind directions with footprints lying within the plantation with homogeneous surface and topography.

In comparison to the eddy covariance method, the Bowen Ratio method overestimated evaporation by about 50 %. The difference is surprisingly large. Other studies showed differences ranging from 23 to 33 % (BROTZGE ET AL., 2002). Considering possible footprint differences, and the sensor's position within the roughness sublayer as unimportant for the Bowen Ratio results obtained here, the large difference between eddy covariance and Bowen Ratio results could be due to the change in sensor response or due to energy budget imbalance, whose reasons

could not be explained during this study. In an overall comparison between the methods used, taking the eddy covariance results as standard, best agreement was found between the Penman and the eddy covariance results, with daily averages of Penman underestimating the results of eddy covariance by 26 %. Daily values of Penman Monteith showed no correlation with the other methods and the overall sum was 32 % smaller than eddy covariance sum.

A Monte Carlo type simulation was calculated to test the hypothesis if there is significant evaporation during fog. Through the analysis significant water vapour fluxes during fog could be determined. These fluxes are mainly due to temperature gradients and occurred at the beginning of fog episodes. Problems in the run of the calculations were discussed in Section 3.7. These problems may lead to small scale changes in the results but do not change the general statement that there were statistically significant water vapour fluxes during fog during this study.

Footprint calculation showed excellent conditions for measurement in south easterly wind directions. As these winds prevailed during daytime with unstable conditions, the calculated footprint areas were relatively small and within optimum fetch ranges (i.e., within the plantation's homogeneous extensions). During day time with south easterly winds, the main part of measured data with high mean values was achieved. Footprints into other wind directions were more difficult to obtain, as Schmid's specifications for input parameters had to be widened to get data. These footprints were the ones from stable conditions and were thus much larger in area and distance to the tower. Two footprints were calculated for north easterly directions. These wind directions did not occur in the data that remained after quality check. As there were few eddy covariance data due to problems, only 19 footprints could be calculated in total. Comparison with the Lagrangian footprint model have shown that results obtained with the analytical model of Schmid (1997) overestimate the longitudinal extensions of the footprint area, and thus provide a 'worst case' scenario concerning source area dimensions (REBMANN, 2004).

A fact that was not regarded in this study is the vertical distribution of sources and sinks within the forest layer. This vertical distribution of sources and sinks and turbulent transport inside the canopy affect concentration and fluxes inside and above the forest. There are further models and ideas on how to describe the distribution of emission by the layer with certain depth at certain height (RANNIK ET AL, 2000). These ideas were not regarded here due to time and instrumental limitations.

Summarizing, the problems with the eddy covariance and the Bowen Ratio set up were large and reasons could not be fully explained. The Penman method gives the best evaporation rates estimates on average basis. If higher time scale resolution is needed, the eddy covariance set up is the best choice, due to its suitability for inhomogeneous surfaces and its comparatively small source areas (Schmid, 1997). The suitability of the Bowen Ratio measurement for forest evaporation was confirmed from other studies, but could not be confirmed here. The pronounced daily cycle of mountain and valley wind was reflected in the determined results, i.e. evaporation rates, footprint size, atmospheric stability etc.

The tower, its location, and the instrumental set up were constructed with an emphasis on the south easterly wind direction, with the main fetch in this direction. For further studies, designed to evaluate the second prevailing wind direction from north and north west, another tower will should be installed. To achieve further detailed information about footprints of this study side and the fluxes measured there it is advisable to have at least one, but preferably several, three dimensional ultrasonic anemometers on each mast.

Appendix

As appendix a compact disc is attached to the printed version of this thesis.

The compact disc contains four folders:

> “Footprint” contains data and program used in the footprint analysis.
>
> “Methods” consists of the calculations and results of the four methods to determine water vapour fluxes.
>
> “Monte Carlo” includes the calculations done for the Monte Carlo type simulation.
>
> “Raw Data” contains the raw data of the Delta-T DL2e data logger and the raw meteorological and wind profile data.

Data is stored either as excel-data or (the raw data) as dat- or bin-data.

In addition, a pdf-file of this thesis is included.

Acknowledgments

I would like to express my thanks to Prof. Dr. Otto Klemm, who initiated this work, supported it and was always available for questions.

I am thankful to Prof. Yue-Joe Hsia, who made the study possible in Taiwan, gave us his trust (and his car), and, above all, his help in scientific and ordinary life questions.

Further I would like to thank Dr. Shih-Chieh Chang, who made us feel at home in Taiwan and had a helping hand and (German-) understanding ear whenever needed.

My special thanks go to Eva Beiderwieden, who was brave enough to enter the jungle with me and stay there for two months. Thank you for a very good time, interesting discussions and your help with my little moment of acrophobia.

Thank you to Dr. Thomas Wrzesinsky and Dr. Andreas Held, who patiently answered questions and discussed scientific and other topics. This includes a special thanks to the whole climatology working group at the Institut der Landschaftsökologie.

I am more than thankful to Robert W. Rooks, who proofread my work and tried to make me sound like a native English speaker.

This study has been made possible by a grant of the German Academic Exchange Service (DAAD). Grant number D/05/42326.

Last but not least I would like to thank all friends and family for their support and especially my twin sister for never switching off her mobile phone.

References

Ammann, C. (1998): On the Applicability of Relaxed Eddy Accumulation and Common Methods for Measuring Trace Gas Surface Fluxes. Doctoral Thesis. Swiss Federal Institute of Technology Zurich

Arya, S. P. (2001): Introduction into Micrometeorology. Academic Press

Aubinet, M.; Chermanne, B.; Vandenhaute, M.; Longdoz, B.; Yernaux, M. & Laitat, E. (2001): Long term carbon dioxide exchange above a mixed forest in the Belgian Ardennes. Agricultural and Forest Meteorology **108**: 293-315.

Barr, A.G.; King, K.M.; Gillespie, T.J.; Hartog, G. Den & Neumann, H.H. (1994): A comparison of Bowen ratio and Eddy correlation sensible and latent heat flux measurement above deciduous forest. Boundary Layer Meteorology **71**: 21-41.

Beiderwieden, E. (2004): Chemische Zusammensetzung von Nebel und Regen am Standort “El Tiro”, Ecuador. Diploma Thesis. Westfälische Wilhelms-Universität Münster (unpublished)

Bernhofer, C. (1992): Estimating forest evapotranspiration at a non-ideal site. Agricultural and Forest Meteorology **60**: 17-32.

Bowen, I. (1926): The Ratio of Heat Losses by Conduction and by Evaporation from any Water Surface. Physical Review **27**: 779-787.

Brotzge, J.A. & Crawford, K.C. (2002): Examination of the Surface Energy Budget: A Comparison of Eddy Correlation and Bowen Ratio Measurement Systems. Journal of Hydrometeorology **4**: 160-178.

Chang, S.C. (2006): personal communication

Chang, S.C.; Lai, I.L. & Wu, J.T. (2002): Estimation of fog deposition on epiphytic bryophytes in a subtropical montane forest ecosystem in northeastern Taiwan. Atmospheric Research **64**, 159-167.

Chou, C.H.; Chen, T.Y.; Liao, C.C. & Peng, C.I. (2000): Long-term ecological research in the Yuen-Yuang Lake forest ecosystem: I. Vegetation composition and analysis. Botanical Bulletin of Academia Sinica **41**, 61-72.

Foken, T. (2003): Angewandte Meteorologie. Mikrometeorologische Methoden. Springer

Hwang, Y.H.; Fan, C.W. & Yin, M.H. (1996): Primary production and chemical composition of emergent aquatic macrophytes, Schoenoplectus mucronatus ssp. Robustus and Sparganium fallax, in the lake Yuang-Yang, Taiwan. Botanical Bulletin of Academia Sinica **37**, 265-273.

Klemm, O.; Chang, S.C. & Hsia, Y.J. (2006): Energy fluxes at a subtropical mountain cloud forest. Forest Ecology and Management **224**: 5-10.

Lauer, W. & Bendix, J. (2004): Klimatologie. Das Geographische Seminar. Westermann

Lutz, Monika (2006): http://www.fh-friedberg.de/users/mlutz/JavaKurs/applets /MonteCarloMethode/MonteCarloMethode.htm (abgerufen am 24.04.2006)

Mangold, A. (1999): Untersuchung der lokalen Einflüsse auf die Turbulenzmessing an der Station Weidenbrunnen. Diploma Thesis. Universität Bayreuth

McNeil, D.D. & Shuttleworth, W.J. (1975): Comparative measurements of the energy fluxes over a pine forest. Boundary Layer Meteorology **9**: 297-313.

Menzel, L. (1997): Modellierung der Evapotranspiration im System Boden-Pflanze-Atmosphäre. Züricher Geographische Schriften **67**. Verlag Geographisches Institut ETH Zürich

Monteith, J.L. & Unsworth, M. (1990): Principles of Environmental Physics. Edward Arnold.

Monteith, J.L. (1965): Evaporation and Environment. Symposium of the Society for Experimental Biology **19**: 205-234.

Ohmura, A. (1982): Objective Criteria for Rejecting Data for Bowen Ratio Flux Calculations. Journal of Applied Meteorology **21**: 595-598.

Oke, T.R. (1987): Boundary Layer Climates. University Press

Penman, H.L. (1948): Natural evaporation from open water, bare soils, and grass. Proc. Roy. Soc. London **A193**: 120-145.

Rannik, Ü.; Aubinet, M.; Kurbanmuradov, O.; Sabelfeld, K.K.; Markkanen, T. & Vesala, T. (2000): Footprint analysis for measurements over a heterogeneous forest. Boundary Layer Meteorology **97**: 137-166.

Schmid, H.P. (1994): Source areas for scalars and scalar fluxes. Boundary Layer Meteorology **67**: 293-318.

Schmid, H.P. (1997): Experimental design for flux measurements: matching scales of observations and fluxes. Agricultural and Forest Meteorology **87**: 179-200.

Spittlehouse, D.L. & Black, T.A. (1980): Evaluation of the Bowen Ratio/Energy Balance Method for Determining Forest Evaporation. Atmosphere-Ocean **18**: 98-116

Stadtmüller, T. (1987): Cloud Forests in the Humid Tropics. A Bibliographic Review. Turrialba: United Nations University, Tokyo and Centro Agronomico Tropical de Investigacion y Ensenanza.

Stull, R. B. (1988): An introduction to Boundary Layer Meteorology. Kluwer Academic Publishers

VDI-Richtlinie VDI 3786, Blatt 4, Meteorologische Messungen für Fragen der Luftreinhaltung – Luftfeuchte.

Wu, J.T.; Chang, S.C.; Wang, Y.S.; Wang, Y.F. & Hsu, M.K. (2001): Characteristics of the acidic environment of the Yuanyuang Lake (Taiwan). Botanical Bulletin of Academia Sinica **42**: 17-22.

Wrzesinsky, T. (2006): personal communication

Wrzesinsky, T. & Klemm, O. (2000): Summertime fog chemistry at a mountainous site in Central Europe. Atmospheric Environment **34**: 1487-1496.

Statement

I assure, that I did this entire thesis myself including figures, tables, and maps, if not mentioned differently, and did not use any other aid than specified in the text. Text, literal or analogous, originating from other sources is marked with its original source.

Münster, 23. Mai 2006 _____